

# **Investigation of a Potential Interaction Between PKD3 and MP-GAP Utilizing Fluorescent Microscopy and FRET**

by Roumina Rouhani Ardeshiri

A thesis submitted to the school of graduate studies in partial fulfillment of the requirements for the Degree of Master of Science in Medicine (Cancer and Development)

Division of Biomedical Sciences, Faculty of Medicine

Memorial University of Newfoundland

**May 2025**

St. John's

Newfoundland and Labrador

## **Abstract:**

Failures in cytokinesis, the final stage of mitosis, can lead to binucleation, which may act as an initiation point for cancer development. Protein kinase D3 (PKD3) is an enzyme that belongs to a family of protein kinases that have key roles in promoting many cellular processes, including proliferation, survival, and adhesion. It has been demonstrated that PKD3 depletion can cause a significant increase in binucleation in mouse embryonic fibroblasts (MEFs). In addition, the M-Phase GTPase-Activating Protein (MP-GAP) is shown to play an important role during the abscission of two daughter cells by inactivating the Ras homolog gene family member A (RhoA). The Leitges group previously showed that MP-GAP is translocated to the cleavage furrow at the late cytokinesis, where it colocalizes with RhoA and PKD3. Considering the effect of PKD3 deficiency on cells and the role of MP-GAP in cytokinesis, we aimed to verify the hypothesis that these two proteins might interact to regulate the final abscission. In this regard, this project was based on fluorescent microscopy imaging to track the dynamics of fluorescent protein-fused PKD3 and MP-GAP to characterize a potential interaction. In conclusion, while some data were collected on the endogenous PKD localization in cells, more experiments are required to establish a definitive strategy to identify a potential interaction.

## **General Summary:**

Cell division is one of the most important fields of cell biology and is required for homeostasis, growth, and reproduction. It comprises a series of tightly coordinated sequential events that are regulated by several proteins. While many of these regulatory mechanisms and the roles of involved proteins have been identified so far, the regulating factors of some pathways are not yet fully understood, including the final separation of two dividing cells. Failure to promote correct cell separation can result in the disruption of their genetic stability and subsequent tumor development, underscoring the clinical significance of studying those regulatory pathways. Herein, we used fluorescent protein to label two proteins that have previously been shown to contribute to successful cell division. Based on previous observations, it was hypothesized that these two proteins might interact, which is crucial for facilitating the final separation. In this regard, the aim of this project was to conduct microscopy investigations to trace the dynamics of these two proteins and characterize a potential interaction. Our experiments revealed that different tools and strategies are required to achieve more reliable results and to conclude if there is an interaction.

## **Acknowledgments:**

I would like to express my deepest gratitude to all those who have supported and contributed to completing this thesis.

First and foremost, I would like to express my sincere gratitude and deepest thanks to my supervisor, Dr. Michael Leitges, for his continuous guidance and support throughout my master's thesis project. My time spent in the lab would not have been nearly as enjoyable without the incredible support system he provided. In addition, I am grateful for the continuous help from the research assistant of the group, Uschi Braun. Her tireless efforts to facilitate the way to success and her experience in troubleshooting have been invaluable assets for my studies. I am also thankful to my past and present fellow members for their kind support. I deeply appreciate the guidance and support from my thesis committee members, Dr. Ken Kao and Dr. Matthew Parsons. With profound appreciation, I also extend my heartfelt thanks to Dr. Ann Dorward, to whom I owe my deepest gratitude for her invaluable academic guidance. A special thank you to Dr. Jacqueline Vanderluit, Nick Newhook, and Stephanie Tucker for all their guidance regarding the microscopy techniques. Gathering all those images would not have been plausible without your kind help. I also thank Dr. Jessica Esseltine, her lab members, and Dr. Parsons' group for kindly sharing aliquots of some materials used in this project. To my family, thank you for your patience, understanding, and unwavering support. Most importantly, I would like to thank my husband, Amirreza, whose encouragement and belief in me have been a source of strength throughout this endeavor.

# Table of Contents

|  |             |
|--|-------------|
| <b>ABSTRACT:</b> .....   | <b>II</b>   |
| <b>GENERAL SUMMARY:</b> .....  | <b>III</b>  |
| <b>ACKNOWLEDGMENTS:</b> .....  | <b>IV</b>   |
| <b>LIST OF TABLES</b> .....  | <b>VII</b>  |
| <b>LIST OF FIGURES</b> .....   | <b>VIII</b> |
| <b>LIST OF ABBREVIATIONS AND SYMBOLS</b> .....   | <b>IX</b>   |
| <b>1-INTRODUCTION:</b> .....   | <b>1</b>    |
| <b>1.1 SIGNAL TRANSDUCTION:</b> .....  | <b>1</b>    |
| <b>1.2 PROTEIN PHOSPHORYLATION AND KINASES:</b> .....                                      | <b>1</b>    |
| <b>1.3 PROTEIN KINASE C FAMILY:</b> .....  | <b>2</b>    |
| <b>1.4 PROTEIN KINASE D FAMILY:</b> .....  | <b>4</b>    |
| 1.4.1 STRUCTURE OF PKDS: .....   | 5           |
| 1.4.2 ACTIVATION OF PKDS: .....  | 8           |
| 1.4.3 INTRACELLULAR LOCALIZATION OF PKDS: .....  | 9           |
| 1.4.4 FUNCTIONS OF PKDS: .....   | 11          |
| <b>1.5 MAMMALIAN CELL CYCLE &amp; MITOSIS:</b> .....                                       | <b>16</b>   |
| 1.5.1 MITOTIC SUBPHASES: .....   | 17          |
| <b>1.6 CYTOKINESIS:</b> .....  | <b>18</b>   |
| 1.6.1 SOME ASPECTS OF MOLECULAR MECHANISMS UNDERLYING THE REGULATION OF CYTOKINESIS: ..... | 20          |
| 1.6.2 INSIGHTS INTO THE ROLE OF PKCE IN THE CYTOKINESIS REGULATION: .....                  | 22          |
| 1.6.3 FINDINGS ABOUT THE CONTRIBUTION OF PKD3 TO THE CYTOKINESIS REGULATION: .....         | 24          |
| <b>1.7 THE PROJECT RATIONALE:</b> .....  | <b>27</b>   |
| 1.7.1 THE METHODOLOGICAL APPROACH:.....  | 30          |
| <b>2-MATERIALS &amp; METHODS</b> .....   | <b>32</b>   |
| <b>2.1 CLONING:</b> .....  | <b>32</b>   |
| 2.1.1 DESIGNING PRIMERS: .....   | 32          |
| 2.1.2 PCR: .....   | 34          |
| 2.1.3 SUBCLONING INTO TOPO-VECTOR: .....   | 35          |
| 2.1.4 HEAT SHOCK TRANSFORMATION AND BACTERIAL CULTURE: .....                               | 36          |
| 2.1.5 PLASMID EXTRACTIONS:.....  | 36          |
| 2.1.6 RESTRICTION SITE DIGESTIONS: .....   | 37          |
| 2.1.7 GEL ELECTROPHORESIS: .....   | 37          |
| 2.1.8 GEL EXTRACTION AND DNA PURIFICATION: .....   | 38          |

|  |                  |
|--|------------------|
| 2.1.9 LIGATION:.....   | 38               |
| <b>2.2 CELL CULTURE: .....</b>   | <b>38</b>        |
| <b>2.3 TRANSFECTION:.....</b>  | <b>39</b>        |
| <b>2.4 CELL CYCLE SYNCHRONIZATION:.....</b>  | <b>40</b>        |
| <b>2.5 IMMUNOSTAINING: .....</b>   | <b>40</b>        |
| <b>2.7 CONFOCAL MICROSCOPY: .....</b>  | <b>42</b>        |
| <b>2.8 LIVE IMAGING: .....</b>   | <b>42</b>        |
| <br>   |                  |
| <b><u>3-RESULTS.....</u></b>   | <b><u>43</u></b> |
| <br>   |                  |
| <b>3.1 GENERATION OF TOOLS TO INVESTIGATE THE LOCALIZATION OF PKD3 AND MP-GAP DURING CYTOKINESIS/CLONING .....</b> | <b>43</b>        |
| <b>3.2 CRITERIA FOR CELL CYCLE STAGE IDENTIFICATION IN MICROSCOPY .....</b>  | <b>46</b>        |
| <b>3.3 TRANSFECTION EXPERIMENTS .....</b>  | <b>47</b>        |
| <b>3.4 IMMUNOSTAINING EXPERIMENTS .....</b>  | <b>55</b>        |
| <b>3.5 MP-GAP CLOVER EXPERIMENTS .....</b>   | <b>62</b>        |
| <br>   |                  |
| <b><u>4-DISCUSSION.....</u></b>  | <b><u>64</u></b> |
| <br>   |                  |
| <b>4.1 CLONING AND TRANSFECTION .....</b>  | <b>64</b>        |
| <b>4.2 IMMUNOSTAINING .....</b>  | <b>68</b>        |
| <b>4.3 MP-GAP .....</b>  | <b>72</b>        |
| <b>4.4 STUDY LIMITATIONS:.....</b>   | <b>73</b>        |
| <b>4.5 CONCLUDING REMARKS: .....</b>   | <b>74</b>        |
| <br>   |                  |
| <b><u>5- REFERENCES:.....</u></b>  | <b><u>75</u></b> |
| <br>   |                  |
| <b><u>6-SUPPLEMENTARY DATA .....</u></b>   | <b><u>83</u></b> |

## List of Tables

|  |    |
|--|----|
| <b>Table 1.1.</b> Summary of PKD functions .....                                       | 14 |
| <b>Table 2.1.</b> List of primers used for the cloning experiments .....               | 34 |
| <b>Table 2.2.</b> PCR cycles.....  | 35 |
| <b>Table 2.3.</b> List of primary and secondary antibodies used in immunostaining..... | 41 |
| <b>Table 3.1.</b> Summary of cell transfection and synchronization experiments.....    | 50 |

## List of Figures

|  |    |
|--|----|
| <b>Figure 1.1.</b> Schematic representation of PKD isoforms .....  | 7  |
| <b>Figure 1.2.</b> Schematic representation of Cytokinesis .....   | 19 |
| <b>Figure 1.3.</b> .....   | 21 |
| Schematic representation of the RhoA GTPase molecular switch, along with the regulators.   |    |
| <b>Figure 1.4.</b> .....   | 29 |
| Schematic representation of the cleavage furrow of a dividing cell, along with PKC $\epsilon$ signaling pathway regulating the contractile ring dissociation and final abscission. |    |
| <b>Figure 1.5.</b> .....   | 31 |
| Schematic representation of FRET between two fluorescent proteins (FPs).   |    |
| <b>Figure 2.1.</b> Flowchart representing cloning steps in brief.....  | 33 |
| <b>Figure 3.1.</b> Schematic representation of the project's cloning strategy.....   | 45 |
| <b>Figure 3.2.</b> .....   | 46 |
| Demonstration of morphological characteristics to identify the cell cycle stage.   |    |
| <b>Figure 3.3.</b> .....   | 49 |
| Schematic pattern of a cell cycle demonstrating the cycle arrest points upon thymidine and nocodazole treatment.   |    |
| <b>Figure 3.4.</b> Figure HeLa Kyoto cells expressing PKD3-mRuby2 .....  | 53 |
| <b>Figure 3.5.</b> .....   | 54 |
| Lack of specific localization of PKD3-mRuby2 in HEK cells during prophase to telophase.  |    |
| <b>Figure 3.6.</b> Localization of PKD during prophase to telophase in MEFs .....  | 57 |
| <b>Figure 3.7.</b> Localization of PKD during prophase to telophase in HEKs .....  | 58 |
| <b>Figure 3.8.</b> .....   | 59 |
| Association of the phosphorylated PKD with structures that might represent central spindle microtubules and intracellular bridge during mitotic phases in HEK cells.               |    |
| <b>Figure 3.9.</b> MEFs expressing endogenous active PKD .....   | 60 |
| <b>Figure 3.10.</b> .....  | 61 |
| Localization of phosphorylated PKD during prophase to telophase in MEFs-Prophase to telophase  |    |
| <b>Figure 3.11.</b> The localization pattern of MP-GAP-Clover in HeLa Kyoto cells.....   | 63 |
| <b>Figure 6.1.</b> Immunostaining validation of PKD3-mRuby2 plasmid.....   | 84 |
| <b>Figure 6.2.</b> .....   | 85 |
| Synchronization and live imaging of GFP::tubulin H2B::mCherry expressing HeLa Kyoto cells  |    |
| <b>Figure 6.3.</b> Controls (Mock samples).....  | 86 |

## List of Abbreviations and Symbols

|                         |  |
|-------------------------|--|
| • <b>AGC</b>            | protein kinase A (PKA), protein kinase G (PKG), and protein kinase C (PKC) |
| • <b>AL</b>             | Activation loop  |
| • <b>AMPK</b>           | AMP-dependent kinases  |
| • <b>APC/C</b>          | Anaphase-Promoting Complex/Cyclosome                                       |
| • <b>aPKC</b>           | Atypical PKC   |
| • <b>BME</b>            | $\beta$ -mercaptoethanol   |
| • <b>BMP</b>            | bone morphogenetic proteins  |
| • <b>BSA</b>            | Bovine serum albumin   |
| • <b>CAMKs</b>          | Ca <sup>2+</sup> /calmodulin-dependent protein kinases                     |
| • <b>CDK1</b>           | Cyclin-dependent Kinase  |
| • <b>CHO</b>            | Chinese hamster ovary  |
| • <b>CO<sub>2</sub></b> | Carbon dioxide   |
| • <b>cPKC</b>           | Conventional PKC   |
| • <b>DAG</b>            | Diacylglycerols  |
| • <b>DAPI</b>           | 4',6-Diamidino-2-Phenylindole  |
| • <b>DTB</b>            | Double thymidine block   |
| • <b>dd</b>             | Double distilled   |
| • <b>dKO</b>            | Double knock out   |
| • <b>DMEM</b>           | Dulbecco's Modified Eagles' Medium   |
| • <b>EB1</b>            | End binding 1  |
| • <b>ERK</b>            | Extracellular receptor kinase  |

|                  |   |
|------------------|---|
| • <b>FBS</b>     | Fetal bovine serum                                  |
| • <b>FP</b>      | Fluorescent protein                                 |
| • <b>FRET</b>    | Fluorescence resonance energy transfer              |
| • <b>GAP</b>     | GTPase activating protein                           |
| • <b>GEF</b>     | Guanine-nucleotide exchange factors                 |
| • <b>GFP</b>     | Green fluorescent protein                           |
| • <b>G phase</b> | Growth phase  |
| • <b>GPCR</b>    | G-protein coupled receptor                          |
| • <b>HBS</b>     | HEPES buffered saline                               |
| • <b>HDAC</b>    | Histone deacetylase                                 |
| • <b>HEK</b>     | Human embryonic kidney                              |
| • <b>HEPES</b>   | 4-(2-Hydroxyethyl)piperazine-1-ethane-sulfonic acid |
| • <b>IEC</b>     | Intestinal epithelial cell                          |
| • <b>IPTG</b>    | Isopropyl $\beta$ -D-1-thiogalactopyranoside        |
| • <b>LB</b>      | Lysogeny broth                                      |
| • <b>MEF</b>     | Mouse embryonic fibroblast                          |
| • <b>MEM</b>     | Minimum essential medium                            |
| • <b>MFF</b>     | Mitochondrial fission factor                        |
| • <b>MP-GAP</b>  | M-Phase GTPase-activating protein                   |
| • <b>MT1-MMP</b> | Membrane type 1 matrix metalloprotease              |
| • <b>NaOAc</b>   | Sodium acetate                                      |
| • <b>NCBI</b>    | National Center for Biotechnology Information       |

|                                    |   |
|------------------------------------|---|
| • <b>NEB</b>                       | New England BioLabs                       |
| • <b>NTDD</b>                      | N-terminal dimerization domain            |
| • <b>nPKC</b>                      | Novel PKC                                 |
| • <b>PANC</b>                      | Pancreatic cancer cell                    |
| • <b>PBS</b>                       | Phosphate buffered saline                 |
| • <b>PBT</b>                       | PBS, Triton X-100, BSA                    |
| • <b>PCM</b>                       | Pericentriolar material                   |
| • <b>PCR</b>                       | Polymerase chain reaction                 |
| • <b>PFA</b>                       | Paraformaldehyde                          |
| • <b>PH</b>                        | Pleckstrin homology                       |
| • <b>PI4KIII<math>\beta</math></b> | Phosphatidylinositol 4-kinase III $\beta$ |
| • <b>pIRES</b>                     | plasmid internal ribosome entry site      |
| • <b>PLC</b>                       | Phospholipase C                           |
| • <b>PKC</b>                       | Protein kinase C                          |
| • <b>PKD</b>                       | Protein kinase D                          |
| • <b>Ras</b>                       | Rat sarcoma                               |
| • <b>RhoA</b>                      | Ras homolog gene family member A          |
| • <b>rpm</b>                       | Revolutions per minute                    |
| • <b>SAC</b>                       | Spindle assembly checkpoint               |
| • <b>SDS</b>                       | Sodium dodecyl sulfate–polyacrylamide     |
| • <b>S phase</b>                   | Synthesis phase                           |
| • <b>SERBP1</b>                    | SERPINE1 mRNA Binding Protein 1           |

|                |  |
|----------------|--|
| • <b>Ser</b>   | Serine   |
| • <b>TAE</b>   | Tris-acetate-EDTA                                      |
| • <b>TE</b>    | Tris-HCl containing EDTA.Na <sub>2</sub>               |
| • <b>TENS</b>  | NaOH in TE buffer and SDS                              |
| • <b>TGN</b>   | Trans-Golgi network                                    |
| • <b>TLR</b>   | Toll-like receptors                                    |
| • <b>Thr</b>   | Threonine  |
| • <b>Tyr</b>   | Tyrosine   |
| • <b>UV</b>    | Ultraviolet  |
| • <b>VEGF</b>  | Vascular endothelial growth factors                    |
| • <b>wt</b>    | Wild type  |
| • <b>X-gal</b> | Bromo-4-chloro-3-indolyl- $\beta$ -D-galactopyranoside |
| • <b>ZEN</b>   | Zeiss efficient navigation                             |

# **1-Introduction:**

## **1.1 Signal Transduction:**

To maintain cellular and tissue-specific homeostasis, signals from the extracellular environment are transferred into the cell through the binding of specific ligands to the receptors, either localized on the plasma membrane or inside the cell. The bound receptors are then activated and transmit the signals through a series of cellular pathways or cascades. Ultimately, the signaling cascades culminate in the activation of proteins and/or enzymes, leading to different cellular responses, such as cell migration or proliferation. These processes are referred to as *signal transduction*, a term that was first employed in biological concepts in the 1970s. It then became ubiquitous in cell-related studies after it was adopted by Nobel Prize winner Martin Rodbell in 1980 to describe guanosine-triphosphate (GTP) and GTP-binding proteins, which are now known to be involved in many key signaling events<sup>1</sup>. Signal transduction is facilitated by changes in the status of proteins, including their activation, subcellular localization, and interactions with other proteins or lipids. These changes are achieved through different approaches, known as post-translational modifications, among which protein phosphorylation is one of the most common and most widely studied in cell signaling events.

## **1.2 Protein Phosphorylation and Kinases:**

The roots of protein phosphorylation are grounded back to 1906 when Levene and Alsberg discovered phosphate as an ingredient of the protein Vitellin<sup>2</sup>. This finding was followed by the identification of phosphorylated serine in the same protein by Levene and Lipmann in 1933<sup>3</sup>.

However, the importance of protein phosphorylation as a dynamic regulatory mechanism of protein function was first recognized by Krebs and Fischer in the 1950s during their studies of glycogen phosphorylase and its reversible phosphorylation<sup>4</sup>. Protein phosphorylation is one of the most common post-translational modifications mediating a variety of fundamental biological processes in cells. The phosphate group has several distinct properties that act as a favorable molecular switch to regulate complex signaling pathways through dynamic and transient phosphorylation modifications. Protein kinases are phosphotransferases that mediate the transfer of the terminal (gamma) phosphate of ATP to the hydroxyl group of amino acid residues in protein substrates<sup>5</sup>. More than 2% of most genomes encode for the kinase superfamily, and the human kinome comprises more than 500 distinct genes, highlighting the importance of these enzymes participating in the regulation of cellular events<sup>1,6,7</sup>. The kinase superfamily is categorized into groups that are subdivided into one or more families, consisting of kinases with similar amino acid sequences sharing a common ancestor gene. Depending on the amino acid specificity, protein kinases predominantly facilitate the phosphorylation of serine (Ser), threonine (Thr), and tyrosine (Tyr) residues<sup>1</sup>. Although less frequently, histidine, lysine, and arginine residues are also phosphorylated by other kinases<sup>8,9</sup>.

### **1.3 Protein Kinase C Family:**

Protein Kinase C (PKC) is a family of Ser/Thr-specific kinases, a branch of the AGC kinases (protein kinase A (PKA), protein kinase G (PKG), and protein kinase C (PKC)) playing crucial roles in several cellular signal transduction<sup>10</sup>. Upon their discovery in the 1980s, they were renowned for regulating cellular signaling pathways due to acting as receptors for phorbol esters, which are potent tumor-promoting compounds, and diacylglycerols (DAGs), which are lipid second messengers<sup>11,12</sup>. Generally, PKC members consist of an N-terminal regulatory domain

(approximately 20–40 kDa) linked by a flexible hinge region to a C-terminal catalytic domain (approximately 45 kDa). Each family member is regulated by precise mechanisms, forming their stable structures, positioning them in the required subcellular localization, and facilitating their functions. In total, the family comprises 11 isozymes that are categorized into three structurally different subgroups based on their N-terminal regulatory domains, which require distinct cofactors: conventional (cPKC:  $\alpha$ ,  $\beta$ I,  $\beta$ II, and  $\gamma$ ), novel (nPKC:  $\delta$ ,  $\epsilon$ ,  $\eta$  and  $\theta$ ) and atypical (aPKC:  $\zeta$  and  $\iota$ ). While the carboxy (C)-terminal catalytic domains are highly conserved among the isoforms, the isoform-specific interactions are known to be linked to variable regions (termed V1–V5)<sup>10,13,14</sup>.

The C1 domain in conventional isozymes contains a tandem repeat of zinc-finger-like cysteine-rich motifs that is the binding site for DAGs and phorbol esters, while the C2 domain binds anionic lipids in a  $\text{Ca}^{2+}$ -dependent manner. Although the C1 domain has the same cysteine-rich motifs and acts the same in novel family members, these isozymes are insensitive to  $\text{Ca}^{2+}$  due to the lack of  $\text{Ca}^{2+}$  binding sites in their C2 domains and, thus, are regulated only by DAGs. Lastly, atypical PKCs comprise a different variant of the C1 domain, lacking cysteine-rich motifs (atypical C1) and not binding to DAGs or phorbol esters. Also not regulated by  $\text{Ca}^{2+}$ , their functions are mainly mediated by protein-protein interactions. Among the similarities between all the isoforms is a conserved carboxyl-terminal tail that performs as a phosphorylation-dependent docking segment for the enzyme's regulators, an auto-inhibitory pseudosubstrate sequence that keeps the enzyme in an inactive state by occupying its substrate binding domain, and an activation loop region that contains phosphorylation sites<sup>13,14</sup>.

Regarding their activation, PKC enzymes (except aPKCs) are activated by DAG, which can be produced in cells mainly following the stimulation of G protein-coupled receptors (GPCR),

tyrosine kinase receptors, or non-receptor tyrosine kinases. Furthermore, phorbol esters can induce PKC activation by mimicking the action of DAG and are extensively used for *in vivo* PKC studies. Both phorbol esters and DAG mediate the membrane recruitment of PKC, which is one hallmark of PKC activation, by hydrophobic anchorage of the enzyme. In addition, phosphatidylserine, which is an acidic lipid exclusively found on the cytoplasmic side of membranes, is required for the regulation of PKC members (αPKCs are differently activated), and Ca<sup>2+</sup> is necessary for the maximum activity of some isozymes. Furthermore, PKC activation involves the dissociation of its pseudosubstrate from the kinase core<sup>13,14</sup>.

Once activated, PKCs mediate various signaling pathways to control key biological processes, including but not limited to cell proliferation and differentiation, apoptosis, inflammation and immune responses, vesicle trafficking and secretion, and gene expression. One of the key downstream targets in PKC signaling is the protein kinase D (PKD) family of kinases. Studies in the 1990s revealed a considerable increase of PKD activation in intact cells following treatment with phorbol ester and DAGs and also showed PKD inhibition after treatment with PKC inhibitors which did not directly impact PKD catalytic activity<sup>15,16</sup>. Together with the demonstration of a PKC-dependent PKD activation upon regulatory peptide induction, they provided the first evidence for the existence of a PKC-PKD signaling axis<sup>17</sup>. Nowadays, the PKC-PKD phosphorylation cascade is known as an established signal transduction pathway regulating multiple fundamental cellular events.

#### **1.4 Protein Kinase D Family:**

PKD is also a family of Ser/Thr phosphorylating kinases but is classified within the Ca<sup>2+</sup>/calmodulin-dependent protein kinases (CAMKs) group<sup>18</sup>. The family comprises three

structurally similar isoforms: PKD1, PKD2, and PKD3. PKDs are recognized for regulating several biological functions crucial for cell proliferation, differentiation, apoptosis, immune regulation, cardiac contraction, cardiac hypertrophy, angiogenesis, and cancer<sup>19-35</sup>. Due to the similarity between the C1 domain of PKDs and the DAG binding domain of PKC enzymes, PKD1 and PKD3 were previously categorized as PKC family members, known as PKC $\mu$  and PKC $\nu$ , respectively<sup>36,37</sup>. However, they were later identified as a distinct Phorbol Ester/DAG-stimulated kinase family following their sequencing and molecular cloning in 1994 and introduced as a potential catalyst for signal transduction with substrate specificity different from that of recognized PKCs<sup>37-39</sup>. Accordingly, it revealed that they belong to the CAMK family owing to the sequence similarities in their kinase domain, separate from the AGC group<sup>40</sup>. Among other predominant characteristics leading to the new classification are very low homology between the catalytic domain of PKDs and the conserved kinase domain of PKCs, the presence of a pleckstrin homology (PH) domain in the N-terminal of PKDs, the lack of an autoinhibitory pseudosubstrate motif present in PKCs, and distinct specificity in substrates and inhibitors<sup>40-42</sup>.

#### **1.4.1 Structure of PKDs:**

Members of the PKD family consist of an N-terminal regulatory domain and a C-terminal catalytic domain. N-terminally, all isoforms share some conserved regions: an N-terminal dimerization domain (NTDD) followed by two cysteine-rich Zn fingers (C1A-C1B) connected with a linker which contains serine-rich stretch only in PKD2, and a PH domain. On the other tail, the C-terminal consists of a conserved kinase domain comprising an activation loop phosphorylation motif and an autophosphorylation site at the very end, which is conserved in PKD1 and PKD2 but not PKD3<sup>40,43-45</sup>. The intricate structure of PKDs is tightly interconnected

with their regulation and function. The tandem C1A/C1B motifs are shown to act in the lipid-membrane anchorage, which is a substantial step in PKD activation, while the PH domain participates in PKD regulation by propagating an intramolecular autoinhibitory interaction<sup>46</sup>. It is worth noting that the autophosphorylation regions present in PKD1/2 are PDZ-binding motifs playing potential roles in PKD trafficking and PKD signaling, while PKD3 is not regulated in this manner due to the lack of the autophosphorylation site<sup>45,47,48</sup>. Moreover, the lack of an autophosphorylation site could potentially change the substrate specificity and catalytic function of PKD3 since the absence of a phosphate group at this site may affect the conformation of the kinase by eliminating a negative charge<sup>49</sup> (Fig1.1).

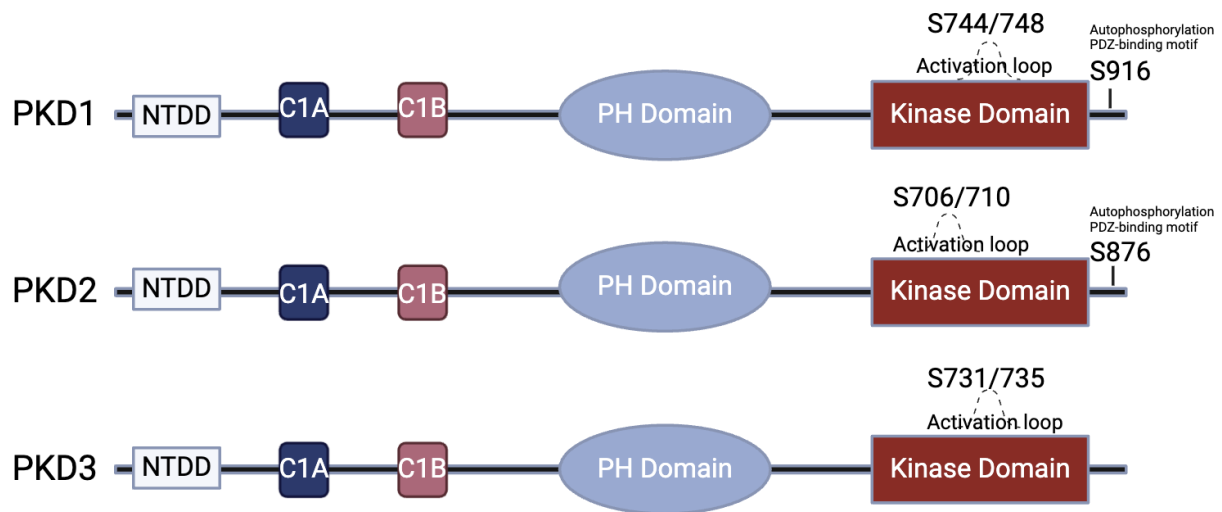


**Figure1.1. Schematic representation of PKD isoforms.** Domain structures of three PKD isoforms comprise conserved NTDD, C1A-C1B, and PH domains in the regulatory region and the kinase domain in the catalytic region. Trans-phosphorylation sites of the isoforms are in the activation loop. PKD1 and PKD2 also contain an auto-phosphorylation motif depicted above.<sup>45</sup> The figure was created by the *BioRender* tool.

### 1.4.2 Activation of PKDs:

PKDs are also directly activated by DAG and phorbol esters based on in vitro kinase studies<sup>16</sup>. The initial model for PKD activation described by Rozengurt et al. is based on receptor-dependent pathways that facilitate the accumulation of DAG and the plasma membrane-colocalization of PKD with its upstream activator PKC<sup>18</sup>. This colocalization mediates PKD activation through the transphosphorylation of conserved serine residues in the activation loop (AL) by novel PKCs. In this model, activated GPCR stimulations lead to the recruitment of PKD at the plasma membrane in close proximity to PKC $\epsilon$ , by which they become activated. It eventually leads to a reverse translocation to their specific subcellular target compartments in order to propagate subsequent signaling. This PKC $\epsilon$ -mediated phosphorylation was shown to be in the activation loop at Ser744/748, resulting in the release of the autoinhibiting PH domain and following stabilization of PKD in its active conformation. These findings were among the first studies providing evidence for establishing a novel PKC $\epsilon$ -dependent mechanism of PKD activation<sup>45,50-52</sup>. Of note, PKD3 is shown to be phosphorylated by novel PKC isozymes, including PKC $\epsilon$ , as the expression of the constitutively active form of those resulted in robust and constant activation of PKDs<sup>53</sup>. Altogether, transphosphorylation of PKDs in their activation loop is known as a key PKD activation pathway in many cell types and can be initiated by a numerous set of stimuli, for example, oxidative stress<sup>54,55</sup>.

On the other hand, a considerable body of recent data suggests that all PKD members can also be activated through an AL autophosphorylation mechanism in a PKC-independent manner during cellular processes such as oxidative stress responses and apoptotic circumstances, which is distinctive for each isoform<sup>45,56</sup>. PKD1 and PKD2, but not PKD3, are also autophosphorylated at a consensus phosphorylation motif within the C terminus tail, which regulates their interaction

with some scaffolding proteins<sup>45,47,48</sup>. Eventually, the activated PKDs mediate the phosphorylation of target substrates, orchestrating a cascade of downstream signaling events that result in a specific cellular function<sup>55</sup>.

### **1.4.3 Intracellular localization of PKDs:**

The intracellular localization of PKDs is predominantly associated with their activation status. In unstimulated cells, PKDs are mainly ubiquitous in the cytoplasm. Through their regulatory domains and upon receptor stimulation, PKDs can possess rapid dynamic translocations to different cellular compartments, including the plasma membrane, the Golgi apparatus, mitochondria, and the nucleus<sup>40</sup>. Understanding the distinctive distribution of each member of the PKD family can reveal additional insights into their unknown isoform-specific characteristics.

In the case of PKD1, it has been shown that a significant portion of them reside in the cytosol of the resting cells, with a lesser presence in the Golgi<sup>40,57,58</sup>. Phosphoinositide-specific phospholipase C (PLC) can stimulate the plasma membrane production of DAG. Cytosolic PKD1 translocates and binds to the DAGs with its cysteine-rich domains. Also, upon GPCR-agonist stimulation, PKD1 translocates from the cytosol to the plasma membrane through its cysteine-rich domain. This translocation was shown to be reversible in a PKC $\epsilon$ -dependent manner, requiring the PKD activation loop (Ser744 and Ser748) in the catalytic domain. Subsequently, catalytically activated PKD1 transiently accumulates in the nucleus from which it is exported, requiring the PH domain<sup>52</sup>.

Similar to PKD1, PKD2 also goes through the same reversible translocations between cytosol and plasma membrane. A subsequent transport to the nucleus was observed for PKD2 upon activation with gastrin in a CCK2 receptor-transfected gastric cancer AGS cells. This localization

was shown to depend on activation loop phosphorylation of Ser706 and Ser710 on PKD2, and also phosphorylation on Ser244 by another group of kinase named casein kinase<sup>57</sup>. These are an illustrative example highlighting the interplay of specific domains, receptors, phosphorylation events, and upstream regulators that lead to isoform-specific subcellular dynamics. and enable them to execute their functions.

In contrast to the other two family members, PKD3 is demonstrated to localize in both the cytosol and nucleus of unstimulated cells. However, there is a significantly increased accumulation of PKC-activated PKD3 in the nucleus upon stimulation with GPCR agonists<sup>59</sup>. Additionally, the nuclear accumulation of PKD3 was shown to depend on its catalytic activity since the catalytic domain-targeted point mutations could inhibit this localization. Moreover, it is demonstrated that PKD3 shuttles between cytosol and plasma membrane and PKC-mediated phosphorylation of the PKD3 activation loop (Ser731 and Ser735) is required for the membrane dissociation<sup>51-53,57</sup>.

It is worth mentioning that most of the information available about PKD isoform subcellular localizations are during the interphase in different cell types, and the data on their mitotic distribution is limited. A study by Papazyan et al. demonstrated that during mitosis, PKD isoforms are phosphorylated in their activation loop and localize to mitotic apparatus, including centrosomes, spindles, and midbody, underscoring a yet unidentified potential role for the enzymes in association with mitotic structures<sup>60</sup>. This is described in detail in the subsequent paragraphs.

#### 1.4.4 Functions of PKDs:

While it was previously suggested that PKD isoforms function redundantly and share many common signaling pathways in different cell types, a growing set of studies highlights isoform-specific roles of PKDs in highly differentiated cell lines<sup>45</sup>. PKDs are shown to contribute to a vast array of cellular functions, including endothelial cell migration and proliferation, cell trafficking and secretion, neuronal and epithelial cell polarity, immune response, inflammation, oxidative stress, and cancer cell proliferation and invasion<sup>55</sup>. The next paragraphs describe some studies focusing on each mentioned function. A summary is provided in [Table 1.1](#).

PKD signaling is linked to regulating vesicle trafficking, secretion, and polarity. PKD1-2 have been shown to localize at the Golgi complex and participate in regulating the formation of secretory vesicles from the trans-Golgi network by phosphorylating substrates present at the Golgi, including phosphatidylinositol 4-kinase III $\beta$  (PI4KIII $\beta$ ). PKD 1-2 inactivation led to impaired fission of trans-Golgi network (TGN) transport carriers, along with cargo-accumulated long tubules at TGN<sup>61-64</sup>. PKD1-2 were shown to define the neuronal and epithelial cell polarity by regulating the sorting and destination of TGN-derived proteins<sup>65,66</sup>. Considering their roles in immunity, many studies demonstrate PKD modulating immune function through different mechanisms such as regulating  $\beta$ 1 integrin activity<sup>24</sup>, controlling pre-T-cell differentiation<sup>67</sup>, and functioning downstream of Toll-like receptors TLR2,5,9<sup>25,26</sup>. Moreover, PKD was introduced to play important roles in fundamental processes such as contraction, hypertrophy and proliferation in cardiac cells, highlighting its function in cardiovascular regulation<sup>23</sup>. It is also worth noting that a growing body of evidence has implicated PKD1 as a mediating factor of NF- $\kappa$ B induction in response to oxidative stress<sup>19-21,68</sup>. Although the mentioned studies and many others have shed light on the existing knowledge about PKDs, conducting isoform-specific studies on substrates

and biological functions of PKDs are commonly ascribed to inconclusive results, basically due to some challenges associated with the redundant nature of PKDs and their compensatory mechanisms for mediating cellular responses<sup>45</sup>.

#### **1.4.4.1 Functions of PKDs related to cell proliferation, differentiation, and cancer:**

One of the most widely studied functions of PKDs is in cell proliferation and differentiation.<sup>22</sup> These cellular events can be stimulated by the intensity and duration of a signaling pathway that includes extracellular receptor kinase (ERK). PKDs have been shown to participate in GPCR-induced DNA synthesis and cell proliferation pathways through the ERK signaling cascade. Accordingly, PKD has been linked to this signaling pathway, thereby concentrating the products of their downstream gene transcription, leading to cell cycle progression. Together, they form a PKD/ERK/DNA synthesis axis, which is demonstrated to stimulate proliferation in fibroblasts and cancer lines with rat sarcoma (Ras) mutation, including pancreatic cancer 1 (PANC-1) cells<sup>33,34,69,70</sup>.

In addition, PKD signaling was shown to be pivotal for the angiogenesis in tumor cells through the vascular endothelial growth factors (VEGFs) pathway<sup>30</sup>. PKDs can regulate proliferation by phosphorylating some members of the Class II histone deacetylases (HDACs) in endothelial cells. HDACs regulate gene expression by modifying the structures of chromatin. The phosphorylation of HDAC5 and HDAC7 by PKD leads to their interaction with 14-3-3 proteins, which sequesters them in the cytosol. Preventing the proteins from accessing DNA structures inhibits their transcription repressive effects, resulting in the corresponding gene expression and proliferation. In this context, VEGF is shown to mediate phosphorylation of HDAC 5,7 by PKD, which leads to their nuclear export and subsequent angiogenesis-associated transcriptions<sup>28,29</sup>.

Lastly, several studies focusing on the implication of PKD signaling in cancer have identified important roles for PKDs regulating proliferation and the tumor microenvironment in cancer cells originating from different malignant tissues, including the pancreas, liver, gastrointestinal tract, breast, prostate, and lung. PRKD1 was revealed to bear recurrent mutations in breast and colon cancer cells<sup>71</sup>. Accordingly, PKD was introduced as a potential therapeutic target for pancreas and prostate cancer<sup>35,72,73</sup>. Although PKDs have been linked to cancer development through various mechanisms, at the time this project's hypothesis was proposed, only a few studies had explored the role of PKDs in cell cycle regulation and their potential connection to cancer. Considering this, the next paragraph focuses on some recent key studies establishing the mentioned link, but through pathways different from those addressed in this project.

**Table 1.1. Summary of PKD functions**

| <b>Function</b>                               | <b>Studies</b>   |
|---|--|
| <b>Vesicle Trafficking and Secretion</b>      | PKD1-2 localize at the Golgi complex and regulate the formation of secretory vesicles by phosphorylating substrates at the Golgi, such as PI4KIII $\beta$ . Inactivation leads to impaired TGN transport carriers <sup>61-64</sup> .   |
| <b>Cell Polarity</b>                          | PKD1-2 define neuronal and epithelial cell polarity by regulating the sorting and destination of TGN-derived proteins <sup>65,66</sup> .   |
| <b>Immune Response</b>                        | PKDs modulate immune functions, regulate $\beta$ 1 integrin activity, control pre-T-cell differentiation, and function downstream of Toll-like receptors (TLR2,5,9) <sup>24 25,26, 67, .</sup>   |
| <b>Cardiovascular Regulation</b>              | PKDs play roles in cardiac cell contraction, hypertrophy, and proliferation, emphasizing their function in cardiovascular regulation <sup>23</sup> .   |
| <b>Oxidative Stress Response</b>              | PKD1 mediates NF- $\kappa$ B induction in response to oxidative stress <sup>19-21,68</sup> .   |
| <b>Cell Proliferation and Differentiation</b> | <p>PKDs participate in GPCR-induced DNA synthesis and cell proliferation pathways through the ERK signaling cascade, forming a PKD/ERK/DNA synthesis axis stimulating proliferation in fibroblasts and cancer cells<sup>33,34,69,70</sup>.</p> <p>PKDs regulate angiogenesis in tumor cells through the VEGF pathway and phosphorylate Class II HDACs in endothelial cells, affecting gene expression and proliferation<sup>28,29</sup>.</p> |
| <b>Cancer Cell Proliferation and Invasion</b> | PKDs regulate proliferation and the tumor microenvironment in various cancer types (pancreas, liver, gastrointestinal tract, breast, prostate, lung) <sup>35,72,73</sup> . PRKD1 mutations are noted in breast and colon cancers <sup>71</sup> .   |

#### 1.4.4.2 PKDs and cell cycle:

While it is essential for dividing cells to maintain chromosomal fidelity, the proper and equal duplication and partitioning of organelles is equally crucial. The proliferation of mitochondria is mediated through the processes of fusion and fission, leading to their growth and division during the cell cycle<sup>74</sup>. In this context, what positions PKDs as an important factor is the demonstration that they induce mitochondrial fission in mammalian cells by phosphorylating the mitochondrial fission factor (MFF) and, thus, are involved in mitosis regulation. PKD-mediated MFF phosphorylation is independent of AMP-dependent kinases (AMPKs) and is proposed to be facilitated by all three members of the PKD family. PKD inhibition in HeLa cells and PKD depletion in mouse embryonic fibroblasts (MEFs) were characterized by inhibition and reduction in mitotic MFF phosphorylation at Ser172, respectively. In a model proposed by Pangou et al. PKD-mediated MFF phosphorylation links mitochondrial fission to chromosome segregation during mitosis. It was also shown that this phosphorylation might be required to avoid the spindle assembly checkpoint (SAC) adaptation, which enables the cells to complete mitosis despite the chromosomal alignment defects. In addition, PKD2/3 double knockout (dKO) HeLa cells showed mitotic defects similar to MFF KO cells, highlighting the role of PKD-MFF signaling in the regulation of mitosis<sup>75</sup>. As cancer cells are marked with a high proliferation rate, the upregulation of PKD activation may guarantee their fast progression and survival, making the PKD-MFF signaling axis a strategic therapeutic target<sup>75,76</sup>. Another organelle whose proper division is pivotal for successful mitosis is the Golgi complex. To be divided between two daughter cells, the Golgi complex turns into vesicular compartments, a process that starts with Golgi fragmentation. The correct segregation of the Golgi complex that takes place in the G2 phase of the cycle is pivotal for entry to mitosis, suggesting an additional control for the G2/M checkpoint. This step is

introduced as the Golgi mitotic checkpoint regulated by PKDs through activating the rapidly accelerated fibrosarcoma1/ mitogen-activated protein kinase1 (Raf-1/MEK1) signaling pathway. It was also shown that PKD1/2 depletion results in a G2 phase arrest in HeLa cells<sup>77</sup>. This highlights that PKD-mediated cell cycle regulation may start before the initiation of mitosis. As completing this step is inevitable for a successful proceed to mitosis, it underscores a novel indirect role of PKD involvement in mitosis control. These accumulative data underscore an undefined role of PKDs in proper cell cycle progression in human cells<sup>75</sup>.

### **1.5 Mammalian Cell Cycle & Mitosis:**

The cell cycle refers to a series of sequential events that are tightly coordinated to result in the faithful duplication of cells. A finely coordinated action of numerous biochemical and molecular processes is required to enable the cells to pass through domino-like sequences, leading to a successful cell division. The eukaryotic cell cycle consists of two major phases: interphase and mitosis. Throughout interphase, the cell grows and achieves complexity in organelle localization, transcription, and translation. During this step, the DNA is duplicated through the DNA synthesis stage (S-phase), which prepares the cell for replication. The mitosis or M-phase is shorter but includes highly orchestrated and elaborative mechanisms of cell cycle regulation. It involves condensation and segregation of chromosomes followed by separation and equal distribution of the cytoplasm and cytoplasmic material between two daughter cells. M-phase is further divided into Prophase, Prometaphase, Metaphase, Anaphase, and Telophase. Details about the events linked to each mitotic subphase are described in the following paragraph. The final stage of mitosis, cytokinesis, in which the cytoplasm divides and the final abscission occurs, is also discussed in the next section. Several checkpoints are ascribed to cell cycle progression to ensure

chromosomal fidelity and error-free replication. If the required events are not met, the cell cycle is arrested, resulting in various consequences, including reversible quiescence, apoptosis, or unsuccessful cytokinesis and binucleation. In general, multinucleation affects the ploidy of the cells, disrupting their chromosomal integrity, which is demonstrated as a critical factor in forming cancerous cells. Before mitosis, there is a tight linkage between sister chromatids that is crucial for their bipolar orientation and successful mitosis<sup>78,79</sup>.

### **1.5.1 Mitotic subphases:**

Mitosis is initiated by fundamental events, including chromosome condensation, centrosome separation, and spindle assembly in the prophase. In prometaphase, the nuclear envelopes disappear, and sister chromatids attach to the mitotic spindle. Next, sister chromatids are completely associated with spindles and are positioned at the mitotic plate during prometaphase. Together with the two previous phases, they include the stage termed mitotic entry, which is followed by the next stage, mitotic exit. The hallmark that divides mitotic entry and the mitotic exit is the sister chromatid segregation, serving as the midpoint. Anaphase is the step when the mitotic spindle segregates sister chromatids, pulling them to the spindle poles. Telophase is considered the final stage in mitosis, comprising spindle disassembly, chromosome decondensation, and reformation of the nuclear membrane<sup>79</sup>.

## 1.6 Cytokinesis:

Cytokinesis, the final step of cell division, is the separation of the cytoplasm of two daughter cells during late mitosis. It is initiated following the spatial definition of the division plane between the separating chromosomes by the central microtubules<sup>80</sup>. Subsequently, signaling pathways lead to the concentration and activation of a small Rho GTPase, Ras homolog gene family member A (RhoA), which is the upstream mediator for the assembly of an actomyosin contractile ring at the equatorial cortex of the cell.<sup>81,82</sup> Formation of the ring is followed by contractility at this site and relaxation at the polar cortex. During contraction, the plasma membrane invaginates, and a cytokinetic cleavage furrow forms, partitioning the cytoplasm of daughter cells. As ingression continues, the central spindle compacts until there is a dense cluster of antiparallel microtubule bundles overlapping at the center, flanked by cytoplasmic domains. At this stage, the cells remain connected through a cytoplasmic bridge that forms the midbody, an organelle proposed to control the final separation. The ultimate physical separation of two sister cells is termed abscission, an actin-independent irreversible process that is completed by the division of the plasma membrane in the midbody. The microtubule bundle becomes resolved, and the plasma membrane seals in place (Fig1.2). The faithful inheritance of the genome to daughter cells requires the final abscission to be tightly coordinated with the spatiotemporal state of the segregating chromosomes<sup>83-86</sup>.

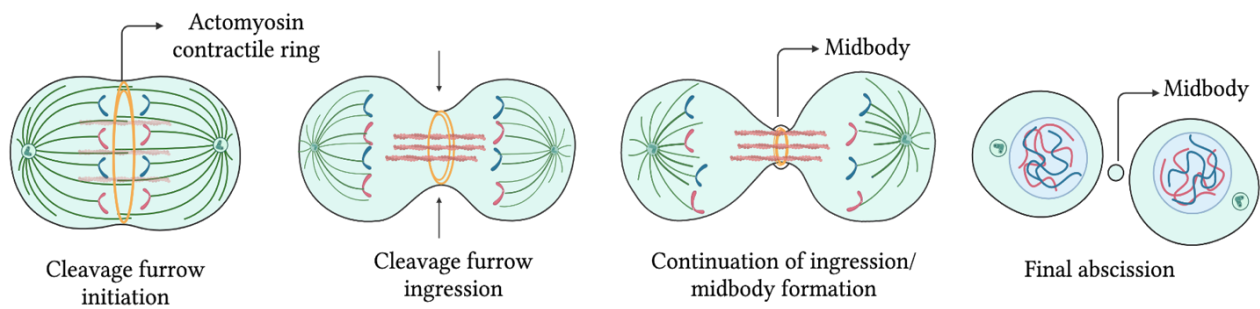


**Figure 1.2. Schematic representation of Cytokinesis-** Cleavage furrow initiates upon contraction of actomyosin contractile ring. The contraction continues until there is an intracellular bridge between two dividing cells that contain the midbody. Dissociation of the contractile ring is required for the final separation. The midbody can be asymmetrically inherited by one daughter cell or released in the extracellular environment.<sup>87</sup> The figure was created by the *BioRender* tool.

### 1.6.1 Some Aspects of Molecular Mechanisms Underlying the Regulation of Cytokinesis:

During cytokinesis, an actomyosin contractile ring is required to constrict the membrane at the site of the nascent furrow and partition the cytoplasm of the dividing cells. Together with the central spindle microtubules, they comprise the key elements of the cytokinesis regulation machinery. By recruiting the RhoA regulators at the centralspindlin complex, the central spindle microtubules contribute to this regulation<sup>88</sup>. RhoA, commonly referred to as a master regulator of cytokinesis, regulates the actomyosin ring assembly by indirectly promoting the nucleation of unbranched actin filaments and activation of myosin II<sup>89,90</sup>. The myosin-II filaments slide actin filaments and provide the required motor activity, facilitating the driving force for the contraction similar to what takes place in muscle sarcomeres<sup>91</sup>.

The spatiotemporal activation of RhoA is crucial to ensure a reliable separation. Like most Rho GTPases, RhoA constantly cycles between active GTP-bound to inactive GDP-bound states<sup>92,93</sup> (Fig1.3). This switch continually takes place at the equatorial plasma membrane upon the onset of cytokinesis. It is facilitated by the RhoA activators, guanine-nucleotide exchange factors (GEFs), that catalyze the exchange of GDP for GTP and RhoA inactivators, GTPase activating proteins (GAPs), that enhance the intrinsic GTP hydrolysis rate of the GTPase<sup>89,94</sup>. While the epithelial cell transforming 2 (Ect2) protein is an upstream activator of RhoA during cytokinesis<sup>90</sup>, male germ cell Rac GTPase-activating protein (MgcRacGAP) is a major GAP constraining the RhoA concentration at the cleavage furrow facilitating the cytokinesis<sup>95</sup>. In contrast, MgcRacGAP also forms a complex with Ect2 to activate RhoA at earlier cytokinesis, thus promoting the process by indirect RhoA activation<sup>96,97</sup>.

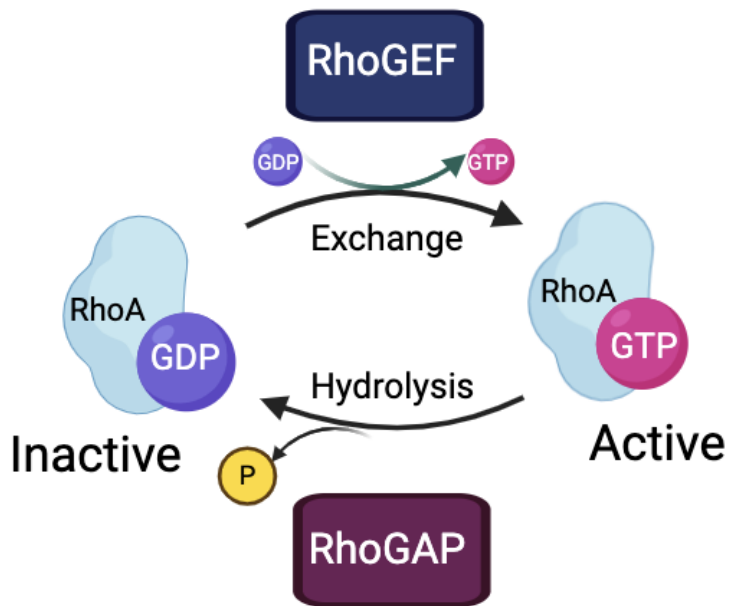


**Figure 1.3. Schematic representation of the RhoA GTPase molecular switch, along with the regulators.** RhoA continually switches between active GTP-bound and inactive GDP-bound states. This cycling is driven by guanine-nucleotide exchange factors (GEFs), which exchange GDP for GTP, and GTPase activating proteins (GAPs), which increase the rate of GTP hydrolysis.<sup>92</sup> The figure was created by the *BioRender* tool.

A novel study by Zanin et al. identified MP-GAP (also known as ARHGAP11A) as the primary GAP that dampens RhoA activation at the cell cortex during cytokinesis<sup>98</sup>. They showed MP-GAP depletion in HeLa cells is characterized by cortical-hypercontractility and protrusions, particularly during mitosis and cytokinesis, a pattern that can be suppressed by inactivating RhoA. Importantly, a significant portion of depleted cells exhibited late cytokinesis failures. In this study, the pattern of Ect2 localization at the spindle midzone was not altered in MP-GAP-depleted cells, suggesting MP-GAP inactivates RhoA rather than affecting its upstream activator<sup>98</sup>. A subsequent study identified p190RhoAGAP-A (ARHGAP35) as a Rho GAP downregulating RhoA-GTP in the cytokinetic furrow, demonstrated by cytokinesis failure and multinucleation upon p190 depletion in HeLa cells<sup>99</sup>. While it is undisputed that all these studies provide valuable data to comprehend the signaling pathways engaged in cytokinesis, they also manifest the complexity of the regulatory mechanisms, underscoring the requirement for more studies to reveal the intricate interplay and balance that govern those processes.

### **1.6.2 Insights into the Role of PKC $\epsilon$ in the Cytokinesis Regulation:**

While the activation of RhoA promotes the ring formation and subsequent contractions, the inactivation of RhoA and dissociation of the contractile ring is essential for successfully completing abscission<sup>100</sup>. Until recently, the mechanism underlying the reversion of the cytokinesis contractility was not well understood. Even though many activators and inactivators for RhoA have been discovered, the upstream regulators controlling these mechanisms and the redundant pathways that can compensate for each other have yet to be unraveled. One of the most prominent findings in the field has been achieved by Peter.J. Parker et al., introducing PKC $\epsilon$  as a key component of the signaling pathway for abscission control<sup>88</sup>. Those studies were initiated by

the finding that PKC $\epsilon$ -deficient MEFs were characterized by delayed cytokinesis, which was recovered by re-expression of wild-type PKC $\epsilon$ . In addition, an acute knock-down of PKC $\epsilon$  in HeLa cells resulted in the same cytokinesis defect. Utilizing an approach introduced in the Shokat laboratory<sup>101</sup>, the inhibited form of PKC $\epsilon$  also exhibited similar cytokinesis failure in human embryonic kidney (HEK) 293 cells. However, there were variations for different cell lines in the severity of the phenotype and the time required for cells to recover, suggesting that cells differentially rely on PKC $\epsilon$ . Notably, the distribution of the PKC $\epsilon$  was also affected upon inhibition, with inclusive cytosolic localization for the active state and robust accumulation around the contractile ring when inactivated, highlighting a key role for PKC $\epsilon$  in abscission control by regulating a potential actor in the furrow. Interestingly, failure in cytokinesis after the PKC $\epsilon$  inhibition was associated with prolonged localization of activated RhoA at the midbody and delayed dissociation of the actomyosin ring. Accordingly, a number of mechanisms were hypothesized to be responsible for the extended presence of RhoA, including direct phosphorylation of RhoA, indirect inactivation of GEFs, and activation of GAPs. While some specific GEF and GAP candidates were proposed, including ECT2, GEF-H1, MgcRacGAP, and p190 RhoGAP, it was mentioned that more investigations are required to identify an established pathway. Nevertheless, more studies revealed several roles for PKC $\epsilon$  in regulating cytokinesis through other signaling pathways<sup>100</sup>.

PKC $\epsilon$  was demonstrated to translocate to the furrow and facilitate the final abscission through its interaction with 14-3-3 proteins. Three phosphorylation sites have been linked to this interaction, and the mutations that hinder the phosphorylation or the 14-3-3 binding result in incomplete cytokinesis and cell cycle arrest. This can result in the formation of binucleated cells followed by aneuploidy state, highlighting the significance of this regulatory pathway in

carcinogenesis<sup>100</sup>. DNA catenation refers to the attachment of sister chromatids during anaphase and later stages of mitosis and can lead to chromosome aberrations if it remains unresolved. In the case of DNA catenation in cleavage furrow, cytokinesis is delayed by the Aurora B abscission checkpoint until the DNA retention is completely resolved. The S227 phosphorylated Aurora B is proposed to activate TopoII $\alpha$ , enhancing the decatenation and facilitating the checkpoint exit. Accordingly, PKC $\epsilon$  was shown to play an essential role in the checkpoint release by phosphorylating Aurora B S227 at the midbody, thus inhibiting an abscission failure and subsequent binucleation<sup>102,103</sup>. Furthermore, a catalytic PKC $\epsilon$ -dependent genome protective pathway was described in which SERPINE1 mRNA Binding Protein 1 (SERBP1), a PKC $\epsilon$  substrate, is pivotal for successful chromosome segregation and cell division<sup>104</sup>. Although the above studies have deepened our knowledge of the PKC $\epsilon$  functions in successful cell division, the exact mechanism for the contribution of PKC $\epsilon$  to the abscission through RhoA inactivation remains unclear, suggesting further studies are needed to elucidate this regulatory pathway.

### **1.6.3 Findings about the Contribution of PKD3 to the Cytokinesis Regulation:**

A set of experiments has been previously implemented by our group to elucidate the consequences of PKD3 depletion on cells, aiming to establish defined isoform-specific *in-vivo* functions for PKD3. For this purpose, PKD3-deficient MEFs were generated, which were characterized by reduced proliferation rates upon immortalization. Intriguingly, they also demonstrated cytokinesis failures similar to those observed with PKC $\epsilon$ -deficient MEFs, resulting in an increased binucleation phenotype<sup>105</sup>. It should be highlighted that binucleation can lead to chromosomal instability and subsequent development of cancer<sup>106</sup>, indicating the potential role of PKD3 in carcinogenesis. Interested in filling the knowledge gap for a defined signaling pathway

involving PKC $\epsilon$  and RhoA, and whether PKD3 acts in between, subcellular localization of PKD3 during the cell cycle was probed using exogenously expressed GFP-tagged PKD3 in wild type (wt) MEFs (unpublished data). Of note, PKD3-GFP was localized to the furrow during telophase, with a remaining signal at the midbody. The specificity of the PKD3 function responsible for this phenotype was confirmed by the rescue experiment of exogenous PKD3 expression in PKD3-deficient MEFs and by dominant negative expression in wt-MEFs. Interestingly, this localization was shown to be PKC $\epsilon$  dependent, and reintroduction of PKD3 rescued the aberrant cytokinesis, suggesting that PKD3 is sufficient to re-establish furrow localization, but only in a context where PKC $\epsilon$  is functional. This localization was demonstrated to be isoform-specific, as neither PKD1 nor PKD2 could compensate for PKD3's function (unpublished data). The prominent observation of the study linking PKD3 to the mentioned PKC $\epsilon$  pathway is that PKD3 and RhoA co-localized during cytokinesis, with prolonged RhoA activity in PKD3-deficient MEFs. But how might PKD3 regulate RhoA? While it can be postulated that RhoA is a direct downstream substrate of PKD3, it is also important to investigate the established RhoA-GAPs, which may account for the extended RhoA activation/furrow localization. Based on the findings about the role of MP-GAP in cytokinesis failure and RhoA inactivation, it was hypothesized to be the potential RhoA regulator that might act downstream of PKD3. Interestingly, MP-GAP was observed to co-localize with RhoA during the later stages of cytokinesis, but it was not present in the early furrow, suggesting the expected time-point when the RhoA starts to be inactivated before the final abscission. Given the possibility that PKD3 may interact with MP-GAP to regulate RhoA and that there are other GAPs functioning as RhoA inactivators, more experiments are required to unravel the specific interactions and regulatory mechanisms involved and to identify the precise role of PKD3 in this

context. Together with previously published data on PKD3, these intracellular localizations and potential functions comprise the basis of this project.

## 1.7 The Project Rationale:

Since PKD family members were identified, the knowledge about their isoform-specific functions and mechanisms of action has expanded. Nevertheless, there are a limited number of studies focusing on isoform-specific functions of PKD3. To elucidate information about the fundamental roles of this member of the PKD family in regulating cellular processes, PKD3-deficient mice were previously generated by the Leitges group. Two important phenotypic alterations were observed after immortalizing MEFs originating from those mutant mice. First, there was a reduction in their proliferation rate, and second, a significant increase in the number of binucleated cells up to 40% was observed (unpublished data). Since binucleation is an outcome of aberrant cytokinesis, it was proposed that PKD3 might function in the pathways that are linked to facilitating a successful division of the cytoplasm. Saurin et al. had previously shown that PKC deficiency led to increased binucleation and that PKC participates in the completion of cytokinesis in HeLa cells by regulating the dissociation of contractile ring and final abscission.<sup>88</sup> To further analyze the role of PKD3 in this context, an exogenous GFP-tagged PKD3 was used to study its localization during cytokinesis. Using fluorescent microscopy, it was demonstrated that active PKD3 accumulates in the cleavage furrow during cytokinesis, where it colocalizes with RhoA. In addition, western blotting experiments revealed that the presence of RhoA was prolonged for 2.5 hours more than the time in intact cells, an increase which was also shown in PKC-deficient cells. Interestingly, MP-GAP, which is a RhoA GAP shown to downregulate the RhoA activity and facilitate cytokinesis, was demonstrated to colocalize with RhoA at late cytokinesis. Considering the function of PKC in activating PKDs in many cellular pathways, it was hypothesized that **PKD3 might interact downstream of PKC and upstream of MP-GAP to regulate cytokinesis in the**

**context of immortalization.** A summary of the proposed signaling pathway is illustrated in [Fig 1.4.](#)

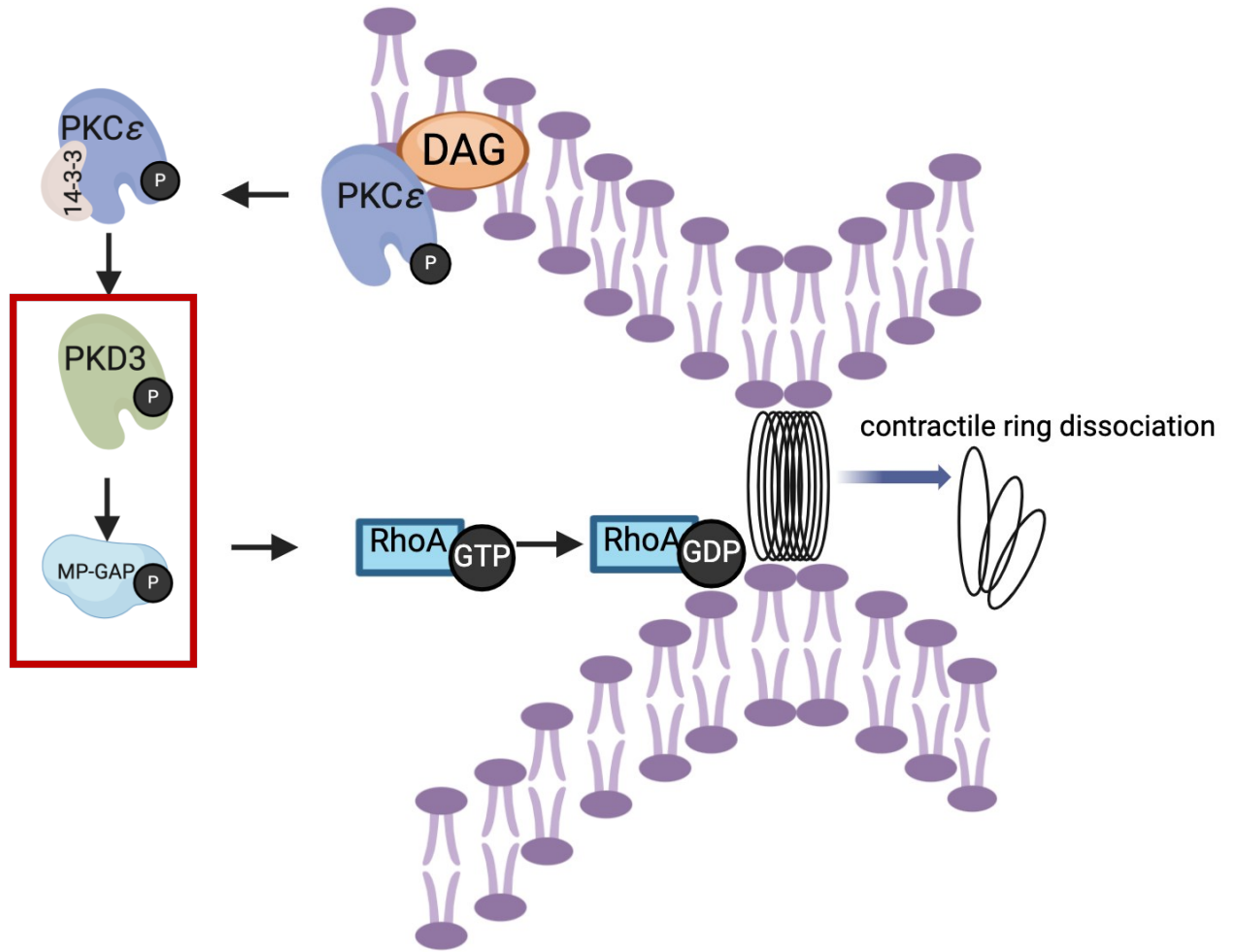


**Figure 1.4 Schematic representation of the cleavage furrow of a dividing cell, along with PKC $\epsilon$  signaling pathway regulating the contractile ring dissociation and final abscission.** PKC $\epsilon$  is activated by DAG at the cell membrane and is demonstrated to translocate to the furrow and facilitate the final abscission through its interaction with 14-3-3 proteins<sup>100</sup>. PKD3 might interact with the MP-GAP, a RhoA inactivator, to facilitate the abscission process downstream of PKC $\epsilon$ , which constitutes the hypothesis of this project. The hypothesized signaling pathway is highlighted in red border. The figure was created using the *BioRender* tool.

### **1.7.1 The methodological Approach:**

Given the increased binucleation phenotype observed upon PKD3 deficiency and that binucleation serves as an initial step in cancer development, studying the interplay of PKD3 in cytokinesis is crucial in the field of carcinogenesis research. Fluorescent tagging has been extensively used as a versatile tool to study protein localization and signaling pathways. In addition, fluorescence resonance energy transfer (FRET) is the most widely employed technology for studying the dynamics of protein kinases<sup>107</sup>. This technique is based on non-radiative energy transfer between two biomacromolecules and is significantly useful to study interactions owing to its inherent robust distance dependence.<sup>108</sup> In this regard, a project was designed to tag PKD3 and MP-GAP with fluorescent proteins to trace their dynamics during cytokinesis by fluorescent microscopy, providing detailed insights into the localization of these two proteins. Furthermore, the project's goal was to utilize FRET (Fig1.5) to determine if a potential interaction exists between the two proteins, with the ultimate aim of introducing a novel signaling pathway as an approach to cancer therapeutics.

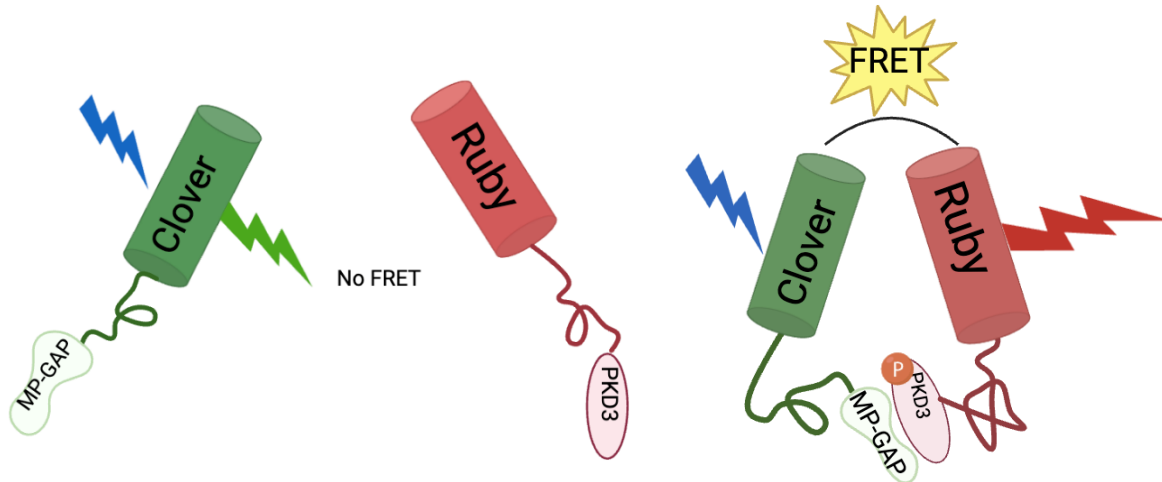


**Figure 1.5. Schematic representation of FRET between two fluorescent proteins (FPs).** This figure illustrates the mechanism of Fluorescence Resonance Energy Transfer (FRET) between two fluorescent proteins (FPs). The proteins under study, MP-GAP and PKD3, are labeled with FPs that function as FRET pairs, performing as a donor and acceptor. FRET occurs only if the proteins are in very close proximity (typically 1-10 nm), enabling the energy transfer from the donor to the acceptor, which indicates a potential interaction between the proteins. In this schematic: The donor FP, Clover (green), emits energy upon excitation. The acceptor FP, mRuby2, (red) excites by the emitted energy if positioned sufficiently close to the donor, re-emitting a different wavelength. This is an energy transfer, and its efficiency highly depends on the distance between FRET pairs. The occurrence of FRET can serve as an interaction indicator for the studied proteins. The cartoon was created by the *BioRender* tool.

## 2-Materials & Methods

### 2.1 Cloning:

The pcDNA3.1 vector containing mRuby2 and the pcDNA3.1 vector containing Clover were purchased from Addgene, while the plasmids encoding PKD3 and MP-GAP were provided by GenScript. Primers were designed to amplify PKD3 and MP-GAP encoding sequences with polymerase chain reaction (PCR). This enabled harvesting multiple copies of the fragments for subcloning and introducing restriction sites flanking the intended fragment for the final cloning. The PKD3 encoding sequence was amplified, with the restriction site BamHI at the 5'end and HindIII at the 3'end. The MP-GAP encoding fragment was also amplified, with restriction site BamHI at the 5'end and BstXI at the 3'end. Next, they were subcloned into the pCR 2.1-TOPO vector using the TOPO-TA cloning kit to obtain single and clean inserts, ensuring the homogeneity and purity of the DNA fragments used in the ligation. Last, the inserts were excised and ligated into the mRuby2 vector for PKD3 and into the Clover vector for MP-GAP. The cloning resulted in successfully generating mRuby2-tagged PKD3 and Clover-tagged MP-GAP. The cloning approach is described in brief in [Figure 2.1](#).

#### 2.1.1 Designing Primers:

Key factors were considered when designing the primers, including length of primers, Kozak sequence, specificity, melting temperature ( $T_m$ ), and GC content by the National Center for Biotechnology Information (NCBI) primer designing tool. Each primer included nucleotides corresponding to the recognition sites of the restriction enzymes used for subsequent cloning. [Table 2.2](#) provides a list of primers used for cloning experiments in this project.

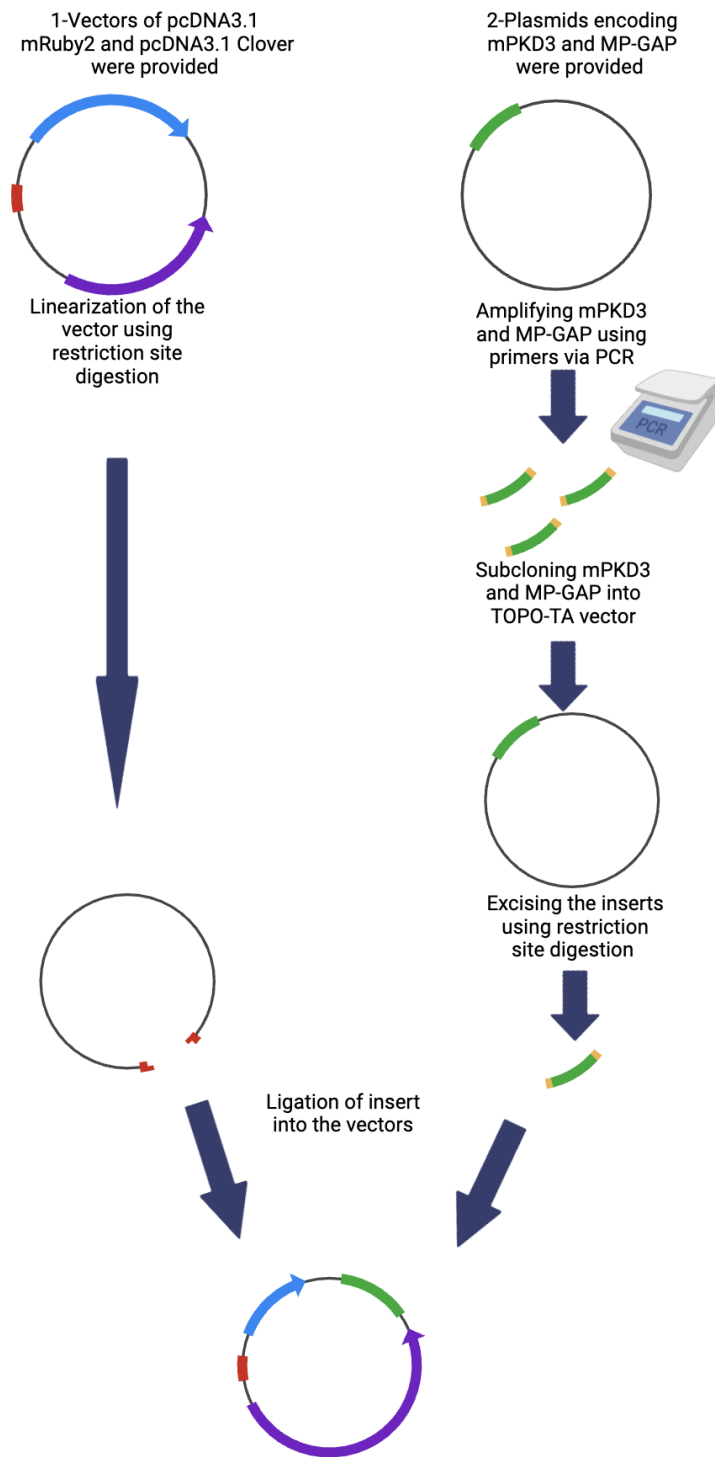


**Figure 2.1. A flowchart representing cloning steps in brief.**

**Table 2.1. List of primers used for the cloning experiments.**

| <b>Construct</b>                          | <b>Orientation</b> | <b>Sequence 5'to3'</b>                  | <b>Restriction Site, T<sub>m</sub>, and GC Content</b> |
|---|--------------------|---|--|
| <b>PKD3-mRuby2<br/>in pcDNA 3.1</b>       | <b>5'</b>          | GAAGCTTGCCACC <b>ATG</b> TCTGCAAATAATTC | HindIII T <sub>m</sub> 63°C, GC 45%                    |
|   | <b>3'</b>          | CGGATCCGGAGGATGCTCCTCCATTGTCGTC         | BmHI T <sub>m</sub> 69°C, GC 63                        |
| <b>MP-GAP-Clover<br/>in pcDNA 3.1</b>     | <b>5'</b>          | GCTCGGATCCGCCACC <b>ATG</b> TGG         | BamHI T <sub>m</sub> 66°C, GC 68%                      |
|   | <b>3'</b>          | CCAGCACACTGGCCTTATCGTCGTCATC            | BstXI T <sub>m</sub> 66°C, GC 57%                      |
| <b>PKD3-mRuby2<br/>in psLenti100092</b>   | <b>5'</b>          | GAATCCGCCACC <b>ATG</b> TCTGCAAATAATTC  | EcoRI T <sub>m</sub> 63°C, GC 47%                      |
|   | <b>3'</b>          | CTCGAGCGGCCGCTTGTACAGCTCGTCC            | NotI, T <sub>m</sub> 71°C, GC 68%                      |
| <b>MP-GAP-Clover<br/>in psLenti100092</b> | <b>5'</b>          | GCTCGGATCCGCCACC <b>ATG</b> TGG         | BamHI, T <sub>m</sub> 66°C, GC 68%                     |
|   | <b>3'</b>          | CTCGAGCGGCCGCTTGTACAGCTCGTCC            | NotI, T <sub>m</sub> 71°C, GC 68%                      |

### 2.1.2 PCR:

PCR method was used to amplify the sequence coding for PKD3, MP-GAP, and also PKD3-mRuby2 and MP-GAP-Clover. The PCR mixture was prepared by adding the template DNA and primers to the PCR master mix based on the provider's protocol (Platinum SuperFi II PCR from Invitrogen by Thermo Fisher Scientific-12368010). The PCR cycling conditions are described in [Table 2.2](#). After amplification, another PCR was implemented to add an 'A' nucleotide to the 3' end of the products, in order to facilitate the next subcloning steps. For this purpose, 10 µl of PCR product was mixed with 10 µl of a *Taq* enzyme. Those steps are also mentioned below in [Table 2.2](#).

**Table 2.2 - Left- PCR cycles for PKD3, MP-GAP, PKD3-mRuby2 and MP-GAP-Clover  
Right- PCR cycles for Adding A-overhangs**

| Steps | Temp   | Time<br>mm:ss |
|-------|--------|---------------|
| 1     | 98.0°C | 00:30         |
| 2     | 98.0°C | 00:10         |
| 3     | 60.0°C | 00:10         |
| 4     | 72.0°C | 02:00         |
| 5     | 72.0°C | 05:00         |
| 6     | 4.0°C  | ∞             |

x32

| Steps | Temp   | Time<br>mm:ss |
|-------|--------|---------------|
| 1     | 95.0°C | 02:00         |
| 2     | 95.0°C | 00:30         |
| 3     | 60.0°C | 00:30         |
| 4     | 70.0°C | 02:00         |
| 5     | 70.0°C | 10:00         |
| 6     | 4.0°C  | ∞             |

x19

### 2.1.3 Subcloning into TOPO-Vector:

The amplified segments were put through another PCR step using a *Taq* polymerase enzyme (JumpStart Taq ReadyMix (Sigma Aldrich, P2893)) to add 3' A-overhangs to the products. Then, the segments were subcloned into pCR 2.1-TOPO vector (TOPO-TA cloning kit from Invitrogen by Thermo Fisher Scientific-45-0641) vectors, following the protocols specified by the manufacturer. Those vectors contain a cloning site with a 3' T-overhang, which is complementary to the 3' A-overhangs found on the PCR products. The subcloned plasmids were used to transform competent bacteria by heat shock transformation.

#### **2.1.4 Heat Shock Transformation and Bacterial Culture:**

For DH5 $\alpha$  bacteria, the time was 1 minute and 45 seconds at 42°C, followed by 10 minutes on ice. For the One Shot Top 10 bacteria (from Invitrogen by Thermo Fisher Scientific-40-4010), the time was 30 seconds at 42°C and 30 minutes on ice. The transformed bacteria were then inoculated to Lysogeny Broth (LB) agar plates containing the antibiotic, which aligned the antibiotic resistance of the plasmids, and incubated shaking at 245 rpm overnight at 37°C in a bacterial culture incubator. The blue/white screening method was executed by adding 80  $\mu$ l 5-Bromo-4-chloro-3-indolyl- $\beta$ -D-galactopyranoside (X-gal) + 40  $\mu$ l isopropyl  $\beta$ -D-1-thiogalactopyranoside (IPTG) to the plates at the time of incubation. To identify the white colonies with the correct plasmids, some were randomly chosen and inoculated in 2ml of LB broth with the proper antibiotics. For each chosen colony, a backup was taken on LB agar plates (LB Broth, Miller by Fisher bioreagents-BP1426-2 and LB Broth with agar, Lennox by SIGMA-AIDRICH-L2897). After an overnight incubation, the plasmids were extracted for further analysis.

#### **2.1.5 Plasmid Extractions:**

A Miniprep kit was used to extract plasmids from several randomly picked colonies for screening, following the protocols specified by the manufacturer (GeneJET Plasmid Miniprep kit by Thermo Scientific- K0503). In some cases, dirty miniprep was performed to isolate DNA without a kit. In this method, the bacterial culture was centrifuged at 14000 revolutions per minute (rpm) for 30 seconds, and the supernatant was discarded, leaving a small volume behind for the bacterial pellet to be dissolved. Amount of 300 $\mu$ l TENS (0.1M NaOH in Tris-HCl containing EDTA.Na<sub>2</sub> (TE) buffer and SDS (sodium dodecyl sulfate–polyacrylamide)) buffer was used as lysis buffer per each microtube, flipped, and vortexed. Next, 150 $\mu$ l of sodium acetate (NaOAc) was added to neutralize the buffer and precipitate DNA, flipped, and vortexed, followed by 10

minutes of centrifugation at 14000 rpm. Then, 95% ethanol was added and they were centrifuged for another 10 minutes at the same speed. Subsequently, the same step was repeated with 70% ethanol for 5 minutes. The ethanol was discarded, and extracted DNA was dissolved in 50µl of TE + RNase buffer. All the extracted DNAs were digested with restriction site enzymes to reveal if they aligned with the expected pattern for each plasmid. A midiprep kit was used to isolate the plasmids from colonies that had confirmed restriction site analysis patterns, following the protocols specified by the manufacturer (QIAGEN Plasmid Midi Kit-12143).

### **2.1.6 Restriction Site Digestions:**

To digest the plasmids, a master mix was prepared to contain double distilled (dd) water, enzymes, plasmids, and proper buffer with which the enzymes have their maximum function and minimum star activity, to a 1:10 ratio. All the enzymes and buffers were from New England BioLabs (NEB). The mixture was incubated at 37°C for a duration varying between 2 to 5 hours depending on the experiments, plasmids, and enzymes. To reveal the outcome of digestions, a portion of them were subjected to gel electrophoresis, subsequently visualized by the Analytikjena device (Analytikjena, Upland, CA, USA).

### **2.1.7 Gel Electrophoresis:**

When the plasmids were fully digested by the proper restriction site enzymes to cut the segment out, they were mixed with gel loading buffer (by New England BioLabs-B7024A and/or BlueJuice by Invitrogen-10816015) and loaded into the wells in the casted agarose gels. To prepare the 1% agarose gel, 100 mg of agarose powder (by Fisher bioreagents-BP1356) was dissolved in 100 ml of 1x TAE buffer (Tris-acetate-EDTA) with 2µl of nucleic acid stain (GelRed by Biotium-41003) and poured into the gel casts to cool down and solidify. After loading the DNA, the

electrophoresis was performed at the voltage of 110-120V. The duration varied depending on the size of the fragments, and it was between 20 and 40 minutes to get distinctive bands.

### **2.1.8 Gel Extraction and DNA Purification:**

After separating the DNA bands by gel electrophoresis, the gel containing the inserted segment was cut out using a scalpel under ultraviolet (UV) light and transferred to a microtube. The DNA was extracted from the gel with the Quick Gel Extraction kit following the protocols specified by the manufacturer (Invitrogen by Thermo Fisher Scientific- K210012).

### **2.1.9 Ligation:**

The vectors were linearized using the restriction site enzymes that flanked the inserts and were dephosphorylated by phosphatase enzyme using Antarctic Phosphatase Reaction Buffer (by NEB-B0289S). The extracted inserts were ligated into the linearized vectors by adding them to the master mix with T4 DNA Ligase (by NEB-M0202M), 10X buffer for the ligase (by NEB-B0202A), and dd water. After overnight incubation at 16 °C, the ligated plasmids were transformed into competent bacteria by heat shock transformation, and the next steps were performed as previously described to find the right colony. The colonies from backup plates were re-inoculated to broth medium to harvest large replicants of plasmids by midiprep (QIAGEN Plasmid Midi Kit- 12143).

## **2.2 Cell Culture:**

Cells were housed in a humidified cell culture incubator at 37°C in a 5% carbon dioxide (CO<sub>2</sub>) atmosphere. The cell lines used in this study including Chinese hamster ovary (CHO), COS7, and HEK 293 were provided by ATCC, and the HeLa Kyoto cells were a kind gift from Dr. Tiaple's lab at the University of Toronto. The H2B::mCherry expressing HeLa Kyoto cells were

brought to the lab as a kind gift from Dr. D'Avino's lab at the University of Cambridge. The cell culture medium used for growing the cells was high-glucose Dulbecco's modified eagles' medium (DMEM) (D5796-SIGMA Life Science) supplemented with 10% fetal bovine serum (FBS by HyClone-SH30396.03, heat-inactivated), minimum essential medium (MEM) non-essential amino acids (by Cytiva- SH40003.01), Penicillin Streptomycin (15070-063, Gibco), and  $\beta$ -mercaptoethanol (BME, (FisherScientific, Gibco, 21985023)). Cells were plated in 100mm or 6-well plates as necessary. For splitting and replating cells, diluted 0.5% Trypsin-EDTA (by Gibco- 15400-054) was used as the cell-dissociating agent, and phosphate-buffered saline (1x PBS, Cytiva, SH30256.01) was used for washing. The Trypsin exposure time was 8-10 minutes, depending on the cell type.

### **2.3 Transfection:**

For transfection experiments, cells were plated on coverslips to achieve 60-80% confluency. On the day of transfection, the medium was aspirated and replaced by a transfection mixture, which was prepared using different amounts of DNA and reagents. The transfection buffer was commonly Reduced Serum Medium OPTI-MEM (by gibco-31985-062). The electroporation was performed by the Neon Transfection System 10  $\mu$ L Kit (Life Technologies Inc., Burlington, ON). In addition, Lipofectamine Reagent (Invitrogen by Thermo Fisher Scientific-18324-012) and FuGENE 4k Transfection Reagent (by Promega-E5911) were also used for chemical transfections. All the experiments were conducted according to the protocols and ratios recommended by the manufacturer. For calcium phosphate transfection, HEPES (4-(2-Hydroxyethyl)piperazine-1-ethane-sulfonic acid) buffered saline (HBS) and  $\text{CaCl}_2$  were prepared in our lab and filtered to be sterilized. Before transfection, cells were seeded on 24 well plates to reach almost 70 % confluency. On the day of transfection, 10 $\mu$ g DNA was diluted in ddH<sub>2</sub>O and volumed to 438 $\mu$ l,

followed by adding 62µl 2M CaCl<sub>2</sub> to a final volume of 500µl. Then 500µl of 2x HEPES was added dropwise while being vortexed. After 2 minutes, the mixture was poured dropwise on the medium, and the cells were incubated for 2-3 days.

## **2.4 Cell Cycle Synchronization:**

Cells were plated and grown to reach 70% confluency. For the double thymidine followed by nocodazole synchronization, cells were first treated with thymidine (by SIGMA-T9250) with 200mM in PBS, released from arrest after 16h by 3x PBS wash, and grown for 8h in normal medium, followed by the same steps for the second thymidine block. Then, they were treated with 100 ng/mL nocodazole (by SIGMA-M1404) and released after 10h by 3x PBS wash. Thymidine is a chemical compound that interferes with DNA synthesis, and nocodazole perturbs microtubule polymerization. Cells were fixed with 4% paraformaldehyde (PFA) 110 minutes post-release to harvest cells in cytokinesis. The single nocodazole treatment was the same but without previous thymidine exposure. All the release steps were accomplished by gentle room temperature PBS washing three times, followed by adding prewarmed DMEM. The effects of drugs were alleviated by the washing steps, enabling the cells to recover normal cycle progression.

## **2.5 Immunostaining:**

Cells were plated on 15mm round coverslips. (CELL TREAT-229172) Upon 70-90% confluency, the media was aspirated, and live cells were washed 3x with room temperature PBS, followed by fixation with 4% PFA for 10 minutes. Then, cells were washed 3x with PBS, each time for 5 minutes. Next, cells were incubated in the PBT blocking/permeabilization buffer (PBS, 0.5% [v/v] Triton X-100 (by Fisher bioreagents BP151), and 5% [w/v] BSA (Bovine Serum Albumin-SIGMA-A9647)) for 1 h at room temperature, and then incubated overnight (16 hours)

with primary antibodies at 4°C. The primary antibodies were diluted in PBT (PBS, 0.1% [v/v] Triton X-100 and 1% [w/v] BSA). The next day, cells were washed twice with PBT, each for 5 minutes, incubated with the secondary antibody (Rabbit Secondary Antibody, Alexa Fluor™ 488), and fluorescent-conjugated phalloidin (Alexa Fluor 647 phalloidin-A22287) diluted in PBT with the concentration of 0.5µl 400x stock solution in 200µl for one hour. Phalloidin is a toxin that specifically binds to F-actin. Finally, cells were washed 3x in PBS, and coverslips were mounted on the slides (United Scientific Supplies-MSLF01) once dried. When using mounting media without DAPI (SouthernBiotech-0100-01), cells were stained with 4',6-Diamidino-2-Phenylindole (DAPI) for 15 minutes before being mounted. Most slides were prepared using mounting media containing DAPI (Fluoroshield by Abcam-AB104139), and some slides were prepared using Hoechst for DNA staining. [Table 2.3](#) provides a list of antibodies used in the immunostaining experiments.

**Table 2.3. List of primary and secondary antibodies used in immunostaining.**

| <b>Target</b> | <b>Host Species</b> | <b>Antibody Type</b>   | <b>Concentration</b> | <b>Vendor/Cat#</b>                    |
|---------------|---------------------|--|----------------------|---------------------------------------|
| PKD1,2,3      | Rabbit              | PKD1/2/3/PKCmu Polyclonal Antibody                                   | 1:250                | ThermoFisher Scientific<br>PA5-99550  |
| pPKD1,2,3     | Rabbit              | Phospho-PKD1/2/3/PKCmu (Ser738, Ser742) Polyclonal Antibody          | 1:500                | ThermoFisher Scientific<br>PA5-104996 |
| Rabbit        | Goat                | Rabbit IgG (H+L) Cross-Adsorbed Secondary Antibody, Alexa Fluor™ 488 | 2mg/ml               | ThermoFisher Scientific<br>A-11008    |

## **2.7 Confocal Microscopy:**

The acquisition of images was performed by Zeiss LSM 900 unless otherwise stated. It is a confocal microscope run by Zeiss Efficient Navigation (ZEN) software and equipped with Plan-Apochromat 63x/1.40 Oil DIC f/ELYRA and PApo 20X/0.8 objectives. The intensity and sensitivity of lasers were adjusted to visualize the best signal-to-noise ratio with minimized backgrounds. Depending on the experiments, the following lasers were used to excite the fluorophores: DAPI/Hoechst 33342 (405 nm laser); Alexa Fluor 488 for green fluorophore including EGFP, Clover, and conjugated secondary antibody, Alexa Fluor 568 for mRuby2 and mCherry, and Alexa Fluor 647 for phalloidin. All images were taken in a single optical section. For post-processing purposes, images were adjusted for brightness and contrast and pseudocolored, when necessary, using ZEN software.

## **2.8 Live Imaging:**

The live imaging experiments were conducted with the Zeiss LSM 900 microscope using a 20x objective. Images were taken at 5-minute intervals with multi-channel image acquisition. The device was equipped with features to facilitate uninterrupted cell growth and proliferation, including a glass beaker as a humidifier linked to a chamber with 37°C temperature and 5% CO<sub>2</sub>.

## 3-Results

### 3.1 Generation of Tools to Investigate the Localization of PKD3 and MP-GAP During Cytokinesis/Cloning

To study the localization and dynamics of PKD3 and MP-GAP, a set of constructs was established aiming to label the proteins, enabling us to track them during cytokinesis by fluorescent microscopy. Accordingly, FPs were C-terminally fused to the encoding DNA. To characterize a potential interaction with FRET technology in the future, the fluorescent proteins were chosen to be FRET pairs (Fig1.5). The mRuby2 and Clover are high-efficiency established FRET pairs used in many studies<sup>109</sup>, which were used in this project to label PKD3 and MP-GAP, respectively (Fig3.1.A). The map of the created plasmid constructs is shown in (Fig3.1.B). More details about cloning are elaborated on in the materials and methods section. The cloning accuracy of MP-GAP-Clover was validated using Sangar sequencing and restriction site analysis (Fig3.1.C). Furthermore, the accuracy of cloning for PKD3-mRuby2 was demonstrated by Sangar sequencing, restriction site analysis (Fig3.1.C), and, later in this study, by immunostaining (Fig.S6.1). As shown in the immunostaining experiment, anti-PKD antibody staining overlaps red signals in PKD3-mRuby2 expressing cells.

Once protein labeling was accomplished, the aim was to generate cell lines that stably express the PKD3-mRuby2 or MP-GAP-Clover using the lentivirus method. For this purpose, another cloning experiment was conducted to clone the PKD3-mRuby2 and MP-GAP-Clover plasmids into a lentiviral vector, followed by transfection experiments. All the steps of the cloning strategy were the same as described for the previous constructs except for the designed primers and restriction sites. For MP-GAP-Clover EcoRI at the 5' and NotI at the 3', and for PKD3-

mRuby2, BamHI at the 5' and NotI at the 3' were introduced, respectively. The cloning approach is the same as described previously in brief in Fig2.1, and the map of the created constructs is shown in Fig3.1.B. The accuracy of cloning for these constructs was verified by sequencing and restriction site analysis (Fig3.1.C). After stable transfection, cells were kept under antibiotic selection for several weeks to harvest a population of cells that integrated the plasmids into their genome and stably expressed the transfected proteins along with the antibiotic resistance protein. However, no expressing cells survived the recommended antibiotic concentration despite trials for three different cell lines (HeLa, CHO, and HEKs). Interestingly, some cells survived higher antibiotic concentrations compared to the non-transfected control cells, in which no signal was detected for FPs. It was postulated that this could result from protein cleavage, which led us to design new primers and utilize the plasmid internal ribosome entry site (pIRES) cloning strategy for stable transfection.

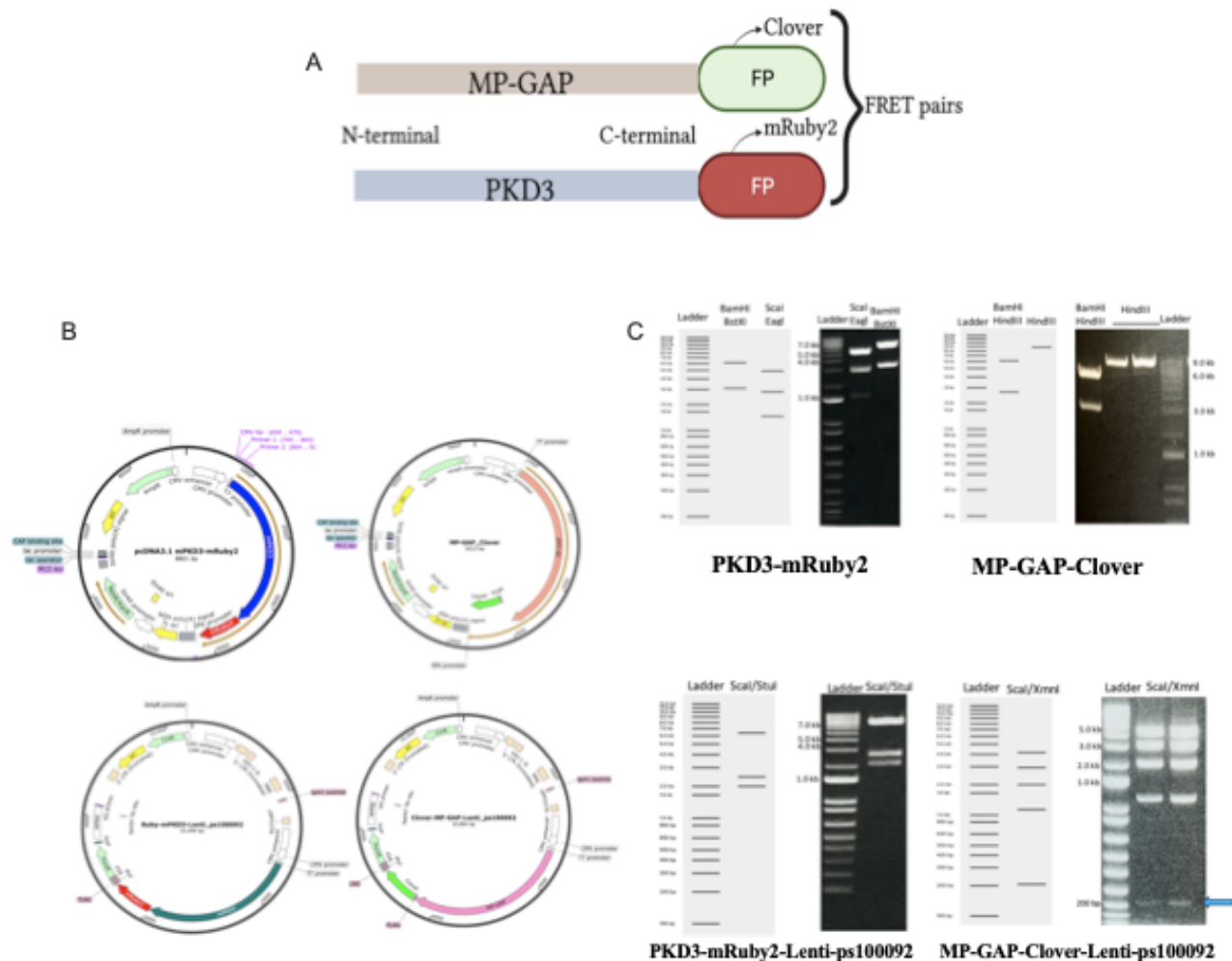


**Figure 3.1. A- Schematic representation of the project's cloning strategy.** This figure depicts the cloning strategy employed in the project. The FRET pair fluorescent proteins (FPs) selected for this project are Clover and mRuby2. Clover, a green fluorescent protein, is used to visualize MP-GAP, while mRuby2, which emits red fluorescence, is used to exhibit PKD3. Both FPs were C-terminally fused to their respective target proteins. **B-** Annotated DNA map for the generated constructs, including pcDNA 3.1 PKD3-mRuby2, pcDNA 3.1 MP-GAP-Clover, PKD3-mRuby2-Lenti-ps100092, and MP-GAP-Clover-Lenti-ps100092. Maps are created using SnapGene Viewer, highlighting key genetic elements and their positions within the sequence. They depict features associated with the plasmid, including promoters, coding sequences, restriction sites, origin of replication (Ori), and antibiotic resistance genes. **C-** The panels on the left with a white background show the virtual double digests of plasmid sequence using the indicated restriction enzymes, performed with the Benchling online tool. The expected fragment sizes for each digest are indicated, providing an expected profile of the restriction analysis. The panels on the right with a dark background display the gel electrophoresis results of the same digests performed on the plasmid constructs generated in the lab. The blue arrow points to the band associated with the smallest fragment. This figure demonstrates the alignment between the in-silico restriction digest predictions and the actual laboratory results, validating the correct construction and sequence of the plasmids.

### 3.2 Criteria for Cell Cycle Stage Identification in Microscopy

In this study, actin staining based cell shape and nuclei structure were considered as criteria to distinguish the cell cycle stage for all the cell imaging. The presence of a contractile ring represented the cytokinesis stage. Nucleic acid and actin staining were employed to visualize DNA and actin filaments, respectively (Fig 3.2).

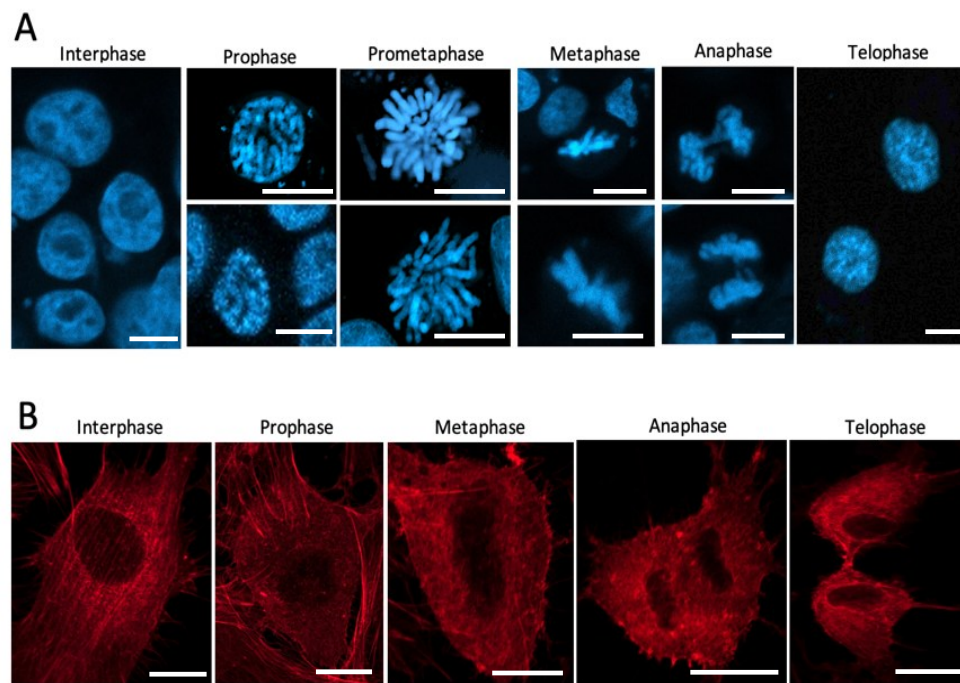


**Figure 3.2. Demonstration of morphological characteristics to identify the cell cycle stage. A-** This panel demonstrates different DNA structures representing various stages of the cell cycle in CHO cells. The cells were fixed and stained with DAPI. This staining highlights the chromatin organization, allowing the identification of different cell cycle stages based on DNA condensation and distribution. **B-** This panel shows the staining of actin filaments to represent phases of the cell cycle in HeLa Kyoto cells based on cell morphology. It reveals changes in the actin cytoskeleton during the cell cycle. The cells were fixed and stained with fluorescent-conjugated phalloidin, emitting red fluorescence. The images were acquired at 63x magnification. In both panels, the staining techniques highlight distinct cellular structures that correspond to different phases of the cell cycle. Scale bars: 10 μm

### 3.3 Transfection Experiments

To study the mitotic dynamics of PKD3 and MP-GAP, HeLa cells were used for transient transfection to express the tagged proteins. HeLa cells are human cervical carcinoma cell line extensively employed as mammalian cancer cell models in cell-cycle-related studies due to their simple culture conditions, morphology, and short cycles.<sup>110</sup> However, those HeLa cells showed very poor viability, and almost no expressing cell was alive after continuous attempts with electroporation. Different cell confluency, DNA concentrations, reagent dilution, and DNA/reagent ratios were employed. Despite several attempts and different transfection methods, switching from electroporation to chemical transfection, including traditional calcium phosphate, the issue remained, and no troubleshooting was helpful. For the next step, we decided to use Chinese hamster ovary cells (CHO) to investigate the transfection and protein expression experiments in this model. The key features of these cells are high transfection efficiency and cytoplasmic:nuclear ratio, positioning them as an ideal replacement for the project.<sup>111</sup> Those transfection experiments were characterized by acceptable viability as they could recover the 70% confluency 24 hours post-transfection. Since the study focused on analyzing the localization of the proteins, particularly during cytokinesis, the experiments aimed to spot cells that met two conditions in parallel: 1- to be in mitosis and 2-to be expressing the fluorescent-tagged proteins. However, the transfection efficiency was less than expected, leading to cells appearing either with expression signals or in mitosis, yet not fulfilling both conditions. At least 10 independent transfection experiments were conducted, but no expressing mitotic cell was found. Then, we aimed to incorporate cell cycle synchronization methods to enhance the number of mitotic cells in the population under study and find expressing mitotic cells. Cell cycle synchronization is an approach to arrest cells in a specific phase of the cycle using chemical compounds, and release

leads to harvesting a population of cells with similar synchronized cycles (Fig 3.3.A). Those experiments resulted in establishing a protocol with double thymidine and nocodazole block for synchronization of CHO cells with a 30% efficiency (Fig3.3.B). It should be noted that the protocol was initially taken from a study by A.Surani et al.,<sup>112</sup> and then slight changes were made for the optimization. Even though seemingly low, the rate was enough to catch many cells in mitosis per field of view. However, finding mitotic cells that express the transfected proteins remained a challenge. A summary of transfection and synchronization results is provided in Table 3.1.

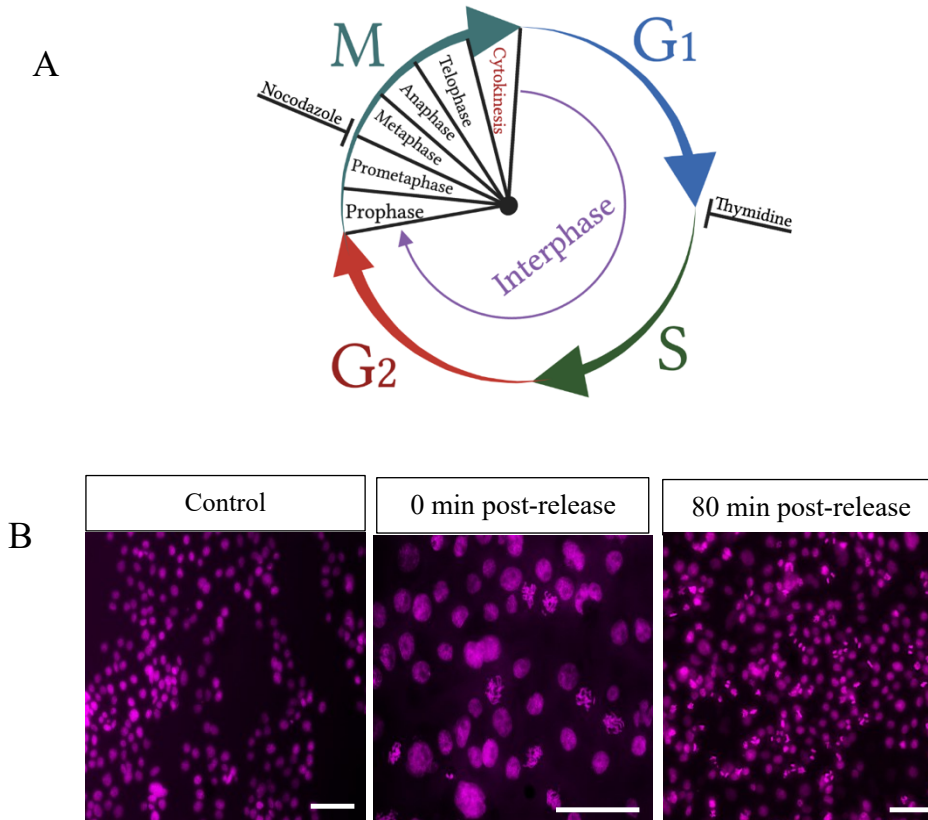


**Figure 3.3. A- Schematic pattern of a cell cycle demonstrating the cycle arrest points upon thymidine and nocodazole treatment.** This figure depicts the cell cycle stages and shows the time points when thymidine and nocodazole halt the cycle. The cell cycle initiates with the G1 phase (blue arrow) when cells grow and prepare for the S phase (green arrow), where DNA duplication occurs. Thymidine blocks the cycle in the G1-to-S transition. During the G2 phase (red arrow), the cell prepares for mitosis, and organelles duplicate. G1, S, and G2 comprise the interphase, followed by mitosis (M phase). Mitosis (blue-green arrow) consists of several subphases (divided in black), including prometaphase when DNA starts to accumulate at the mitotic plate, and metaphase when DNA accumulation at the center is completed by microtubules. Nocodazole arrests the cycle at the prometaphase to metaphase transition. The figure was created by *BioRender* tool. **B-** Synchronization of CHO cells. Control cells were not treated with drugs. The synchronized cells were double-treated with thymidine followed by nocodazole to arrest them in prometaphase. Post-release, cells were fixed and stained with Hoechst DNA staining. The purple appearance of the DNA is a pseudo-colour applied in the Axioimager. Images are representative of 4 independent experiments. The DNA structure of 1000 cells was analyzed to calculate the synchronization efficiency. The images were taken with a Zeiss AXIO Observer.A1 Inverted Fluorescence Microscope. Scale bars: 20  $\mu\text{m}$ .

**Table 3.1. Summary of cell transfection and synchronization experiments. \***

|   | Cell Line                                  | Transfection Efficiency |                          | Synchronization                                |
|---|--|-------------------------|--------------------------|--|
|   |  | Chemical                | Electroporation          |  |
| 1 | HeLa                                       | Very poor<br>Below 5%   | Very poor<br>Below 5%    | Not performed due to<br>poor viability         |
| 2 | CHO  | 25%                     | Very low<br>Not measured | 30% Efficiency -<br>DTB+Noc**                  |
| 3 | HEK 293                                    | 45%                     | Very low<br>Not measured | Unsuccessful at the<br>first trial             |
| 4 | HeLa Kyoto<br>GFP::tubulin<br>H2B::mCherry | Not measured            | Not performed            | 55%<br>DTB+Noc**                               |
| 5 | HeLa Kyoto<br>(unlabeled)                  | Average 60%             | Not performed            | Not required due to<br>high proliferation rate |

\*All experiments were performed at least 3 times independently, except for HEK 293 synchronization since it was no longer required for this project. The transfection efficiency was calculated by counting the number of signaling cells per 1000 cells 48h post-transfection. The synchronization efficiency was calculated by counting the number of mitotic cells per 1000 cells, from which the number of mitotic cells in the untreated control population of cells was subtracted. DTB+Noc\*\* is a double thymidine block followed by nocodazole treatment.

To resolve this issue, we aimed to bring another strain of HeLa cells to the lab. First, GFP::tubulin and H2B::mCherry expressing HeLa Kyoto cells were brought to the lab. Those cells are named after Kyoto University, where they were first obtained by Prof. Shuh Narumiya. HeLa Kyoto cells display characteristics important for our imaging experiments. It is widely used as a standard model in GFP localization-based studies and has high adherence to glass and plastic surfaces and low sensitivity to prolonged light exposure.<sup>113</sup> Those cells were already labeled with a red fluorescent protein (mCherry) to exhibit DNA and a green fluorescent protein (GFP) to show tubulins. They were successfully synchronized for the cell cycle (55%) (Fig S6.2.A) and were used for the transfection with PKD3-mRuby2, followed by 16-hour live cell imaging, aiming to track the dynamics of the protein (Fig S6.2.B). Even though the excitation wavelength for mRuby2 (558) stands different than mCherry (587), they are close enough for bleed-through to take place. Hence, upon excitation with Alexa568 to detect PKD3-mRuby2, H2B was also excited and emitted sharp and strongly bright, masking the PKD3 signals in the same cell. It is worth noting that we took advantage of the cloning strategy used to develop those stably exogenous protein-expressing HeLa Kyoto cells<sup>113</sup> for our project and generated PKD3-mRuby2 and MP-GAP- Clover plasmids on pIRES backbones. Due to time limitations, those plasmids were not employed for experiments in my project, but they will be potentially useful for future experiments in our lab.

Subsequently, other unlabeled HeLa Kyoto cells were brought to the lab for the transfection experiments. Those cells were characterized by high transfection efficiency in their research. Similarly, the cells demonstrated higher transfection efficiency (average 60%) in our experiments Fig 3.4.A,B, resulting in the identification of exogenous protein-expressing cells during cytokinesis. Since these cells' proliferation rate was relatively high, no synchronization was applied during those experiments. However, those cells were characterized by no specific

localizations for PKD3-mRuby2 in the furrow or microtubular structures (Fig 3.4.C). The signal either appeared as accumulations linked to no specific compartments (punctate) Fig 3.4.E,a or ubiquitously distributed in the cytoplasm (scattered) (Fig 3.4.E,b, Fig 3.4.F). On the other hand, the cells in the resting phase were commonly characterized by a vesicular signaling pattern (Fig 3.4.D). The same experiments were conducted with HEK 293 cells in which the signals were indistinctly scattered (Fig 3.5). Additionally, immunostaining experiments were implemented for HeLa Kyoto cells transfected with Flag-tagged PKD3 constructs from Addgene. The signaling pattern appeared the same as PKD3-mRuby2 constructs (data not included).

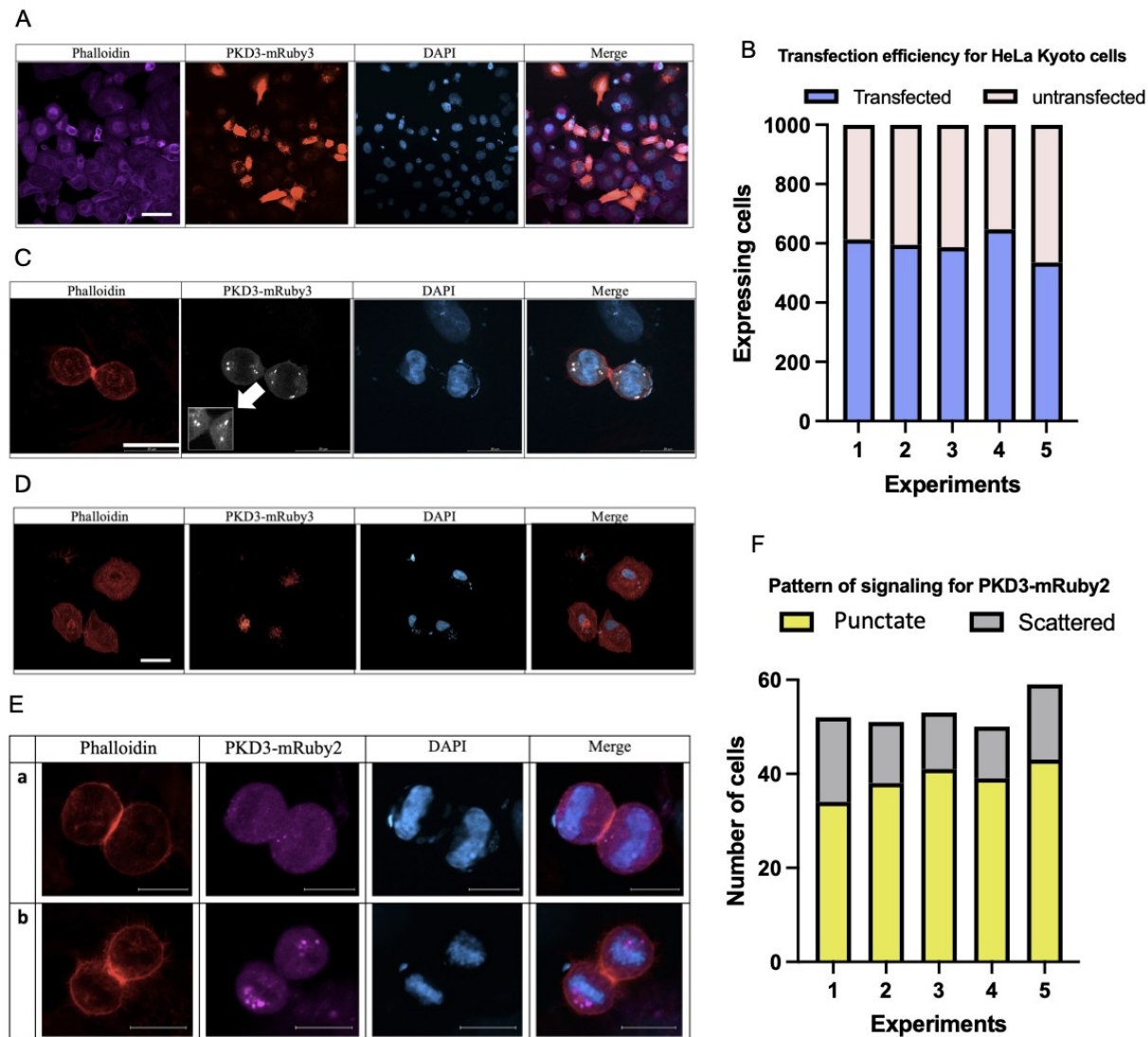


**Figure 3.4. Figure HeLa Kyoto cells expressing PKD3-mRuby2** Representative images of at least five independent experiments. HeLa Kyoto cells were transiently transfected to express exogenous mRuby2-tagged PKD3. After 48 hours, they were fixed and stained with DAPI to detect DNA (blue) and Phalloidin to detect actin (pseudocolor-purple in A, red in C,D,E). **A-** Representative images of HeLa Kyoto cells expressing PKD2-mRuby2. Scale bar: 10  $\mu$ m. **B-** Graph shows the number of transfected cells per 1000 counted cells in each individual experiment. The average transfection efficiency was 60%. **C-** Representative image showing the lack of furrow localization of the PKD3-mRuby2 during cytokinesis in furrowing. The separating DNA and the presence of a contractile ring are used as criteria to stage cytokinesis. The magnification shown by the white arrow demonstrates the cleavage furrow. Scale bar: 20  $\mu$ m. At least 250 furrowing cells were observed without the mentioned localization. **D-** Localization of PKD3-mRuby2 in cells during interphase. Scale bar: 20  $\mu$ m **E-** Two different signaling patterns were observed for PKD3-mRuby2 localization. Scale bar: 10  $\mu$ m. **F-** Graph showing the frequency of each observed pattern. At least 50 cells were considered for each experiment. The images were taken at 20x and 63x magnification.

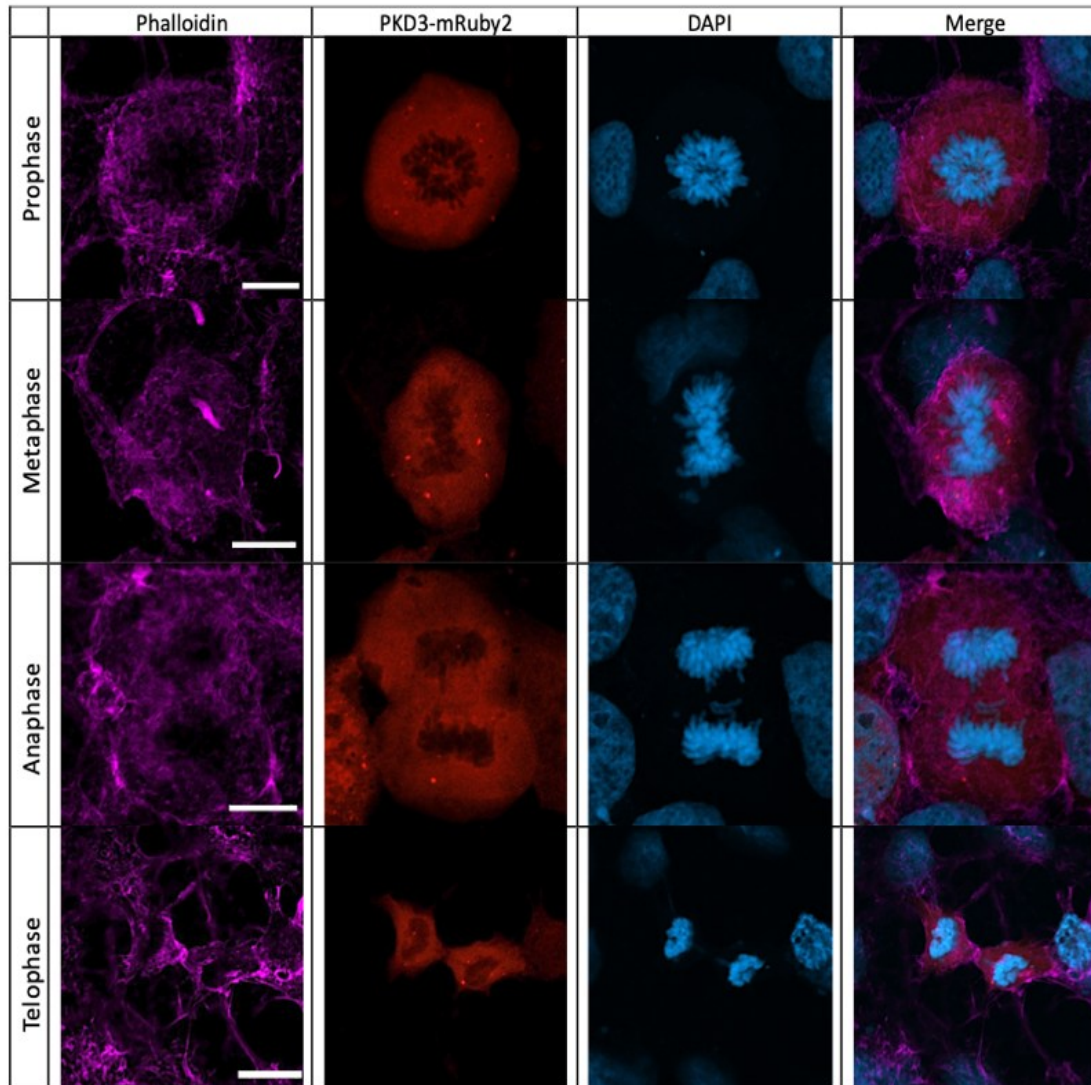


**Figure 3.5. Lack of specific localization of PKD3-mRuby2 in HEK cells during prophase to telophase-** Representative images of at least three independent experiments. HEK cells were transiently transfected to express exogenous mRuby2-tagged PKD3(red). After 48 hours, they were fixed and stained with DAPI to detect DNA (blue) and Phalloidin to detect actin (pseudocolor-purple). The transfection efficiency was 45%. Signaling cells were enumerated per 1000 cells to measure transfection efficiency. The images were taken at 63X magnification. Scale bar: 10  $\mu$ m.

### 3.4 Immunostaining Experiments

The next step was utilizing anti-PKD antibodies to visualize endogenous PKD3 and gain more insights into its localization during cytokinesis. While we tried a set of antibodies against each of the isoforms, the most informative data were taken from PKD pan antibodies that do not provide isoform-specific information. Other immunostainings were mainly characterized by unmeaningful and ubiquitous signals (Data not included). The anti-PKD pan antibody, which detects a locus shared between all members of the PKD family, was used to visualize PKD in mouse embryonic fibroblasts (MEFs) (Fig 3.6) and HEKs (Fig 3.7). According to the images presented for MEFs, PKD accumulates in the nuclei and localizes in the structures that might represent centrosomes upon condensation of DNA in prophase. PKD remains localized in there until telophase. It also colocalizes with the structures that may represent mitotic spindle throughout metaphase and anaphase. In late cytokinesis, PKD accumulates in the midbody. In HEK cells, the most dominant localizations of PKD are in the structures that we postulate are centrosomes (Fig 3.7). Interestingly, upon exposure of HEK cells with nocodazole, a microtubule-interfering compound, a sharp and punctate pattern was observed for phosphorylated PKD at areas that are likely to be mitotic spindle midzone (Fig 3.8). Phosphorylated PKD shows strong nucleic localization in the prophase compared to resting MEFs, highlighting the elevated activity of PKD in the nuclei of early mitotic cells upon chromosome condensation (Fig 3.9.D). Furthermore, phosphorylated PKD colocalizes with structures that could represent microtubules, but this has not been verified with tubulin markers (Fig 3.9.E). In addition, the signal accumulation is more intense at the tip of those presumably microtubules (Fig 3.9.C, pointed by white arrow). In the other stages of mitosis in MEFs, the signaling pattern for phosphorylated PKD is the same as pan-PKD (Fig 3.10). In MEFs, phosphorylated PKD localizes to the furrow and maintains the localization until

the very late stages of cytokinesis in the midbody (Fig 3.9.B,C). In general, the PKD activity is considerably higher in mitotic cells compared to resting cells (Fig 3.9.A). The control panel for immunostaining experiments is also provided (Fig S.5.3).

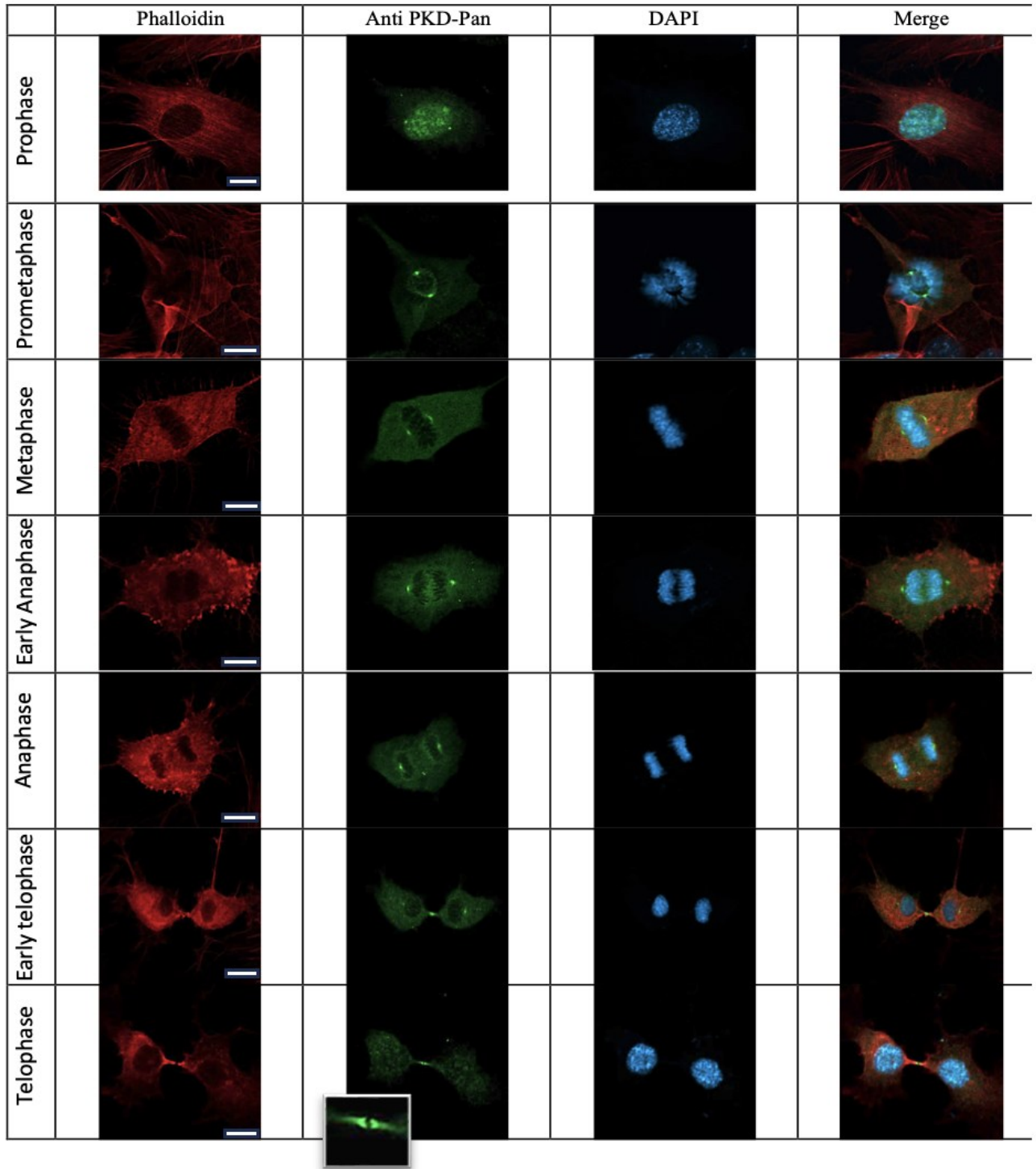


**Figure 3.6. Localization of PKD during prophase to telophase in MEFs-** Representative immunostaining images of at least six independent experiments showing MEFs expressing endogenous PKD. The images were taken at 63X magnification. The magnification square at the bottom row shows the accumulation of PKD signal at the split domain. Scale bars: 10  $\mu$ m.

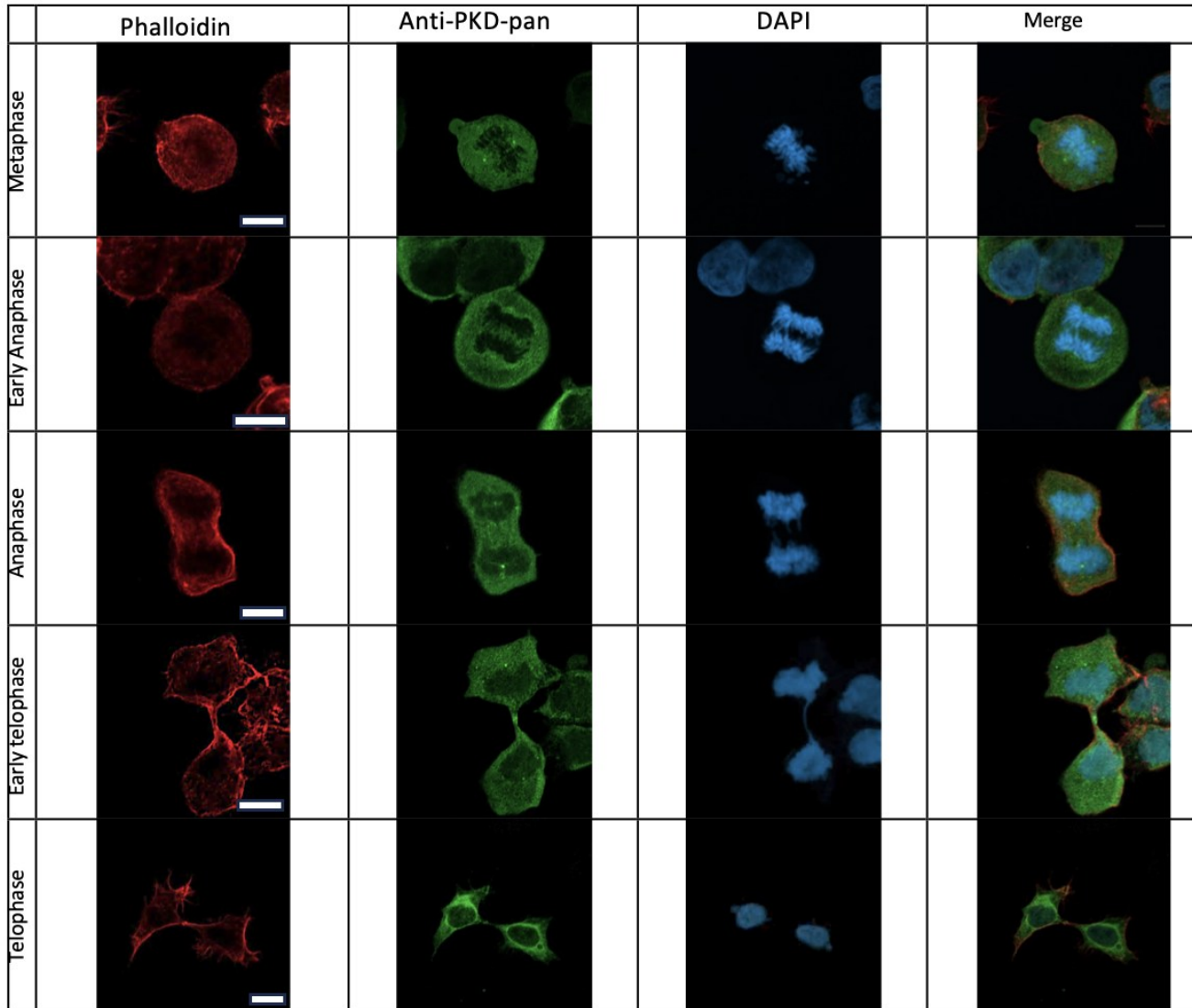


**Figure 3.7. Localization of PKD during prophase to telophase in HEKs** - Representative immunostaining images of at least six independent experiments showing HEKs expressing endogenous PKD. The images were taken at 63X magnification. Scale bars: 10  $\mu$ m

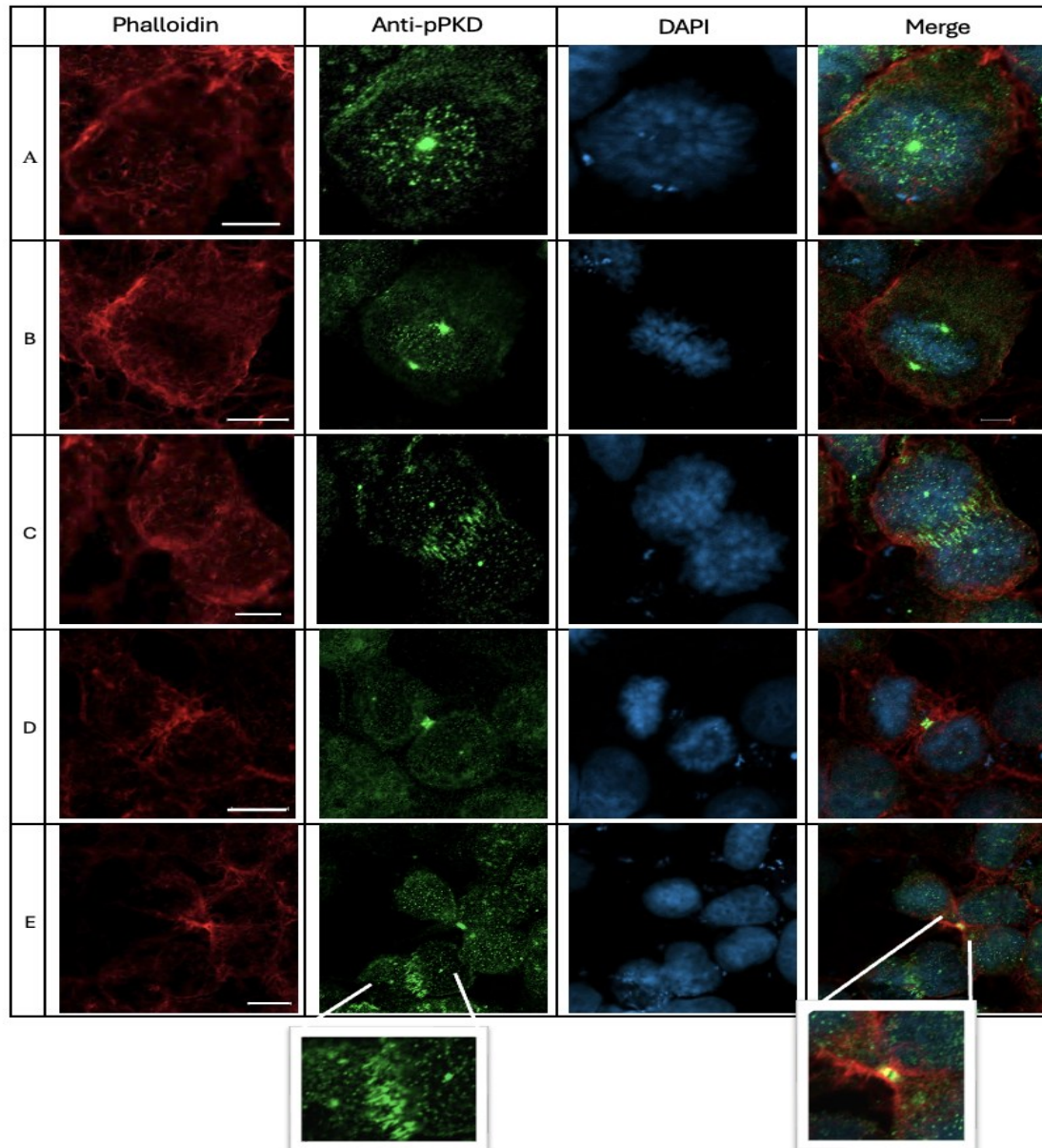


**Figure 3.8. Association of the phosphorylated PKD with structures that might represent central spindle microtubules and intracellular bridge during mitotic phases in HEK cells-** Representative immunostaining images of at least two independent experiments showing HEKs expressing endogenous active PKD. **A-** Localization of phosphorylated PKD in prophase. **B-** Localization of phosphorylated PKD in metaphase. **C-** Localization of phosphorylated PKD in anaphase. **D-** Localization of phosphorylated PKD in telophase. **E-** Localization of phosphorylated PKD in intracellular bridge in 2 different cells. The images were taken at 63X magnification. Scale bars: 10  $\mu$ m.

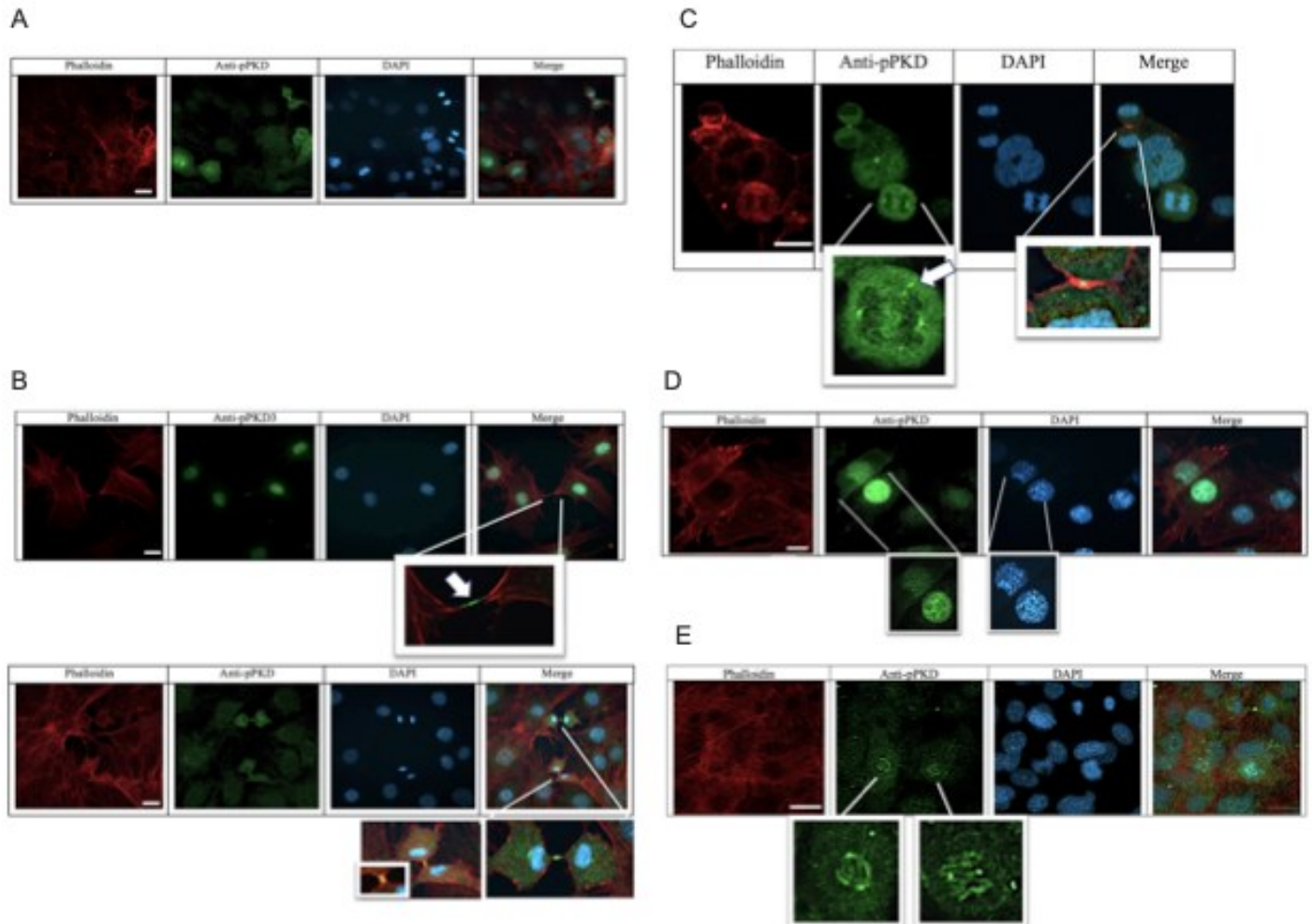


**Figure 3.9. MEFs expressing endogenous active PKD** Representative immunostaining images of at least four independent experiments. **A**-Localization and accumulation of phosphorylated PKD in mitotic MEFs. The image highlights the higher expression of phosphorylated PKD in mitotic cells compared to the resting cells. Scale bar: 20  $\mu\text{m}$ . **B**-Association of phosphorylated PKD with midbody in MEFs. Phosphorylated PKD accumulates at the intracellular bridge in two mitotic cells. The magnification square shows an overlap of PKD and actin signals at the split domain. Scale bar: upper panel is 10  $\mu\text{m}$  and below is 20  $\mu\text{m}$ . **C**-Association of the phosphorylated PKD with structures that might represent central spindle microtubules during anaphase and cytokinesis in MEFs. The magnification square on the left shows the accumulation of phosphorylated PKD at centrosomes and at the tip of structures that could represent microtubules, and on the right shows phosphorylated PKD at the center of the cleavage furrow. Scale bar: 10  $\mu\text{m}$ . **D**-Translocation of phosphorylated PKD to the nucleus upon chromosome condensation. Magnification squares show intensified active PKD signaling adjacent to condensed chromosomes and centrosomes. Scale bar: 10  $\mu\text{m}$ . **E**-Localization of the phosphorylated PKD with structures that might represent microtubules during prometaphase and metaphase in MEFs. Scale bar: 20  $\mu\text{m}$ . The images were taken at 63X magnification.

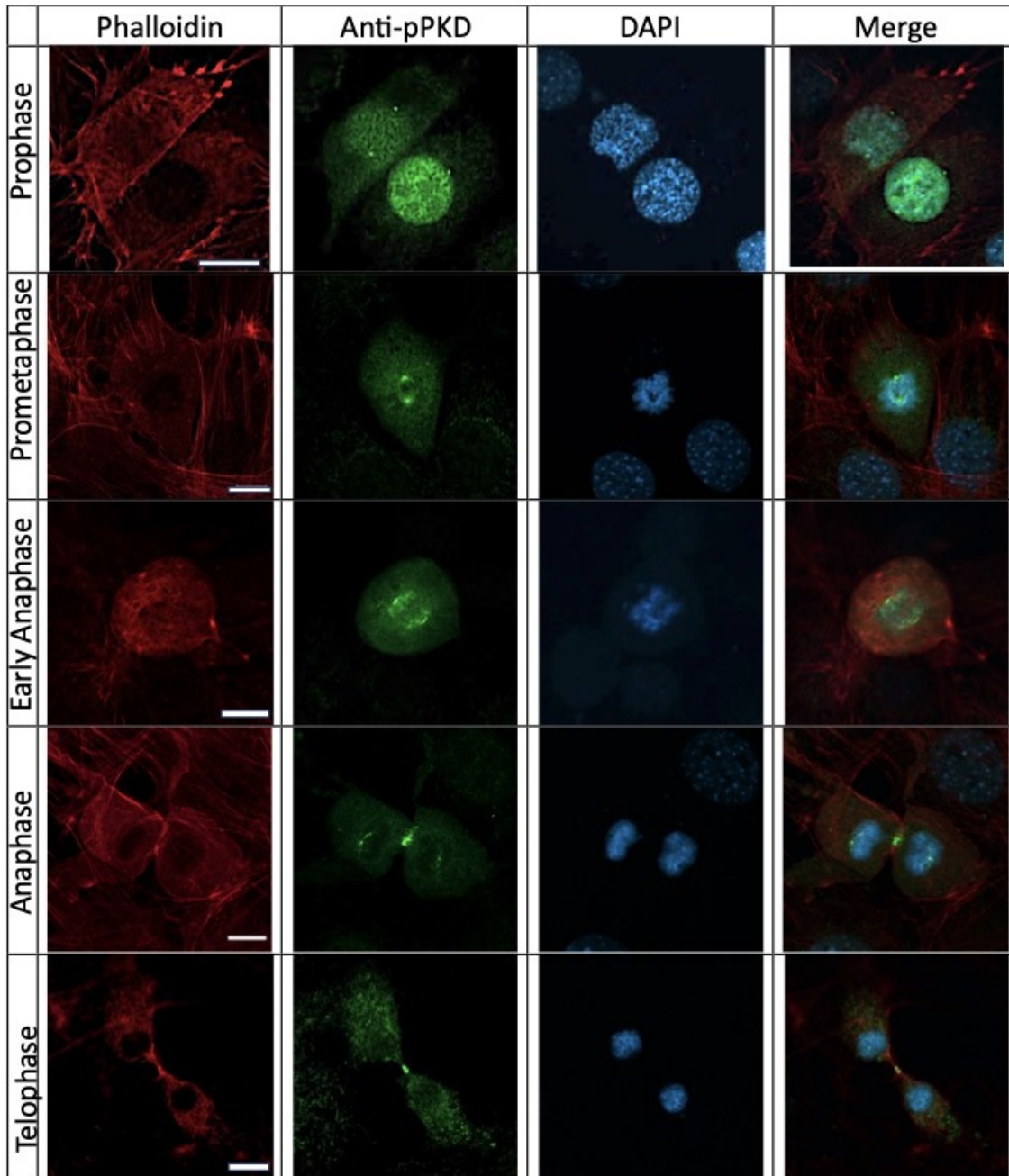


**Figure 3.10. Localization of phosphorylated PKD during prophase to telophase in MEFs-** Prophase to telophase- Representative immunostaining images of at least six independent experiments showing MEFs expressing endogenous phosphorylated PKD. The images were taken at with 63X magnification. Scale bars: 10  $\mu$ m.

### **3.5 MP-GAP Clover experiments**

All the transient transfection experiments using MP-GAP-Clover constructs were conducted at least 5 times for both CHO and HeLa Kyoto cells (Fig 3.11). In all those experiments, many cells showed strong signals in their nucleus during interphase or telophase. In the furrow of very few mitotic HeLa cells, an accumulation of green signals was observed, but they might represent an overlap of signals from two daughter cells. Those images were not included here since signaling patterns were considerably rare and thus might not be reliable. In addition, the quality of images was low due to the small number of cells to choose from. No immunostaining results are available since the commercially provided antibody against MP-GAP that we used did not work as expected.

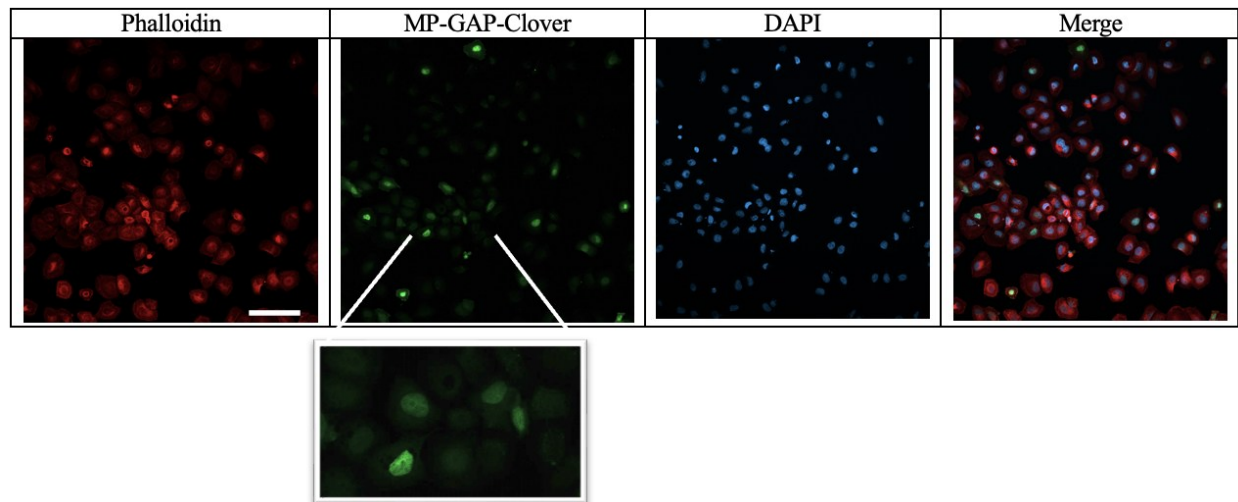


**Figure3.11. The localization pattern of MP-GAP-Clover in HeLa Kyoto cells-** Representative images of at least five independent experiments. HeLa Kyoto cells were transiently transfected to express exogenous MP-GAP-Clover (green). After 48 hours, they were fixed and stained with DAPI to detect DNA (blue) and Phalloidin to detect actin (red). The transfection efficiency was above 60%. Signaling cells were enumerated per 1000 cells to measure transfection efficiency. The images were at 20X magnification. The magnification square shows the nuclear localization during interphase. Scale bar: 20  $\mu$ m.

## **4-Discussion**

Since the beginning of studies on mitosis, scientists have been focused on figuring out the pathways and proteins regulating each step of this highly orchestrated event. Accordingly, many key factors have been established to participate in the regulation of cytokinesis. Leitges group has long been interested in the *in-vivo* roles of the third member of the protein kinase D family in regulating cell mechanisms. In this regard, PKD3-deficient MEFs were generated, and they became characterized by lower proliferation rates and aberrant cytokinesis. This observation, along with the prolonged RhoA presence and colocalization with PKD3 and MP-GAP during cytokinesis, led to the development of the hypothesis of this project. It proposes a potential interaction between PKD3 and MP-GAP, essential for contractile ring dissociation and successful cytokinesis to take place. Protein interactions are a prominent feature in determining the protein function. In addition, flawless cytokinesis is a requirement for cells to avoid binucleation and subsequent cancer development, highlighting the biological and clinical significance of this project.

### **4.1 Cloning and Transfection**

Here, molecular cloning was utilized to generate plasmids encoding fluorescent-tagged PKD3 and MP-GAP, aiming to ultimately visualize a potential interaction by FRET. It should be noted that the PKD3 used in these experiments had a murine origin (mPKD3) since the lab had been unsuccessful in isolating human PKD3 (hPKD3) plasmid-expressing bacteria before. To study the localizations and potential interaction between the proteins, the transient transfection method was used in the HeLa cell model, which is excessively employed in cell cycle-related studies. However, both the physical (electroporation) and chemical (lipofectamine, calcium

phosphate) transfection methods resulted in almost no survival for the HeLa cells despite numerous attempts and troubleshooting. Interestingly, the HeLa cells appeared healthy and proliferative prior to the transfection experiments while showing a considerable death rate 24 hours after transfection and a whole plate/well washout post-48 hour. Comparing the post-transfection cell viability for those cells and the subsequently available HeLa cell line (Kyoto) led to figuring out that those old HeLa cells were unable to resist transfection stress even to a very low extent. This conclusion was confirmed by conducting experiments on HeLa Kyoto cells with entirely similar factors except for the cell type, excluding the effect of any other variables, such as plasmid endotoxicity. To the knowledge of the Leitges group, this observation has not been described in any studies thus far. It is worth mentioning that this situation is quite different from “untransfectable” cells, which are viable yet not easily expressing the exogenous proteins. This intolerance or lack of viability could result from transfection reagent effects or activation of apoptotic pathways in response to exogenous DNA/proteins. To resolve this problem, a switch was made to the CHO cells available in the lab. In the case of CHO cells, even though it was possible to synchronize the cycles to harvest more mitotic cells and, considering the viability and transfection efficiency of those cells, finding the expressing cells in mitosis remained a major challenge for this project, leading to exploring more opportunities outside Memorial University.

By conducting transient experiments, HeLa Kyoto cells successfully expressed the PKD3-mRuby2 construct, and many expressing cells were detected during mitosis. However, the signaling pattern was not in accordance with the expected PKD3 localization based on previously published data. Considering the cause for the lack of furrow, centrosome, and nuclear localization, this could be an outcome of our cloning strategy. Proteins depend on their specific domains for anchorage, subcellular localization, interaction, and functions. In this regard, the attachment of

labeling tags, including FPs, could possibly affect the subcellular localization of mRuby2-tagged PKD3. While protein tagging has been extensively employed in molecular biology studies and has enhanced the knowledge in the field, it also bears the potential to perturb the localization and function of the native protein to which it is fused due to the size or domain interference. Most of the fluorescent tagging can be applied at either N or C-terminus, not within the sequence. A study by Davidi et al. demonstrated that tagging at opposite termini resulted in differential localizations for 515 proteins in yeast <sup>114</sup>. Accordingly, another study titled “The price of tags in protein localization studies” was conducted to gauge whether C or N terminal tagging is more successful in representing the correct and physiologically relevant localizations in the same group of proteins. Interestingly, C-terminal tagging was more linked to mitochondrial and nuclear localization, while N-terminal was more ascribed with ER and vesicular accumulation. An example is Apc11, a catalytic core subunit of the Anaphase-Promoting Complex/Cyclosome (APC/C), demonstrating ER localization when C-terminally tagged contrary to a punctuate localization for the N-terminus tagging <sup>115</sup>. Another group compared the subcellular localization of the same protein with two different FPs, which have been separately employed in publications.<sup>116,117</sup> Interestingly, the membrane type 1 matrix metalloprotease (MT1-MMP) shows clear, considerably different subcellular localization patterns in HeLa cells when labeled with EGFP or mCherry.<sup>118</sup> Thus, it can be concluded that variation in tagging each terminus can impact the protein to an extent that entirely changes its native localization.

Considering our project, many HeLa Kyoto cells in the resting phase showed a vesicular pattern for the PKD3-mRuby2, which might be a localization artifact linked to the mRuby2 tagging. In addition, due to their considerable size, GFP derivatives and the coral FPs (27kDa) can cause modifications to the proteins to which they are fused, thereby altering their folding, function,

and localization <sup>119–121</sup>. The mitotic HeLa Kyoto cells did not show the localizations in the furrow, centrosomes, and mitotic spindle as described in previous studies. The pattern was the same for the immunostaining experiment using C-terminally Flag-tagged PKD3, suggesting that C-terminal tagging might affect the PKD3 localization, regardless of the tag size. In this regard, a study by Rey et al. showed spindle localization when exogenous PKD3 is expressed in HEK cells. Hence, more experiments were conducted with PKD3-mRuby2 in HEK cells to investigate if the pattern is specific to the cell line. As shown in [Fig 3.3.E](#), PKD3-mRuby2 is characterized by localizations at no distinctive compartment during different mitotic phases. It is worth mentioning that the short C-terminal tail of the PKDs was proposed to control the cytoplasmic/nuclear localization in a study by Rey et al <sup>122</sup>. In this study, the nuclear accumulation of GFP-tagged PKD was totally inhibited upon point mutation in the catalytic domain shown by real-time imaging. Notably, the experiments by Rey et al. that showed nuclear localization of PKD3 were conducted using N-terminally tagged GFP-PKD3 and Flag-PKD3 <sup>123</sup>. A paper by E. Snapp discusses some useful FP fusion cloning strategies for when the functional and targeting domains are identified or when they are unknown. It also underscores the importance of validating whether the signaling pattern of the FP-tagged proteins is similar to the wild-type protein. Unless the native localization and functionality of the tagged protein are confirmed, researchers should be skeptical about the results of those studies <sup>119</sup>.

In addition, the lack of expected localization could result from studying murine PKD3 in human cell models (HeLa-HEK), even though the peptide sequence for both human and mouse PKD3 is highly similar. The lack of PKD-specific localization in HEKs and HeLa Kyoto cells excludes the cell line-specific effects on the lack of localizations, as this was repeated and observed in more than one cell line, while still not answering the question of whether it results from expressing murine proteins in human cells. It might be possible that the lack of mPKD3

localization in the subcellular compartments that hPKD3 localizes to, lies in their slight sequence difference, highlighting that the different domains could be possible for hPKD3-specific localization. One approach to elucidate this would be implementing a point mutation at the candidate domains related to localization in hPKD3 and comparing the localization of the truncated PKD3 and wt-PKD3 in human cells.

Lastly, the overexpression of exogenous protein in the transient transfection method could impact the localization of the proteins, leading them to mis-localize as vesicular structures in cytoplasm. The abundance of plasmids encoding for the protein and a promoter different from the wild-type state are two factors that could cause over-expression in the transient transfections. An example of overexpression artifacts is described in a study on end binding 1 (EB1) protein, which only localizes at the plus ends of microtubules at its native state expression but accumulates all along the microtubules in addition to the ends when overexpressed <sup>124</sup>.

## **4.2 Immunostaining**

In MEFs, phosphorylated PKD localizes in the nucleus and centrosomes during interphase. Upon initiation of mitosis and when the chromosomes condense, the PKD nuclear accumulation sharply increases, and centrosomes show a more distinctive enhanced PKD signal. This highlights a potential role for PKDs in the early stages of mitosis related to chromosomal structure. Interestingly, phosphorylated and non-phosphorylated PKD accumulate at the structures originating from centrosomes and expanding to the center of the mitotic plate. Even though this has not been validated with any tubulin markers in this study, this structure might represent the mitotic spindle. Accordingly, immunostaining investigation in Zhang et al. study demonstrated that a significant population (40%) of the PKD3-deficient MEFs lacked centrosome-associated  $\alpha$ -

$\beta$  tubulin staining and spindle-like structures until metaphase, which resulted in a disrupted chromosome alignment at the mitotic plate, cell cycle arrest at the metaphase, and consequently, apoptosis. Despite the presence of centrosomes represented by  $\gamma$ -tubulin immunostaining, the microtubule nucleation and the subsequent polymerization dynamics were interrupted. It was also postulated that the kinase substrate might be present among the many microtubule-associated proteins in the pericentriolar material (PCM), but no candidate was suggested to be phosphorylated by PKD3 to act in the proposed spindle establishment pathway<sup>105</sup>. This assumption is supported by a previous study on  $\beta$ -tubulin being phosphorylated by the kinase Cyclin-dependent Kinase1(CDK) at Ser172, interference of which was reported to adversely impact the ability of  $\beta$ -tubulin to bind and interact with GTP<sup>125</sup>. Nevertheless, most PKD3-deficient MEFs (60%) were characterized by the formation of functional spindles, which could possibly be compensated through redundant mechanisms by another member of the family, PKD1. However, the cell cycle was resumed with a decelerated pace in those cells. Notably, PKD3-GFP signaling, along with the active-specific phosphorylated PKD staining, overlapped with mitotic microtubule structures, suggesting a potential role of PKD3 in microtubule dynamics during mitosis<sup>105</sup>. This observation was in line with those of Papazyan et al. on microtubule-associated localization of PKD3 in HEK293 cells, while no candidate substrate or possible function was proposed<sup>60,105</sup>.

By synchronizing the cell cycle in HEK 293 cells, another group showed that PKD1 and PKD3 are phosphorylated in their activation loop during early mitosis, while their expression level was not changed<sup>60</sup>. Activation loop phosphorylated and catalytically active PKD isoforms were demonstrated to colocalize and associate with mitotic microtubular apparatus, including centrosomes, spindles, and midbody in different cell lines in addition to HEK 293 cells such as intestinal epithelial IEC-18 cells, human pancreatic cancer Panc-1 cells, murine Swiss 3T3

fibroblasts, and human primary keratinocytes.<sup>60</sup> The immunostaining findings of this project also demonstrate the same localizations for phosphorylated PKDs, hence providing evidence for active PKD recruitment to the mitotic apparatus during mitosis.

Treatment with nocodazole and other microtubule interfering compounds resulted in a longer recovery time for PKD3 deficient compared to wt MEFs to re-establish their microtubule networks and return to their initial states in the study by Zhang et al<sup>105</sup>. This led to the hypothesis of PKD3-specific involvement in microtubule dynamics through  $\alpha/\beta$ -tubulin polymerization<sup>105</sup>. Interestingly, in our study, nocodazole treatment in HEKs led to a significant increase in the presumably spindle midzone association of phosphorylated PKDs, which might represent active PKD3 [Fig 3.8](#). While the images were taken after the release from nocodazole, the concentration of the drug might have been more than some cells could recover, resulting in longer arrests. Of note, the phosphorylated PKD signals in those cells exhibit a sharp condensed accumulation mainly at the edge of the structures that are likely microtubules ([Fig 3.9.C](#)), which may represent the plus end of microtubules, where microtubule polymerization takes place. Regarding this, investigating a potential overlap between phosphorylated PKD and microtubule plus end tracker protein EB1 could be an interesting step for future studies.

It is worth mentioning other studies revealing key roles for PKD in successfully completing mitosis. It is demonstrated that all PKD isozymes mediate mitochondrial fission, which is an important step in cell division. Pangou et al. generated PKD2/3 depleted HeLa cells using CRISPR-Cas9 gene editing to investigate mitotic defects<sup>75</sup>. The PKD2/3 KO cells exhibited chromosomal segregation errors, prolonged prometaphase-like stage, and polylobed nuclei. Interestingly, a 10-minute delay in the transition between prophase to anaphase was observed, indicating a crucial role for PKDs in mitosis. Moreover, the PKD2/3 phosphorylation in

Ser744/748 was significantly increased during mitosis despite the lack of difference in the expression of these proteins<sup>75</sup>. Since chromosome segregations are mediated by spindle microtubules, this failure might be linked to the observations of this study about increased phosphorylated PKD accumulation at presumably spindle structures upon nocodazole treatment, suggesting a potential role for PKDs in prophase to anaphase transition by regulating microtubule dynamics. According to a study by Kienzle et al, PKD1/2 depletion prohibits HeLa cells from entering mitosis by arresting them in the G2 phase of the cell cycle<sup>77</sup>. It should be noted that while they employed the general PKD term for the statements in the paper, their findings were primarily based on PKD1 and PKD2. However, the mentioned cell cycle arrest was before mitosis and likely due to aberration in a pathway that couldn't be executed in a redundant mechanism by PKD3.

Moreover, the application of different PKC inhibitors revealed the presence of a mechanism in which PKCs mediate the phosphorylation of PKDs during mitosis. Remarkably, inhibitory approaches also showed that other important enzymes that facilitate mitosis from the G2 phase to cytokinesis, including Aurora Kinase A and B and Rho GTPases, are not regulating the PKD phosphorylation<sup>60</sup>. This result was in line with previous findings about the involvement of conventional and novel PKCs in regulating the G2/M cell cycle transition and in activating the PKDs through phosphorylation of Ser744 in the activation loop,<sup>126-128</sup> and supporting the hypothesis of PKC $\epsilon$ -PKD RhoA mediating signaling axis.

What piques interest is the observation by Papazyan et al. that stimulated overexpression of PKD1 and PKD3 was correlated with cytokinetic failure marked by multinucleation and mitotic bridges.<sup>60</sup> While initially it may appear contradictory to the cytokinetic failures resulting from PKD3-deficiency in MEFs, it might account for the presence of a pathway that is tightly dependent on the intensity of total kinase activity. PKD3-deficient cells may lack the necessary signaling to

inactivate the RhoA and properly mediate abscission at the right time during late cytokinesis, while highly expressing PKD3 cells can undergo an elevated PKD3 activity that might lead to premature RhoA inactivation before DNA catenations are resolved. This early initiation of ring dissociation could cause furrow regression, ultimately resulting in the binucleation phenotype.

Lastly, our observation that phosphorylated PKD accumulates in the nucleus is in line with findings from Rey et al., showing a catalytic activity-dependent PKD3 nuclear accumulation<sup>122</sup>. However, in the study, it was not identified whether the catalytic-domain dependence accounts for an autophosphorylation requirement or a protein interaction site. Not excluding the protein interaction, it is shown here that phosphorylation is at least a requirement for PKD nuclear entrance upon initiation of mitosis. Although the antibody used in this study is not specific to the PKD3 isoform, it can be interpreted that the nuclear signals might represent activated PKD3 based on the findings of the mentioned study<sup>122</sup>.

### **4.3 MP-GAP**

Using a GFP-tagged MP-GAP, Zanin et al. showed that GFP-MP-GAP mainly accumulates concentrated in the nucleus from late telophase through interphase but concentrates at the cell cortex from prophase through anaphase in HeLa cells. Furthermore, our group previously identified a colocalization of MP-GAP with RhoA at the late furrow (unpublished data). While there were many cells with nuclear MP-GAP-Clover accumulations during interphase in this study, very few mitotic cells were characterized by cortex and/or furrow association. More investigations are required to elucidate the dynamics of MP-GAP and its potential interaction with PKD3 during cytokinesis.

#### **4.4 Study Limitations:**

Designing studies based on exogenous protein expression should be accompanied by some key precautions, particularly when labeled in cell models. The size of the tag, the site of fusion, and the level of expression are essential factors in localization-based investigations. Finding the proper transfection method with high efficiency and viability is essential to obtain consistent and reproducible results. Furthermore, when the subject of the study is protein kinases, it is important to note the redundant pathways that can result in misinterpretation of isoform-specific functions. Moreover, conducting the experiments using more than one cell line as a model leads to more reliable findings since cell lines might differ in their dependence on a specific enzyme for facilitating signaling pathways. Lastly, it should be noted that findings from cancer cell lines do not necessarily represent intact cells, owing to their genetic aberrations.

Even though unsuccessful, the initial experiments in this project, including cloning and transfection experiments, were conducted to utilize FRET as the final goal of the project. It is noteworthy to consider that even finding a practical FP-fusion cloning strategy that preserves the native subcellular localization, dynamics, and activity of a protein cannot guarantee the identification of a potential interaction by FRET. That is because the interaction domains might be positioned away from the tagging site, leading to false negative results. Designing several different cloning strategies and proper controls is suggested to overcome this issue<sup>120</sup>. Finally, the FRET technology has several advantages, including accessibility, minimal limitations, and sample preparation, positioning it as a decent approach to studying protein interactions compared to other high-resolution techniques, such as X-ray crystallography<sup>108</sup>. However, to harvest the accurate cellular and molecular tools and the setup to practice FRET successfully, one must consider several key steps along with trials and errors.

#### **4.5 Concluding Remarks:**

This study provides an overview of the localization of endogenous PKD and phosphorylated PKD during mitosis in two cell types. Considering the previous findings about cell division defects caused by their deficiency and current mitotic dynamics shown by immunostaining experiments, PKDs are presumably among the intertwined network of protein kinases regulating the intricate signaling pathways during cell division. By the initiation of mitosis, phosphorylated PKD accumulates in the nucleus and centrosomes and then proceeds to translocate in the mitotic spindle and midbody. The midbody recruitment of PKDs lasts even after completion of abscission. In addition, when the microtubule polymerization is disrupted by drugs, there is an increased accumulation of phosphorylated PKDs in the mitotic spindle, particularly at structures that could represent the plus ends of microtubules, demonstrating a previously uncharacterized PKD localization. In conclusion, while there are proposed candidates to be PKD3 interacting partners, more experiments are required to identify them. Together with finding the specific PKD3 domains that mediate the mitotic translocations and interactions, we can move towards a deeper understanding of the precise mechanism by which they are linked to the regulation of cell division. Hence, the upcoming results might shed light on the PKD3 signaling cascades that can be targeted in cancer therapeutics.

## 5- References:

1. Gomperts BD, PET and IMKramer. *Signal Transduction.*; 2016.
2. Levene PA, Alsberg CL. The Cleavage Products of Vitellin. *Journal of Biological Chemistry.* 1906;2(1):127-133. doi:10.1016/S0021-9258(17)46054-6
3. Lipmann FA, Levene PA. Serinephosphoric acid obtained on hydrolysis of vitellinic acid. *Journal of Biological Chemistry.* 1932;98(1):109-114. doi:10.1016/S0021-9258(18)76142-5
4. Krebs EG. An Accidental Biochemist. *Annu Rev Biochem.* 1998;67(1):xiii-xxxii. doi:10.1146/annurev.biochem.67.1.0
5. Schwartz PA, Murray BW. Protein kinase biochemistry and drug discovery. *Bioorg Chem.* 2011;39(5-6):192-210. doi:10.1016/j.bioorg.2011.07.004
6. Manning G, Whyte DB, Martinez R, Hunter T, Sudarsanam S. The Protein Kinase Complement of the Human Genome. *Science (1979).* 2002;298(5600):1912-1934. doi:10.1126/science.1075762
7. Taylor SS, Kornev AP. Protein kinases: evolution of dynamic regulatory proteins. *Trends Biochem Sci.* 2011;36(2):65-77. doi:10.1016/j.tibs.2010.09.006
8. Cieřła J, Frączyk T, Rode W. *Phosphorylation of Basic Amino Acid Residues in Proteins: Important but Easily Missed.*; 2011. www.actabp.pl
9. Kee JM, Muir TW. Chasing Phosphohistidine, an Elusive Sibling in the Phosphoamino Acid Family. *ACS Chem Biol.* 2012;7(1):44-51. doi:10.1021/cb200445w
10. Newton AC. Protein kinase C: poised to signal. *American Journal of Physiology-Endocrinology and Metabolism.* 2010;298(3):E395-E402. doi:10.1152/ajpendo.00477.2009
11. Newton AC. Diacylglycerol's affair with protein kinase C turns 25. *Trends Pharmacol Sci.* 2004;25(4):175-177. doi:10.1016/j.tips.2004.02.010
12. Battaini F, Mochlyrosen D. Happy birthday protein kinase C: Past, present and future of a superfamily. *Pharmacol Res.* 2007;55(6):461-466. doi:10.1016/j.phrs.2007.05.005
13. Mellor H, Parker PJ. The extended protein kinase C superfamily. *Biochemical Journal.* 1998;332(2):281-292. doi:10.1042/bj3320281
14. Newton AC. Protein Kinase C: Structure, Function, and Regulation. *Journal of Biological Chemistry.* 1995;270(48):28495-28498. doi:10.1074/jbc.270.48.28495
15. Matthews SA, Pettit GR, Rozengurt E. Bryostatin 1 Induces Biphasic Activation of Protein Kinase D in Intact Cells. *Journal of Biological Chemistry.* 1997;272(32):20245-20250. doi:10.1074/jbc.272.32.20245
16. Zugaza JL, Sinnott-Smith J, Lint J Van, Rozengurt E. *Protein Kinase D (PKD) Activation in Intact Cells through a Protein Kinase C-Dependent Signal Transduction Pathway.* Vol 15.; 1996.
17. Zugaza JL, Waldron RT, Sinnott-Smith J, Rozengurt E. Bombesin, Vasopressin, Endothelin, Bradykinin, and Platelet-derived Growth Factor Rapidly Activate Protein Kinase D through a Protein Kinase C-dependent Signal Transduction Pathway. *Journal of Biological Chemistry.* 1997;272(38):23952-23960. doi:10.1074/jbc.272.38.23952
18. Rozengurt E, Rey O, Waldron RT. Protein Kinase D Signaling. *Journal of Biological Chemistry.* 2005;280(14):13205-13208. doi:10.1074/jbc.R500002200

19. Döppler H, Storz P. A Novel Tyrosine Phosphorylation Site in Protein Kinase D Contributes to Oxidative Stress-mediated Activation. *Journal of Biological Chemistry*. 2007;282(44):31873-31881. doi:10.1074/jbc.M703584200
20. Song J, Li J, Qiao J, Jain S, Mark Evers B, Chung DH. PKD prevents H<sub>2</sub>O<sub>2</sub>-induced apoptosis via NF- $\kappa$ B and p38 MAPK in RIE-1 cells. *Biochem Biophys Res Commun*. 2009;378(3):610-614. doi:10.1016/j.bbrc.2008.11.106
21. Storz P, Döppler H, Toker A. Activation Loop Phosphorylation Controls Protein Kinase D-Dependent Activation of Nuclear Factor  $\kappa$ B. *Mol Pharmacol*. 2004;66(4):870-879. doi:10.1124/mol.104.000687
22. Rozengurt E. Protein Kinase D Signaling: Multiple Biological Functions in Health and Disease. *Physiology*. 2011;26(1):23-33. doi:10.1152/physiol.00037.2010
23. Avkiran M, Rowland AJ, Cuello F, Haworth RS. Protein Kinase D in the Cardiovascular System. *Circ Res*. 2008;102(2):157-163. doi:10.1161/CIRCRESAHA.107.168211
24. Medeiros RB, Dickey DM, Chung H, et al. Protein Kinase D1 and the  $\beta$ 1 Integrin Cytoplasmic Domain Control  $\beta$ 1 Integrin Function via Regulation of Rap1 Activation. *Immunity*. 2005;23(2):213-226. doi:10.1016/j.immuni.2005.07.006
25. Ivison SM, Graham NR, Bernales CQ, et al. Protein Kinase D Interaction with TLR5 Is Required for Inflammatory Signaling in Response to Bacterial Flagellin. *The Journal of Immunology*. 2007;178(9):5735-5743. doi:10.4049/jimmunol.178.9.5735
26. Park JE, Kim YI, Yi AK. Protein Kinase D1: A New Component in TLR9 Signaling. *The Journal of Immunology*. 2008;181(3):2044-2055. doi:10.4049/jimmunol.181.3.2044
27. Lemonnier J, Ghayor C, Guicheux J, Caverzasio J. Protein Kinase C-independent Activation of Protein Kinase D Is Involved in BMP-2-induced Activation of Stress Mitogen-activated Protein Kinases JNK and p38 and Osteoblastic Cell Differentiation. *Journal of Biological Chemistry*. 2004;279(1):259-264. doi:10.1074/jbc.M308665200
28. Wang S, Li X, Parra M, Verdin E, Bassel-Duby R, Olson EN. Control of endothelial cell proliferation and migration by VEGF signaling to histone deacetylase 7. *Proceedings of the National Academy of Sciences*. 2008;105(22):7738-7743. doi:10.1073/pnas.0802857105
29. Ha CH, Wang W, Jhun BS, et al. Protein Kinase D-dependent Phosphorylation and Nuclear Export of Histone Deacetylase 5 Mediates Vascular Endothelial Growth Factor-induced Gene Expression and Angiogenesis. *Journal of Biological Chemistry*. 2008;283(21):14590-14599. doi:10.1074/jbc.M800264200
30. Ochi N, Tanasanvimon S, Matsuo Y, et al. Protein kinase D1 promotes anchorage-independent growth, invasion, and angiogenesis by human pancreatic cancer cells. *J Cell Physiol*. 2011;226(4):1074-1085. doi:10.1002/jcp.22421
31. Ernest Dodd M, Ristich VL, Ray S, Lober RM, Bollag WB. Regulation of Protein Kinase D During Differentiation and Proliferation of Primary Mouse Keratinocytes. *Journal of Investigative Dermatology*. 2005;125(2):294-306. doi:10.1111/j.0022-202X.2005.23780.x
32. Jadali A, Ghazizadeh S. Protein Kinase D Is Implicated in the Reversible Commitment to Differentiation in Primary Cultures of Mouse Keratinocytes. *Journal of Biological Chemistry*. 2010;285(30):23387-23397. doi:10.1074/jbc.M110.105619
33. Wong C, Jin ZG. Protein Kinase C-dependent Protein Kinase D Activation Modulates ERK Signal Pathway and Endothelial Cell Proliferation by Vascular Endothelial Growth Factor. *Journal of Biological Chemistry*. 2005;280(39):33262-33269. doi:10.1074/jbc.M503198200

34. Sinnett-Smith J, Jacamo R, Kui R, et al. Protein Kinase D Mediates Mitogenic Signaling by Gq-coupled Receptors through Protein Kinase C-independent Regulation of Activation Loop Ser744 and Ser748 Phosphorylation. *Journal of Biological Chemistry*. 2009;284(20):13434-13445. doi:10.1074/jbc.M806554200
35. LaValle CR, George KM, Sharlow ER, Lazo JS, Wipf P, Wang QJ. Protein kinase D as a potential new target for cancer therapy. *Biochimica et Biophysica Acta (BBA) - Reviews on Cancer*. 2010;1806(2):183-192. doi:10.1016/j.bbcan.2010.05.003
36. Prestle J, Pfizenmaier K, Brenner J, Johannes FJ. *Protein Kinase C Ix Is Located at the Golgi Compartment*.
37. Valverde AM, Sinnett-Smith J, Van Lint J, Rozengurt E. Molecular cloning and characterization of protein kinase D: a target for diacylglycerol and phorbol esters with a distinctive catalytic domain. *Proceedings of the National Academy of Sciences*. 1994;91(18):8572-8576. doi:10.1073/pnas.91.18.8572
38. Van Lint J, Sinnett-Smith J, Rozengurt E. Expression and characterization of PKD, a phorbol ester and diacylglycerol-stimulated serine protein kinase. *Journal of Biological Chemistry*. 1995;270(3):1455-1461. doi:10.1074/jbc.270.3.1455
39. Nishikawa K, Toker A, Johannes FJ, Songyang Z, Cantley LC. Determination of the Specific Substrate Sequence Motifs of Protein Kinase C Isozymes. *Journal of Biological Chemistry*. 1997;272(2):952-960. doi:10.1074/jbc.272.2.952
40. Rykx A, De Kimpe L, Mikhalap S, et al. Protein kinase D: A family affair. *FEBS Lett*. 2003;546(1):81-86. doi:10.1016/S0014-5793(03)00487-3
41. Iglesias T, Rozengurt E. Protein kinase D activation by mutations within its pleckstrin homology domain. *Journal of Biological Chemistry*. 1998;273(1):410-416. doi:10.1074/jbc.273.1.410
42. Gschwendt M, Dieterich S, Rennecke J, Kittstein W, Mueller HJ, Johannes FJ. Inhibition of protein kinase C  $\mu$  by various inhibitors. Inhibition from protein kinase c isoenzymes. *FEBS Lett*. 1996;392(2):77-80. doi:10.1016/0014-5793(96)00785-5
43. Steinberg SF. Regulation of Protein Kinase D1 Activity. *Mol Pharmacol*. 2012;81(3):284-291. doi:10.1124/mol.111.075986
44. Rozengurt E, Rey O, Waldron RT. Protein Kinase D Signaling. *Journal of Biological Chemistry*. 2005;280(14):13205-13208. doi:10.1074/jbc.R500002200
45. Steinberg SF. Decoding the Cardiac Actions of Protein Kinase D Isoforms. *Mol Pharmacol*. 2021;100(6):558-567. doi:10.1124/molpharm.121.000341
46. Iglesias T, Rozengurt E. Protein Kinase D Activation by Mutations within Its Pleckstrin Homology Domain. *Journal of Biological Chemistry*. 1998;273(1):410-416. doi:10.1074/jbc.273.1.410
47. Sánchez-Ruiloba L, Cabrera-Poch N, Rodríguez-Martínez M, et al. Protein Kinase D Intracellular Localization and Activity Control Kinase D-interacting Substrate of 220-kDa Traffic through a Postsynaptic Density-95/Discs Large/Zonula Occludens-1-binding Motif. *Journal of Biological Chemistry*. 2006;281(27):18888-18900. doi:10.1074/jbc.M603044200
48. Kunkel MT, Garcia EL, Kajimoto T, Hall RA, Newton AC. The Protein Scaffold NHERF-1 Controls the Amplitude and Duration of Localized Protein Kinase D Activity. *Journal of Biological Chemistry*. 2009;284(36):24653-24661. doi:10.1074/jbc.M109.024547

49. Huynh QK, McKinsey TA. Protein kinase D directly phosphorylates histone deacetylase 5 via a random sequential kinetic mechanism. *Arch Biochem Biophys.* 2006;450(2):141-148. doi:10.1016/j.abb.2006.02.014
50. Waldron RT, Rozengurt E. Protein kinase C phosphorylates protein kinase D activation loop Ser744 and Ser748 and releases autoinhibition by the pleckstrin homology domain. *Journal of Biological Chemistry.* 2003;278(1):154-163. doi:10.1074/jbc.M208075200
51. Rey O, Reeve JR, Zhukova E, Sinnett-Smith J, Rozengurt E. G protein-coupled receptor-mediated phosphorylation of the activation loop of protein kinase D: Dependence on plasma membrane translocation and protein kinase C $\epsilon$ . *Journal of Biological Chemistry.* 2004;279(33):34361-34372. doi:10.1074/jbc.M403265200
52. Rey O, Young SH, Cantrell D, Rozengurt E. Rapid Protein Kinase D Translocation in Response to G Protein-coupled Receptor Activation: Dependence on protein kinase C. *Journal of Biological Chemistry.* 2001;276(35):32616-32626. doi:10.1074/jbc.M101649200
53. Matthews SA, Dayalu R, Thompson LJ, Scharenberg AM. Regulation of Protein Kinase C $\gamma$  by the B-cell Antigen Receptor. *Journal of Biological Chemistry.* 2003;278(11):9086-9091. doi:10.1074/jbc.M211295200
54. Storz P, Döppler H, Toker A. Activation Loop Phosphorylation Controls Protein Kinase D-Dependent Activation of Nuclear Factor  $\kappa$ B. *Mol Pharmacol.* 2004;66(4):870-879. doi:10.1124/mol.104.000687
55. Rozengurt E. Regulation and Function of Protein Kinase D Signaling. In: *Protein Kinase C in Cancer Signaling and Therapy.* Humana Press; 2010:117-154. doi:10.1007/978-1-60761-543-9\_7
56. Cobbaut M, Van Lint J. Function and Regulation of Protein Kinase D in Oxidative Stress: A Tale of Isoforms. *Oxid Med Cell Longev.* 2018;2018:1-10. doi:10.1155/2018/2138502
57. Rey O, Sinnett-Smith J, Zhukova E, Rozengurt E. Regulated Nucleocytoplasmic Transport of Protein Kinase D in Response to G Protein-coupled Receptor Activation. *Journal of Biological Chemistry.* 2001;276(52):49228-49235. doi:10.1074/jbc.M109395200
58. Recruitment of protein kinase D to the trans-Golgi network via the first cysteine-rich domain.
59. Rey O, Yuan J, Young SH, Rozengurt E. Protein kinase C $\gamma$ /protein kinase D3 nuclear localization, catalytic activation, and intracellular redistribution in response to G protein-coupled receptor agonists. *Journal of Biological Chemistry.* 2003;278(26):23773-23785. doi:10.1074/jbc.M300226200
60. Papazyan R, Doche M, Waldron RT, Rozengurt E, Moyer MP, Rey O. Protein kinase D isozymes activation and localization during mitosis. *Exp Cell Res.* 2008;314(16):3057-3068. doi:10.1016/j.yexcr.2008.07.014
61. Nhek S, Ngo M, Yang X, et al. Regulation of Oxysterol-binding Protein Golgi Localization through Protein Kinase D-mediated Phosphorylation. *Mol Biol Cell.* 2010;21(13):2327-2337. doi:10.1091/mbc.e10-02-0090
62. Fugmann T, Hausser A, Schöffler P, Schmid S, Pfizenmaier K, Olayioye MA. Regulation of secretory transport by protein kinase D-mediated phosphorylation of the ceramide transfer protein. *J Cell Biol.* 2007;178(1):15-22. doi:10.1083/jcb.200612017
63. Hausser A, Storz P, Märten S, Link G, Toker A, Pfizenmaier K. Protein kinase D regulates vesicular transport by phosphorylating and activating phosphatidylinositol-4 kinase III $\beta$  at the Golgi complex. *Nat Cell Biol.* 2005;7(9):880-886. doi:10.1038/ncb1289

64. Liljedahl M, Maeda Y, Colanzi A, Ayala I, Van Lint J, Malhotra V. Protein Kinase D Regulates the Fission of Cell Surface Destined Transport Carriers from the Trans-Golgi Network. *Cell*. 2001;104(3):409-420. doi:10.1016/S0092-8674(01)00228-8
65. Yeaman C, Ayala MI, Wright JR, et al. Protein kinase D regulates basolateral membrane protein exit from trans-Golgi network. *Nat Cell Biol*. 2004;6(2):106-112. doi:10.1038/ncb1090
66. Yin DM, Huang YH, Zhu YB, Wang Y. Both the Establishment and Maintenance of Neuronal Polarity Require the Activity of Protein Kinase D in the Golgi Apparatus. *The Journal of Neuroscience*. 2008;28(35):8832-8843. doi:10.1523/JNEUROSCI.1291-08.2008
67. Marklund U, Lightfoot K, Cantrell D. Intracellular Location and Cell Context-Dependent Function of Protein Kinase D. *Immunity*. 2003;19(4):491-501. doi:10.1016/S1074-7613(03)00260-7
68. Waldron RT, Rey O, Zhukova E, Rozengurt E. Oxidative Stress Induces Protein Kinase C-mediated Activation Loop Phosphorylation and Nuclear Redistribution of Protein Kinase D. *Journal of Biological Chemistry*. 2004;279(26):27482-27493. doi:10.1074/jbc.M402875200
69. Sinnott-Smith J, Zhukova E, Hsieh N, Jiang X, Rozengurt E. Protein Kinase D Potentiates DNA Synthesis Induced by Gq-coupled Receptors by Increasing the Duration of ERK Signaling in Swiss 3T3 Cells. *Journal of Biological Chemistry*. 2004;279(16):16883-16893. doi:10.1074/jbc.M313225200
70. Sinnott-Smith J, Zhukova E, Rey O, Rozengurt E. Protein kinase D2 potentiates MEK/ERK/RSK signaling, c-Fos accumulation and DNA synthesis induced by bombesin in Swiss 3T3 cells. *J Cell Physiol*. 2007;211(3):781-790. doi:10.1002/jcp.20984
71. Kan Z, Jaiswal BS, Stinson J, et al. Diverse somatic mutation patterns and pathway alterations in human cancers. *Nature*. 2010;466(7308):869-873. doi:10.1038/nature09208
72. Kisfalvi K, Hurd C, Guha S, Rozengurt E. Induced overexpression of protein kinase D1 stimulates mitogenic signaling in human pancreatic carcinoma PANC-1 cells. *J Cell Physiol*. 2010;223(2):309-316. doi:10.1002/jcp.22036
73. Yamamoto H, Oue N, Sato A, et al. Wnt5a signaling is involved in the aggressiveness of prostate cancer and expression of metalloproteinase. *Oncogene*. 2010;29(14):2036-2046. doi:10.1038/onc.2009.496
74. Otera H, Ishihara N, Mihara K. New insights into the function and regulation of mitochondrial fission. *Biochimica et Biophysica Acta (BBA) - Molecular Cell Research*. 2013;1833(5):1256-1268. doi:10.1016/j.bbamcr.2013.02.002
75. Pangou E, Bielska O, Guerber L, et al. A PKD-MFF signaling axis couples mitochondrial fission to mitotic progression. *Cell Rep*. 2021;35(7). doi:10.1016/j.celrep.2021.109129
76. Bielska O, Strasbourg U DE, Romeo R. *The Role of PKD in Mitochondrial Fission during Mitosis THÈSE Présentée Par : The Role of PKD in Mitochondrial Fission during Mitosis THÈSE Dirigée Par*. <https://theses.hal.science/tel-03270889>
77. Kienzle C, Eisler SA, Villeneuve J, Brummer T, Olayioye MA, Hausser A. PKD controls mitotic Golgi complex fragmentation through a Raf-MEK1 pathway. *Mol Biol Cell*. 2013;24(3):222-233. doi:10.1091/mbc.E12-03-0198
78. Israels ED, Israels LG. The Cell Cycle. *Oncologist*. 2000;5(6):510-513. doi:10.1634/theoncologist.5-6-510

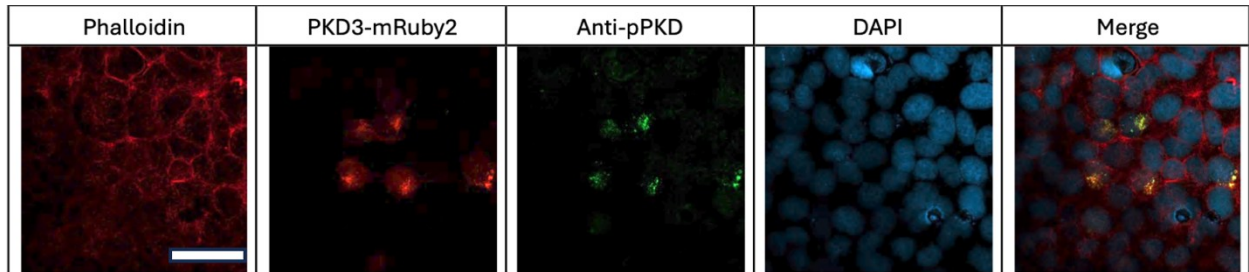
79. MAZIA D. Mitosis and the Physiology of Cell Division. In: *The Cell*. Elsevier; 1961:77-412. doi:10.1016/B978-0-12-123303-7.50008-9
80. Rappaport R. Establishment of the Mechanism of Cytokinesis in Animal Cells. *Int Rev Cytol*. 1986;105(C):245-281. doi:10.1016/S0074-7696(08)61065-7
81. Bement WM, Benink HA, Von Dassow G. A microtubule-dependent zone of active RhoA during cleavage plane specification. *Journal of Cell Biology*. 2005;170(1):91-101. doi:10.1083/jcb.200501131
82. Basant A, Glotzer M. Spatiotemporal Regulation of RhoA during Cytokinesis. *Current Biology*. 2018;28(9):R570-R580. doi:10.1016/j.cub.2018.03.045
83. Capalbo L, Bassi ZI, Geymonat M, et al. The midbody interactome reveals unexpected roles for PP1 phosphatases in cytokinesis. *Nat Commun*. 2019;10(1). doi:10.1038/s41467-019-12507-9
84. D'Avino PP, Giansanti MG, Petronczki M. Cytokinesis in animal cells. *Cold Spring Harb Perspect Biol*. 2015;7(4). doi:10.1101/cshperspect.a015834
85. Hu CK, Coughlin M, Mitchison TJ. Midbody assembly and its regulation during cytokinesis. *Mol Biol Cell*. 2012;23(6):1024-1034. doi:10.1091/mbc.E11-08-0721
86. Fededa JP, Gerlich DW. Molecular control of animal cell cytokinesis. *Nat Cell Biol*. 2012;14(5):440-447. doi:10.1038/ncb2482
87. Lens SMA, Medema RH. Cytokinesis defects and cancer. *Nat Rev Cancer*. 2019;19(1):32-45. doi:10.1038/s41568-018-0084-6
88. Saurin AT, Brownlow N, Parker PJ. Protein kinase C epsilon in cell division: Control of abscission. *Cell Cycle*. 2009;8(4):549-555. doi:10.4161/cc.8.4.7653
89. Carim SC, Kechad A, Hickson GRX. Animal Cell Cytokinesis: The Rho-Dependent Actomyosin-Anilloseptin Contractile Ring as a Membrane Microdomain Gathering, Compressing, and Sorting Machine. *Front Cell Dev Biol*. 2020;8. doi:10.3389/fcell.2020.575226
90. Koh SP, Pham NP, Piekny A. Seeing is believing: tools to study the role of Rho GTPases during cytokinesis. *Small GTPases*. 2022;13(1):211-224. doi:10.1080/21541248.2021.1957384
91. Takaine M, Numata O, Nakano K. An actin–myosin-II interaction is involved in maintaining the contractile ring in fission yeast. *J Cell Sci*. Published online January 1, 2015. doi:10.1242/jcs.171264
92. Hodge RG, Ridley AJ. Regulating Rho GTPases and their regulators. *Nat Rev Mol Cell Biol*. 2016;17(8):496-510. doi:10.1038/nrm.2016.67
93. Buchsbaum RJ. Rho activation at a glance. *J Cell Sci*. 2007;120(7):1149-1152. doi:10.1242/jcs.03428
94. Peck J, Douglas Iv G, Wu CH, Burbelo PD. *Human RhoGAP Domain-Containing Proteins: Structure, Function and Evolutionary Relationships*. <http://bc.georgetown.edu/pb/RhoGAP>
95. Miller AL, Bement WM. Regulation of cytokinesis by Rho GTPase flux. *Nat Cell Biol*. 2009;11(1):71-77. doi:10.1038/ncb1814
96. Glotzer M. Cytokinesis: GAP Gap. *Current Biology*. 2009;19(4):R162-R165. doi:10.1016/j.cub.2008.12.028
97. Somers WG, Saint R. A RhoGEF and Rho Family GTPase-Activating Protein Complex Links the Contractile Ring to Cortical Microtubules at the Onset of Cytokinesis. *Dev Cell*. 2003;4(1):29-39. doi:10.1016/S1534-5807(02)00402-1

98. Zanin E, Desai A, Poser I, et al. A conserved RhoGAP limits M phase contractility and coordinates with microtubule asters to confine RhoA during Cytokinesis. *Dev Cell*. 2013;26(5):496-510. doi:10.1016/j.devcel.2013.08.005
99. Manukyan A, Ludwig K, Sanchez-Manchinelly S, Parsons SJ, Stukenberg PT. A complex of p190RhoGAP and anillin modulates RhoGTP and the cytokinetic furrow in human cells. *J Cell Sci*. Published online January 1, 2014. doi:10.1242/jcs.151647
100. Saurin AT, Durgan J, Cameron AJ, Faisal A, Marber MS, Parker PJ. The regulated assembly of a PKC $\epsilon$  complex controls the completion of cytokinesis. *Nat Cell Biol*. 2008;10(8):891-901. doi:10.1038/ncb1749
101. Bishop AC, Ubersax JA, Petsch DT, et al. A chemical switch for inhibitor-sensitive alleles of any protein kinase. *Nature*. 2000;407(6802):395-401. doi:10.1038/35030148
102. Kelly JR, Martini S, Brownlow N, et al. The Aurora B specificity switch is required to protect from non-disjunction at the metaphase/anaphase transition. *Nat Commun*. 2020;11(1):1396. doi:10.1038/s41467-020-15163-6
103. Watson L, Soliman TN, Davis K, et al. Co-ordinated control of the Aurora B abscission checkpoint by PKC $\epsilon$  complex assembly, midbody recruitment and retention. *Biochemical Journal*. 2021;478(12):2247-2263. doi:10.1042/BCJ20210283
104. Martini S, Davis K, Faraway R, et al. A genetically-encoded crosslinker screen identifies SERBP1 as a PKC $\epsilon$  substrate influencing translation and cell division. *Nat Commun*. 2021;12(1). doi:10.1038/s41467-021-27189-5
105. Zhang T, Braun U, Leitges M. PKD3 deficiency causes alterations in microtubule dynamics during the cell cycle. *Cell Cycle*. 2016;15(14):1844-1854. doi:10.1080/15384101.2016.1188237
106. Ganem NJ, Godinho SA, Pellman D. A mechanism linking extra centrosomes to chromosomal instability. *Nature*. 2009;460(7252):278-282. doi:10.1038/nature08136
107. Lin W, Mehta S, Zhang J. Genetically encoded fluorescent biosensors illuminate kinase signaling in cancer. *Journal of Biological Chemistry*. 2019;294(40):14814-14822. doi:10.1074/jbc.REV119.006177
108. Algar WR, Hildebrandt N, Vogel SS, Medintz IL. FRET as a biomolecular research tool — understanding its potential while avoiding pitfalls. *Nat Methods*. 2019;16(9):815-829. doi:10.1038/s41592-019-0530-8
109. Bajar B, Wang E, Zhang S, Lin M, Chu J. A Guide to Fluorescent Protein FRET Pairs. *Sensors*. 2016;16(9):1488. doi:10.3390/s16091488
110. Poirson J, Cho H, Dhillon A, et al. Proteome-scale discovery of protein degradation and stabilization effectors. *Nature*. 2024;628(8009):878-886. doi:10.1038/s41586-024-07224-3
111. Prosser SL, Fry AM. Fluorescence Imaging of the Centrosome Cycle in Mammalian Cells. In: ; 2009:165-183. doi:10.1007/978-1-60327-993-2\_10
112. Surani AA, Colombo SL, Barlow G, Foulds GA, Montiel-Duarte C. Optimizing Cell Synchronization Using Nocodazole or Double Thymidine Block. In: ; 2021:111-121. doi:10.1007/978-1-0716-1538-6\_9
113. Schmitz MHA, Gerlich DW. Automated Live Microscopy to Study Mitotic Gene Function in Fluorescent Reporter Cell Lines. In: ; 2009:113-134. doi:10.1007/978-1-60327-993-2\_7
114. Weill U, Krieger G, Avihou Z, Milo R, Schuldiner M, Davidi D. Assessment of GFP Tag Position on Protein Localization and Growth Fitness in Yeast. *J Mol Biol*. 2019;431(3):636-641. doi:10.1016/j.jmb.2018.12.004

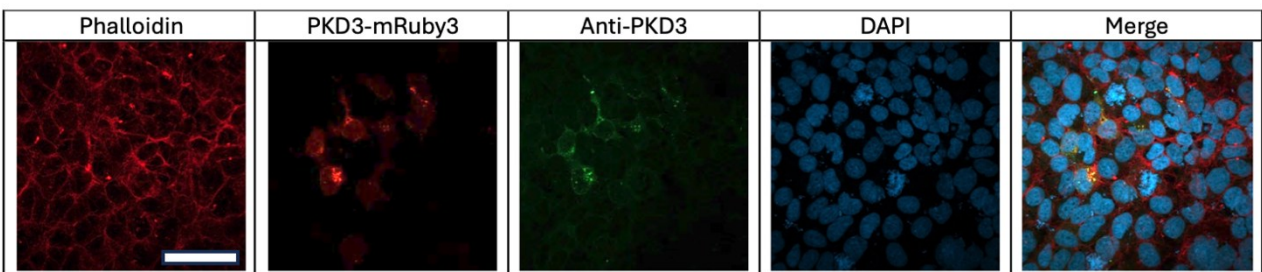
115. Margolin W. The Price of Tags in Protein Localization Studies. *J Bacteriol.* 2012;194(23):6369-6371. doi:10.1128/JB.01640-12
116. Wang Y, McNiven MA. Invasive matrix degradation at focal adhesions occurs via protease recruitment by a FAK–p130Cas complex. *Journal of Cell Biology.* 2012;196(3):375-385. doi:10.1083/jcb.201105153
117. Sakurai-Yageta M, Recchi C, Le Dez G, et al. The interaction of IQGAP1 with the exocyst complex is required for tumor cell invasion downstream of Cdc42 and RhoA. *J Cell Biol.* 2008;181(6):985-998. doi:10.1083/jcb.200709076
118. Ettinger A, Wittmann T. Fluorescence live cell imaging. In: ; 2014:77-94. doi:10.1016/B978-0-12-420138-5.00005-7
119. Snapp E. Design and Use of Fluorescent Fusion Proteins in Cell Biology. *Curr Protoc Cell Biol.* 2005;27(1). doi:10.1002/0471143030.cb2104s27
120. Piston DW, Kremers GJ. Fluorescent protein FRET: the good, the bad and the ugly. *Trends Biochem Sci.* 2007;32(9):407-414. doi:10.1016/j.tibs.2007.08.003
121. Huang SM, Yang F, Cai BY, et al. Genetically Encoded Fluorescent Amino Acid for Monitoring Protein Interactions through FRET. *Anal Chem.* 2019;91(23):14936-14942. doi:10.1021/acs.analchem.9b03305
122. Rey O, Papazyan R, Waldron RT, et al. The Nuclear Import of Protein Kinase D3 Requires Its Catalytic Activity. *Journal of Biological Chemistry.* 2006;281(8):5149-5157. doi:10.1074/jbc.M508014200
123. Rey O, Yuan J, Young SH, Rozengurt E. Protein kinase Cv/protein kinase D3 nuclear localization, catalytic activation, and intracellular redistribution in response to G protein-coupled receptor agonists. *Journal of Biological Chemistry.* 2003;278(26):23773-23785. doi:10.1074/jbc.M300226200
124. Gierke S, Wittmann T. EB1-Recruited Microtubule +TIP Complexes Coordinate Protrusion Dynamics during 3D Epithelial Remodeling. *Current Biology.* 2012;22(9):753-762. doi:10.1016/j.cub.2012.02.069
125. Fourest-Lieuvin A, Peris L, Gache V, et al. Microtubule Regulation in Mitosis: Tubulin Phosphorylation by the Cyclin-dependent Kinase Cdk1. *Mol Biol Cell.* 2006;17(3):1041-1050. doi:10.1091/mbc.e05-07-0621
126. Barboule N, Lafon C, Chadebecq P, Vidal S, Valette A. Involvement of p21 in the PKC-induced regulation of the G2/M cell cycle transition. *FEBS Lett.* 1999;444(1):32-37. doi:10.1016/S0014-5793(99)00022-8
127. Chen D, Purohit A, Halilovic E, Doxsey SJ, Newton AC. Centrosomal Anchoring of Protein Kinase C  $\beta$ II by Pericentrin Controls Microtubule Organization, Spindle Function, and Cytokinesis. *Journal of Biological Chemistry.* 2004;279(6):4829-4839. doi:10.1074/jbc.M311196200
128. Jacamo R, Sinnott-Smith J, Rey O, Waldron RT, Rozengurt E. Sequential protein kinase C (PKC)-dependent and PKC-independent protein kinase D catalytic activation via Gq-coupled receptors: Differential regulation of activation loop Ser744 and Ser748 phosphorylation. *Journal of Biological Chemistry.* 2008;283(19):12877-12887. doi:10.1074/jbc.M800442200

## 6-Supplementary Data

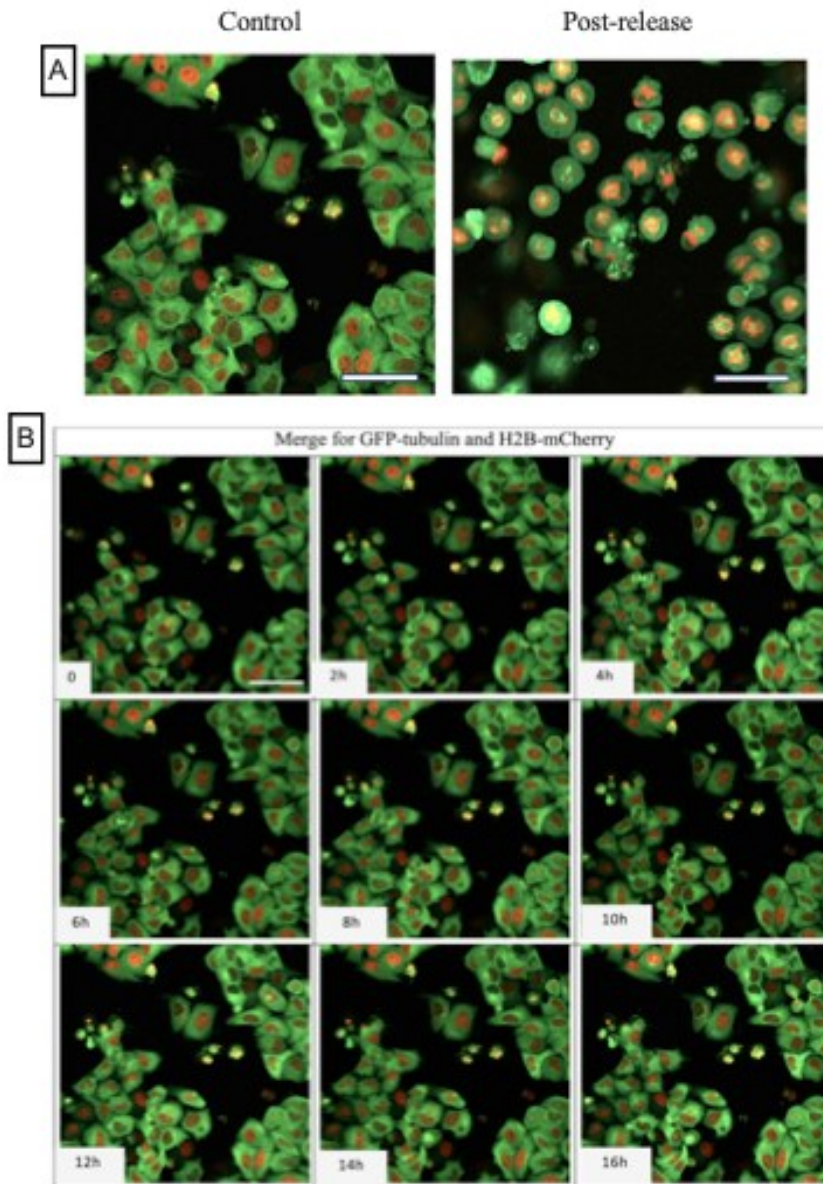
A



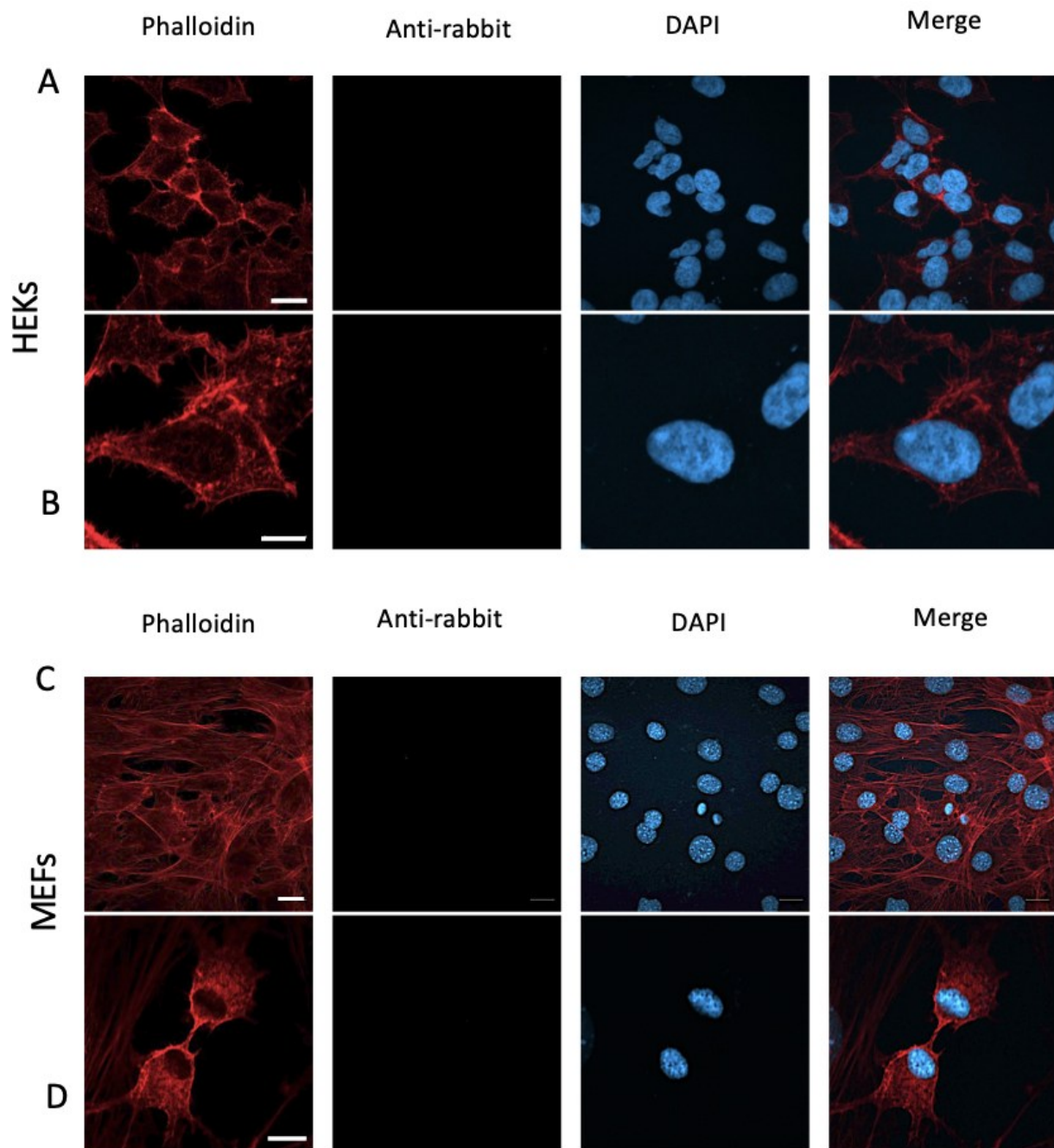
B



**Supplementary Figure 6.1. Immunostaining validation of PKD3-mRuby2 plasmid.** **A-** HeLa Kyoto cells were transiently transfected with the PKD3-mRuby2 construct. After 24 hours of transfection, the cells were fixed and subjected to immunostaining with an anti-phospho-PKD (pPKD) rabbit antibody, followed by a secondary antibody conjugated with a green fluorescent dye. This process highlights the phosphorylated state of PKD3 within the cells. **B-** HeLa Kyoto cells were transiently transfected with the PKD3-mRuby2 construct. Similar to panel A, the cells were fixed 24 hours post-transfection and stained using an anti-PKD3 rabbit antibody, with a green fluorescent-conjugated secondary antibody. This staining specifically identifies the PKD3 protein. In both panels, the overlapping fluorescence signals from the mRuby2 (red) and the green fluorescent-conjugated antibodies indicate successful expression and correct localization of the PKD3-mRuby2 fusion protein. The colocalization of the red and green signals provides additional validation for the accurate construction and expression of the PKD3-mRuby2 plasmid. Scale bar: 20  $\mu\text{m}$



**Supplementary Figure 6.2. A- Synchronization of GFP::tubulin H2B::mCherry HeLa Kyoto cells-** Representative images of HeLa Kyoto cells expressing GFP-tagged tubulins and mCherry-tagged H2B. Above is the result of one synchronization experiment. Cells were double-treated with thymidine followed by nocodazole to arrest them in prometaphase. After release, cells were fixed without any staining. A region with a high number of synchronized cells was chosen for the image. Control untreated cells were fixed without any staining. The DNA structure and tubulin shape of 1000 cells were analyzed to calculate the synchronization efficiency. **B- Live cell imaging of GFP::tubulin H2B::mCherry HeLa Kyoto cells-** Representative images of live cell stills for HeLa Kyoto cells expressing GFP-tagged tubulins and mCherry-tagged H2B. Above is the result of one live imaging experiment, in which images were taken every 5 minutes for 16 hours. The images were taken using Zeiss LSM 900 with 20X magnification Scale bar: 20  $\mu$ m



**Supplementary Figure 6.3. Control (Mock samples)**-The cells were fixed and stained only with a secondary antibody (2mg/2ml) and phalloidin counterstaining. The images were taken using Zeiss LSM 900 with 20x objective for A, C, and 63x for B, D. The phalloidin was excited with Alexa 647, and the secondary antibody (blank) was excited with Alexa 488 lasers. All the laser parameters for the 488 channel were the same as in previous samples in which the fluorescent protein was excited. Scale bars: 10  $\mu$ m.